MHD MIXED CONVECTION STAGNATION-POINT FLOW OF A CHEMICALLY REACTING FLUID OVER A PLATE IN A POROUS MEDIUM WITH RADIATION

NIRANJAN HARI

FACULTY OF SCIENCE
UNIVERSITY OF MALAYA
KUALA LUMPUR

2016

MHD MIXED CONVECTION STAGNATION-POINT FLOW OF A CHEMICALLY REACTING FLUID OVER A PLATE IN A POROUS MEDIUM WITH RADIATION

NIRANJAN HARI

THESIS SUBMITTED IN FULFILMENT OF THE REQUIREMENTS FOR THE DEGREE OF DOCTOR OF PHILOSOPHY

FACULTY OF SCIENCE
UNIVERSITY OF MALAYA
KUALA LUMPUR

2016

UNIVERSITY OF MALAYA

ORIGINAL LITERARY WORK DECLARATION

Name of Candidate: NIRANJAN HARI

Registration/Matric No: SHB120007

Name of Degree: DOCTOR OF PHYLOSOPHY

Title of Thesis ("this Work"): MHD mixed convection stagnation-point flow of a chemically reacting fluid over a plate in a porous medium with radiation

Field of Study: Computational Fluid Dynamics (Mathematics)

I do solemnly and sincerely declare that:

(1) I am the sole author/writer of this Work;
(2) This Work is original;
(3) Any use of any work in which copyright exists was done by way of fair dealing and for permitted purposes and any excerpt or extract from, or reference to or reproduction of any copyright work has been disclosed expressly and sufficiently and the title of the Work and its authorship have been acknowledged in this Work;
(4) I do not have any actual knowledge nor do I ought reasonably to know that the making of this work constitutes an infringement of any copyright work;
(5) I hereby assign all and every rights in the copyright to this Work to the University of Malaya ("UM"), who henceforth shall be owner of the copyright in this Work and that any reproduction or use in any form or by any means whatsoever is prohibited without the written consent of UM having been first had and obtained;
(6) I am fully aware that if in the course of making this Work I have infringed any copyright whether intentionally or otherwise, I may be subject to legal action or any other action as may be determined by UM.

Candidate's Signature Date:

Subscribed and solemnly declared before,

Witness's Signature Date:

Name:

Designation:

ABSTRACT

This thesis deals with the extensive analysis on mathematical modelling of mixed convective flow, heat and mass transfer over a vertical plate embedded in a porous medium near the stagnation point with various effects, such as MHD, slip, chemical reaction, radiation, heat generation/absorption, soret and dufour effects. The working medium is an incompressible, Newtonian, viscous and electrically conducting fluid. A stagnation point occurs whenever a flow impinges on a solid object and it holds the highest pressure. The fluid divided into two streams when the fluid hits at stagnation point and the viscous flow adheres to the plate. The uniform magnetic field is applied in the direction normal to the vertical plate. Since the magnetic Reynolds number is too small, the induced magnetic field is negligible. There is no Hall effect and Joule heating. The porous medium is modeled by Darcy's law and the porous medium is isotropic and homogeneous. The porous medium is in thermodynamic equilibrium with the local fluid. All the fluid properties are taken as constant except the density in the buoyancy term. The physical problem is modelled mathematically by using principles of mass, momentum, energy and species concentration. The governing coupled nonlinear partial differential equations are converted into a system of non-linear ordinary differential equations by using similarity transformation. Then, ordinary differential equations are solved numerically by shooting method along with fourth-order Runge-Kutta integration. The local skin friction, Nusselt number and Sherwood number are calculated and exposed comprehensively. In order to ascertain the accuracy of numerical results, the present results are compared with previously published work and they are found to be in good agreement. The results are depicted in the form of velocity, temperature and concentration profiles for different combination of pertinent parameters involved in the study.

ACKNOWLEDGEMENTS

It is a pleasure to thank the many people who made this thesis possible.

It is difficult to overstate my gratitude to my Ph.D. supervisor, **Dr. S. Sivasankaran,** Institute of Mathematical Sciences, University of Malaya, Kuala Lumpur, Malaysia**.** With his enthusiasm, his inspiration, his great efforts to explain things clearly and simply. Throughout my research period, he provided encouragement, sound advice, good teaching, good company, and lots of good ideas.

Last but not the least, I gratefully acknowledge the encouragement and support received from my family, in particular, my parents, my wife and my son during the preparation of this thesis.

H. Niranjan

TABLE OF CONTENTS

LIST OF FIGURES

LIST OF TABLES

LIST OF SYMBOLS AND ABBREVIATIONS

a	:	constant
b	:	slip parameter
B_0	:	strength of magnetic field
Bi	:	Biot number
C	:	species concentration
Cr	:	chemical reaction parameter
D	:	diffusion coefficient
Df	:	Dufour number
f	:	dimensionless stream function
g	:	gravitational acceleration
Gr_c	:	solutal Grashof number
Gr_T	:	thermal Grashof number
h	:	convective heat transfer coefficient
k	:	thermal conductivity
K	:	permeability parameter
$\tilde{K}$	:	porous medium permeability
K'	:	mean absorption coefficient
M	:	magnetic field parameter
N_1	:	Navier slip coefficient
Nu	:	Nusselt number
Pr	:	Prandtl number
Q	:	heat generation/absorption
Rd	:	thermal radiation parameter
Re_x	:	Reynolds number
Ri_T	:	thermal Richardson number
Ri_c	:	solutal Richardson number
S	:	heat generation parameter
Sc	:	Schmidt number
Sh	:	Sherwood number
Sr	:	Soret number
T	:	temperature

u,v	:	velocity components
x,y	:	cartesian components

Greek Letters

β	:	coefficient of thermal expansion
β^*	:	coefficient of solutal expansion
Γ_0	:	chemical reaction parameter
η	:	similarity variable
θ	:	dimensionless temperature
μ	:	dynamic viscosity
υ	:	kinematic viscosity
ρ	:	density
σ^*	:	Stefan-Boltzmann constant
σ_e	:	electrical conductivity
ϕ	:	dimensionless concentration
ψ	:	stream function

Subscripts

w	:	at wall
∞	:	at free stream

CHAPTER 1: INTRODUCTION

Fluid mechanics is basically the study of fluid behavior when some external forces act over it. It can be divided into two branches, fluid statics-the study of fluids at rest, and fluid dynamics where the fluid is in motion. Fluid dynamics deals with the motion of fluids, the forces that are responsible for motion of fluid. The fluid motion is governed by equation of motion (Navier-Stokes equation). A stagnation point is a point in a flow field where the local velocity of the fluid becomes zero. The stagnation point exists at the surface of objects in the flow field, where the fluid is brought to rest by the object.

1.1 Boundary Layer Theory

The concept of the boundary layer plays a vital role in fluid dynamics. A boundary layer is the layer of fluid in the immediate vicinity of a bounding surface where the effects of viscosity are significant. Ludwing Prandtl (1875–1953) presented his benchmark paper in 1904 and introduced the concept of boundary layer theory of fluid flow for a small viscosity or large Reynolds number. He proved that the Navier-Stokes equations can be simplified to yield approximate solutions for overcoming the limitations associated with the ideal fluid theory.

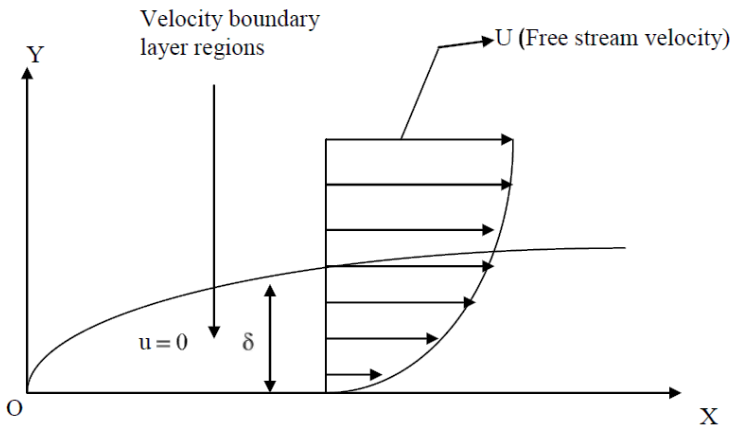

Figure 1.1. Velocity Boundary Layer

1.2 Magneto-hydrodynamics

The study of the motion of an electrically conducting fluid in the presence of a magnetic field is called magneto-hydrodynamics (MHD). In MHD associated with heat transfer problem, the additional body force term viz., the Lorentz force comes into play and the Joule heating appears in the energy equation. The study of MHD of viscous electrically conducting fluids plays a significant role, owing to its practical interest and abundant applications in astro-physical and geo-physical phenomena, such as stellar and planetary processes.

1.3 Heat Transfer

The heat transfer is energy transfer due to a temperature difference between the system and its surroundings. According to Fourier law, the heat flux is given by $q = -k\dfrac{\partial T}{\partial n}$, where k is the constant of proportionality called coefficient of thermal conductivity or thermal conductivity, n is normal to the surface, q is heat flux and T is temperature. Here the negative sign indicates that the heat flow is in the direction of decreasing temperature. There are three modes of heat transfer i.e., conduction, convection and radiation.

1.3.1 Conduction

Conduction is the transfer of heat from molecule to molecule, throughout the material (solids). Heat conduction may be stated as the transfer of internal energy between the molecules. The molecules inside the material which are nearest to the heat source gain kinetic energy. They vibrate vigorously and their movement affects the molecules immediately next to them. They pass on some of their energy spreading heat through the material. Examples: The heating of iron rod, touching a stove and being burned and the ice cooling down from our hand.

1.3.2 Convection

The transfer of heat by circulation or movement of the heated parts of fluids (liquids and gases) is called convection. When a liquid or gas is heated, the part nearest the heat source expands, becomes less dense and rises. This creates a convective motion and it is called convection cell. Convection is classified into two types: free (natural) and forced convection.

1.3.2.1 Free Convection

In this mode, motion of the fluid arises solely by buoyancy force (effect) due to the presence of gravitational acceleration and density variation caused by temperature differences from one fluid layer to another. Examples: the boiling of water, the oceanic currents and the sea-wind formation.

1.3.2.2 Forced Convection

If the heat transfer between the fluid and the solid surface occurs by fluid motion induced by external agencies or forces, then the mode of heat transfer is termed as forced convection. Examples: ovens for baking bread, fluid is circulated by pump or blower, nuclear reactors, air conditioning and car engine.

1.3.2.3 Mixed Convection

This is a combination of forced and natural convections. We imply forced convection where buoyancy forces also exist. Examples: the blood circulation in warm bloodied animals, the shock waves coming from an explosion and a convection oven.

1.3.3 Radiation

The transfer of energy by electromagnetic waves is called radiation. The thermal radiation is electromagnetic radiation generated by the thermal motion of charged particles in matter. In radiation, the heat transfer does not require any intermediate medium, where as in the case of conduction and convection, the medium for heat transfer is essentially required. Examples: the solar energy, the heat from a lightbulb and the heat from a fire.

1.4 Mass Transfer

The process of transfer of mass as a result of the species concentration difference in a mixture is called a mass transfer. Some common examples of mass transfer in everyday life are the diffusion of smoke through tall chimneys into the environment, the transfer of water vapor into dry air, drying and evaporation. The different modes of mass transfer are diffusion and convective mass transfer. Mass transfer which takes place due to random molecular motion in laminar-flow fluid is known as diffusion. Mass transfer which takes place due to concentration difference of species at the surface and the fluid over the surface is known as convective mass transfer. The involvement and application of mass transfer process goes to greater lengths in numerous fields of science, engineering and technology, such as, distillation, absorption of gases, interaction of solids and liquids from their mixtures and crystallization adsorption (solid taking up vapour on its surface).

1.5 Porous Media

A porous medium can be defined as a material consisting of solid matrix with an interconnected void. Soil, sand, fissured rock, karstic lime stone, ceramics, bread, lungs and kidneys, aquifers from which ground water is pumped, reservoirs which yield oil and / or gas, sand filters for purifying water, packed–beds in the chemical engineering industry and the root zone in agriculture are the examples of porous medium domains. The power of free and continuous flow of fluid through fine holes of the surface (or media) is called permeability. Flow through a porous medium is encountered in many applied science and engineering disciplines, namely mechanics (geo-mechanics, soil mechanics, rock mechanics), engineering (petroleum engineering, construction engineering), geosciences (hydrogeology, petroleum geology, geophysics), material science, biology and biophysics. Research in porous media has substantially increased during recent times due to its various practical applications.

1.6 Research Objectives

The objectives of this study are shown as below:

(i) Develop a mathematical model for stagnation point flow.

(ii) Derive the equations for momentum, energy and concentration for stagnation point flow.

(iii) Derive the appropriate boundary conditions for the physical model.

(iv) Find the numerical algorithm to solve the governing equations.

(v) Analyze the solution of velocity, temperature and concentration profiles.

(vi) Calculate the skin friction, heat transfer rate and mass transfer rate.

1.7 Thesis Organization

This thesis consists of nine chapters dealing with MHD stagnation-point flow with heat and mass transfer.

In Chapter 1, a comprehensive introduction of the subject in hand is presented.

In Chapter 2, literature review on the two-dimensional stagnation-point flow and heat (and mass) transfer with various significant effects, such as, magnetic field, porous medium, radiation, chemical reaction, slip and convective boundary conditions, Soret and Dufour effects.

In Chapter 3, the mathematical model is presented and numerical method for analyzing the boundary layer mixed convection flow and heat transfer of an incompressible fluid over a vertical plate embedded in a porous medium near a stagnation-point with various effects is also explained.

Chapter 4 deals with the steady, two-dimensional, viscous incompressible MHD stagnation-point flow towards a vertical plate in a porous medium with chemical reaction.

Chapter 5 presents the study on effect of chemical reaction and radiation of MHD mixed convection stagnation-point flow with convective boundary condition towards a vertical plate in a porous medium.

In Chapter 6, we have investigated the effects of slip, chemical reaction, Soret and Dufour on magneto-convection stagnation-point flow of a viscous fluid over a vertical plate in a porous medium with radiation.

In Chapter 7, an analytical and numerical solution are presented to examine the slip and radiation effects on magneto convection stagnation-point flow of chemically reacting fluid towards a vertical plate in a porous medium.

Chapter 8 deals with analytical and numerical solutions of the effects of slip, chemical reaction and convective boundary condition on MHD mixed convection stagnation-point flow over a vertical plate in a porous medium with radiation.

Chapter 9 gives the conclusions arrived from the above five problems studied in chapters 4 to 8 under various conditions.

CHAPTER 2: LITERATURE SURVEY

The research has been carried out in the area of heat and mass transfer in the boundary layer flow. A detailed review of convective heat transfer in Darcian and non-Darcian porous media is explained here. The detailed reviews of the topic can be found in the books by Vafai (2005) and Nield & Bejan (2006). Many researchers focused on problem of boundary layer flow of an incompressible viscous fluid over a linearly stretching plate under several conditions, (Wang (1984), Surma Devi et al. (1986) and Lakshmisha et al. (1988)). Kafoussias et al. (1998) numerically investigated the local nonsimilarity boundary layer analysis with modified and improved numerical solutions. The forced convection flow of a viscous fluid in a porous medium was analytically investigated by Magyari and Aly (2006a). The mixed convection flow over a vertical surface in a porous medium was investigated by Magyari and Aly (2006b). Fang (2008) investigated an unsteady boundary layer flow over a flat plate. Salleh et al. (2010) numerically studied the steady boundary layer flow with Newtonian heating over a stretching sheet. Fang et al. (2010) and Ramesh (2012) analytically studied the laminar boundary layer flow of a viscous fluid over a plate. Singh and Sharma (2014) explored steady, laminar, heat and mass transfer stagnation point flow embedded in a porous medium over an isothermal vertical plate.

2.1 Boundary Layer Stagnation point Flow

Stagnation point flow is a topic of significance in fluid mechanics, because stagnation-point appears in virtually of all flow fields of science and engineering. Chiam (1994) studied the steady, laminar flow towards a surface that is stretched linearly near the stagnation point. Phillips and Kaye (1999) studied the Stokes number critical value for impaction particle in inviscid stagnation point flow under the influence of viscous boundary layer. Zhu (2000) numerically studied non-stationary flow of a fluid near a stagnation point by using finite difference method. Nazar et al. (2004a) and Cheng et al. (2005) developed an analytic solution for an unsteady mixed convection flow near the stagnation point on a vertical surface in a porous medium. Boutros et al. (2006) studied the steady flow of a viscous fluid on a stretching sheet near the stagnation point by using Lie group method. Santra et al. (2007) examined a steady axisymmetric flow of a Newtonian fluid over a flat disk near the stagnation point. The fluid flow normal to the stagnation point toward a flat plate with constant velocity was examined by Weidman and Sprague (2011). Mahapatra & Gupta (2002), Rosali et al. (2011), Bhattacharyya (2013) and Lok & Pop (2014) obtained the exact similarity solutions for Navier-Stokes equations for which 2-D stagnation point flow of a viscous fluid towards a stretching sheet. The many authors (Ishak et al. (2006), Saleh et al. (2014)) studied the steady mixed convection boundary layer flow of a viscous fluid over a vertical plate embedded in a porous medium near a stagnation point. Zhong and Fang (2011) studied the boundary layer flow of an incompressible fluid in the vicinity of the stagnation point on a body along the perpendicular direction to the wall. The researchers observed that the flow patterns strongly affected on boundary layer thickness generally decreases on decreasing the velocity parameter. Wang et al. (2013) experimentally studied the flow feature near a stagnation vortex pair's. Rohni et al. (2014) theoretically investigated mixed convection flow and heat transfer near a stagnation point over a shrinking vertical sheet in the presence of suction. They observed that the skin friction increases on increasing the buoyancy force. Nazar et al. (2004b) and Bachok et al. (2010) discussed the steady laminar two dimensional boundary layer stagnation point flow towards a horizontal stretching sheet. They observed that the surface heat transfer rate decreases on increasing the melting strength parameter. Fang et al. (2011) investigated the boundary layer of a stagnation point flow near the wall by comprising the mass transfer. They identified that the unsteadiness parameter solution occurs for all parameters of mass transfer. The

Newtonian heating on the surface of the stagnation point flow was discussed by Merkin et al. (2012). Merkin (2013) studied the convective flow near a stagnation point embedded in a porous medium with local heat-generating.

2.2 MHD Stagnation point Flow

In recent years MHD mixed convection flow problems together with heat and mass transfer have attracted a number of scholars because of their possible applications in many branches of science and technology. Engineers employed MHD principle in the design of heat exchangers pumps and flow meters, space vehicle propulsion and creating novel power generating systems. MHD convection flow problems are also very significant in the fields of stellar and planetary magnetospheres, aeronautics, chemical engineering and electronics. Examples include magnetic control of molten iron flow in the steel industry, liquid metal cooling in nuclear reactors and magnetic suppression of molten semi-conducting materials. The application of MHD principles in medicine and biology is of paramount interest owing to their significance in bio medical engineering in general and in the treatment of various pathological state in particular. Applications in biomedical engineering include cardiac MRI, ECG etc. Many authors have made model studies of the above phenomena of MHD convection. Bhutani et al. (1984), Ishak et al. (2009) and Van Gorder et al. (2012) numerically considered the boundary layer flow near a stagnation point in the presence of hydromagnetic field over a stretching/shrinking sheet. The effect of heat source/sink on MHD flow near a stagnation point over a vertical plate in a porous medium was studied by Yih (1998). He observed that the local skin friction and local Nusselt number increase on increasing the buoyancy parameter and permeability parameter in buoyancy assisting flow. Mahapatra & Gupta (2001) and Kumari & Nath (1999) analyzed the effect of magnetic field on the stagnation point flow and heat transfer of a viscous electrically conducting fluid over a stretching sheet.

Geindreau and Auriault (2002) discussed the effect of magnetic field on the explanation of the macroscopic outflow of conductive fluids embedded in a porous medium. Mixed convective boundary layer flow and heat transfer characteristics over a stretching sheet in the presence of a uniform magnetic field was studied by Takhar et al. (2005). Abdelkhalek (2006) numerically examined the heat and mass transfer of MHD mixed convection flow over a vertical semi-infinite heated surface near a stagnation point. Sharma & Singh (2009) analyzed the effects of heat sink/source and thermal conductivity on a convective flow of a viscous fluid over a linearly stretching sheet near a stagnation point, in the presence of magnetic field. As the thermal conductivity parameter increases, the temperature distribution also increases. The researchers concluded that due to the external magnetic field, the shrinking effect is reduced. The MHD flow at a stagnation point with variable surface temperature towards a stretching sheet was examined by Lok et al. (2011). Bhattacharyya et al. (2012) concerned about the distribution of chemically reactive solute in boundary layer stagnation point flow of a viscous fluid over a stretching sheet in the presence of magnetic field and suction or blowing. Mahapatra and Nandy (2013) examined the magneto-convection axi-symmetric steady flow over a shrinking sheet near a stagnation point. Sinha (2014) studied the effect of induced magnetic field of a stagnation-point flow over a shrinking sheet. He noticed that, the velocity of the fluid deceases in the presence of magnetic field.

2.3 Radiation Effect on Stagnation point Flow

The fluid is deliberated to be gray, absorbing releasing radiation but non-scattering medium and the Rosseland approximation is used in the energy equation, to describe the radiative heat flux (Sparrow and Cess (1978)). Pop et al. (2004), Jat and Chaudhary (2010) concerned the effect of radiation of a stagnation point flow over a stretching sheet. The outcomes showed that the boundary layer thickness increases on increasing the radiation parameter. The velocity and temperature profiles decrease on increasing the Prandtl number. Lee et al. (2008) studied free convection and heat transfer of an incompressible fluid over an inclined plate with radiation effect in a saturated porous medium using Lie group analysis. Pal (2009) analyzed the effects of buoyancy force and thermal radiation of mixed convection flow of a Newtonian fluid near a stagnation point over a stretching sheet. The skin friction coefficient, Nusselt number and Sherwood number increase on increasing the thermal radiation parameter in the case of assisting flow. Pop et al. (2011) analyzed the radiation effect on MHD stagnation point flow of electrically conducting fluid over an immersed stretching sheet. Hayat et al. (2010) considered the mixed convection stagnation point flow towards a sheet in a porous medium with magnetic field and radiation by homotopy analysis method. Hayat et al. (2011) considered the mixed convection stagnation point flow towards a sheet in a porous medium with magnetic field and radiation effects using homotopy analysis method. Nandeppanavar et al. (2011) explored the steady, 2-D MHD flow and heat transfer of a visco-elastic fluid over a stretching sheet in the presence of radiation and heat generation/absorption. The effect of radiation on MHD axisymmetric flow of an incompressible fluid near a stagnation point over a heated shrinking sheet was numerically studied by Ashraf and Ahmad (2012). They found that, the thermal boundary layer thickness decreases on increasing the radiation parameter.

2.4 Effect of Internal Heat Generation

Attia (2007) studied the effect of porosity on fluid flow near the stagnation-point over a permeable surface in a porous medium with heat generation. The momentum and thermal boundary layer thicknesses decrease on increasing the porosity parameter. Layek et al. (2007) studied the boundary layer stagnation point flow over a stretching sheet in a porous medium with heat generation and suction/blowing. Cortell (2008) numerically explored the effects of radiation and heat transfer in a viscous fluid flow over a flat sheet in the presence of thermal radiation. Singh et al. (2010) examined the mixed convection stagnation point flow through porous media in the presence of volumetric rate of heat generation/absorption. Chamkha & Ahmed (2011) explored the 3-D convection flows embedded in a porous medium with the combined effects of magnetic field, chemical reaction and heat absorption/generation. It is observed that the heat absorption/generation parameter tends to increase as the velocity distribution increases. Makinde (2012) studied the special effects of internal heat generation and radiation on MHD mixed convection flow immediate stagnation point in a perpendicular plate embedded in a porous medium. Bhuvaneswari et al. (2012) analyzed the effect of internal heat generation on natural convective flow over an inclined surface in a porous medium using the Lie group analysis. They observed that the velocity and temperature increase when the heat generation parameter increases. Mukhopadhyay (2013) investigated the boundary layer variable fluid flow near a stagnation point over a stretching surface with thermal radiation and suction.

2.5 Effect of Chemical Reaction

The study of heat and mass transfer with chemical reaction is of considerable importance in chemical and hydrometallurgical industries and glass fiber production. A chemical reaction is a process that leads to the transformation of one set of chemical substances to another. Chemical reactions can be either spontaneous, requiring no input of energy, or non-spontaneous, typically following the input of some type of energy. Classically, chemical reactions encompass changes that strictly involve the motion of electrons in the forming and breaking of chemical bonds, although the general concept of a chemical reaction, in particular the notion of a chemical equation, is applicable to transformations of elementary particles, as well as nuclear reactions. Chao et al. (1996) theoretically investigated the heat transfer characteristics of a chemically reactive flow near the stagnation point in a catalytic porous bed with finite thickness. Bhuvaneswari et al. (2009) studied the effect of chemical reaction on a semi-infinite inclined surface using the Lie group analysis. Chamkha et al. (2010) obtained the similarity solutions for boundary layer flow over a stretching surface embedded in a porous medium with suction/injection and chemical reaction. Afify and Elgazery (2012) investigated the effect of chemical reaction on MHD flow near a stagnation point embedded in a porous medium. They figured out that the local Nusselt number increases on increasing the Prandtl number. Makinde & Sibanda (2011) examined the effect of chemical reaction over a linearly stretched sheet based on the internal source of heat. Raju et al. (2014) investigated the MHD flow over a vertical surface embedded in porous medium with chemical reaction and thermal radiation. The velocity and concentration increase on increasing the chemical reaction parameter in the case of generative reaction and decrease for the case of destructive reaction. The viscous dissipation and chemical reaction effects on mixed convection MHD flow of a second-grade fluid over a stretching sheet with thermal radiation and thermal diffusion was examined by Das (2014). Shateyi and Marewo (2014) numerically investigated the unsteady laminar flow of a fluid at a stagnation point with combined effects of magnetic field, thermal radiation and heat generation/absorption. Shehzad et al. (2015) examined the boundary layer flow of thixotropic fluid near a stagnation point with chemical reaction and mass transfer.

2.6 Soret and Dufour Effect

In most of the studies related to heat and mass transfer process, Soret and Dufour effects are neglected on the basis that they are of a smaller order of magnitude than the effects described by Fourier's and Fick's laws. But these effects are considered as second order phenomena and may become significant in areas such as hydrology, petrology, geosciences, etc. The experimental investigation of the thermal diffusion effect on mass transfer related problems was first performed by Charles Soret in 1879. Thereafter this effect is termed as Soret effect in the honor of his name. Alam and Rahman (2006) numerically explained the effects of Dufour and Soret on boundary layer mixed convection flow over a vertical plate embedded in a porous medium with variable suction. Kandasamy et al. (2011) investigated the combined effects of thermal diffusion and diffusion thermo on convective laminar flow and heat and mass transfer of Newtonian fluid in the presence of thermophoresis particle deposition over a stretching sheet with variable stream conditions. Postelnicu (2007), Pal and Mondal (2011) and Al-Odat and Al-Ghamdi (2012) studied the effects of magnetic field and thermal diffusion on flow over a stretching surface in a porous medium in the presence of Dufour and Soret effects. Postelnicu (2010) examined the convective flow with heat and mass transfer of a fluid embedded in a porous medium near a stagnation point with Dufour and Soret effects using the Darcy-Boussinesq model. Bhattacharyya et al. (2014) studied the Soret and Dufour effects on convective stagnation point flow, heat and mass transfer towards a shrinking surface. Vedavathi et al. (2015) considered the effects of Soret & Dufour on unsteady 2D flow of MHD over a vertical porous plate with thermal radiation.

2.7 Convective Boundary Condition

Another aspect of the present study is the convective boundary condition on the surface/plate. Makinde and Aziz (2010) numerically studied the MHD mixed convection heat and mass transfer flow towards a vertical plate in a porous medium with convective boundary condition using constant surface temperature. They found that the velocity and temperature distributions increase on increasing the Biot number. Ishak et al. (2011) studied the effect of radiation on the laminar thermal boundary flow of a moving fluid over a moving flat plate with convective boundary condition. The heat transfer of a viscous flow in a quiescent fluid over a stretching sheet with convective boundary condition was investigated by Yao et al. (2011), Bachok et al. (2013) and Mohamed et al. (2013). Hamad et al. (2012) reported the steady laminar two-dimensional MHD viscous incompressible flow over a permeable flat plate with thermal convective boundary condition and radiation effects. Alsaedi et al. (2012) theoretically and numerically studied the effect of convective boundary condition of the boundary layer flow of nanofluid over a stretching sheet at a stagnation point with heat generation/absorption. They observed that the temperature increases on increasing the Biot number. Adeniyan and Adigun (2013) examined the effects of chemical reaction with convective boundary conditions of MHD flow near a stagnation point over a vertical plane. They observed that, the thickness of the thermal boundary layer increases on increasing the Biot number. Akeem et al. (2014) investigated the effects of convective surface boundary condition on boundary layer flow over a flat plate with variable viscosity. The heat transfer rate increases on increasing the Biot number. Baag et al. (2014) numerically explored the effects of chemical reaction and heat generation/absorption of a mixed convection MHD flow of a micro polar fluid over a vertical surface towards a stagnation point.

2.8 Effect of Slip Boundary Condition

The no-slip boundary condition (the assumption that a liquid adheres to a solid boundary) is one of the central tenets of the Navier–Stokes theory. However, there are situations wherein this condition does not hold. The non-adherence of the fluid to a solid boundary, known as velocity slip, is a phenomenon that has been observed under certain circumstances. For example, polymer melts often exhibit macroscopic wall slip and that in general is governed by a nonlinear and monotone relation between the slip velocity and the traction. The fluids that exhibit boundary slip have important technological applications such as in the polishing of artificial heart valves and internal cavities. Partial velocity slip may occur on the stretching boundary when the fluid is particulate such as emulsions, suspensions, foams and polymer solutions. The slip flow problem of laminar boundary layer is of considerable practical interest. Micro channels which are at the forefront of today's turbo machinery technologies, are widely being considered for cooling of electronic devices, micro heat exchanger systems, etc. If the characteristic size of the flow system is small or the flow pressure is very low, slip flow happens. If the characteristic size of the flow system tends to the molecular mean free path, continuum physics is no longer suitable. In no-slip flow, as a requirement of continuum physics, the flow velocity is zero at a solid fluid interface and the fluid temperature instantly closest to the solid walls is equal to that of the solid walls. For viscous fluid, the slip flow condition has been used in studies of fluid flow in rough and coated surfaces, and gas and liquid flow in micro devices. Unlike the no-slip case, the velocity does not vanish at stationary surfaces. The mathematical equation of this condition may be stated as: $u(x, y) = L\frac{\partial u}{\partial y}$ which relates the fluid velocity u to the shear rate u_y at the boundary. Here, L is the slip length and y denotes the coordinate perpendicular to the surface L. Seini & Makinde (2014) studied the effect of slip on MHD flow of an incompressible fluid over a linearly shrinking/stretching sheet. Harris et al. (2009) and Bhattacharyya et al. (2011) explored the steady mixed convection flow at a stagnation point in a porous medium over a perpendicular surface with velocity slip condition. Rohni et al. (2012) considered temperature slip effect on a boundary layer flow in a porous medium. Akbar et al. (2014) explored the effects of slip and convective boundary condition of a nanofluid flow towards a stretching sheet at a stagnation point with homogeneous model. Singh and Makinde (2015) examined the slip, convective heating and buoyancy force on the mixed convection flow along a moving plate. The laminar mixed convection flow towards a stretching sheet with the effect of partial slip and convective surface boundary condition was studied by Daba et al. (2015).

CHAPTER 3: MATHEMATICAL ANALYSIS

The basic equations used to interpret and analyze the incompressible viscous natural convection flow, heat and mass transfer, are the partial differential equations which are due to conservation of mass, momentum, energy and molecular species. To obtain these equations on the physical grounds, we assume the following:

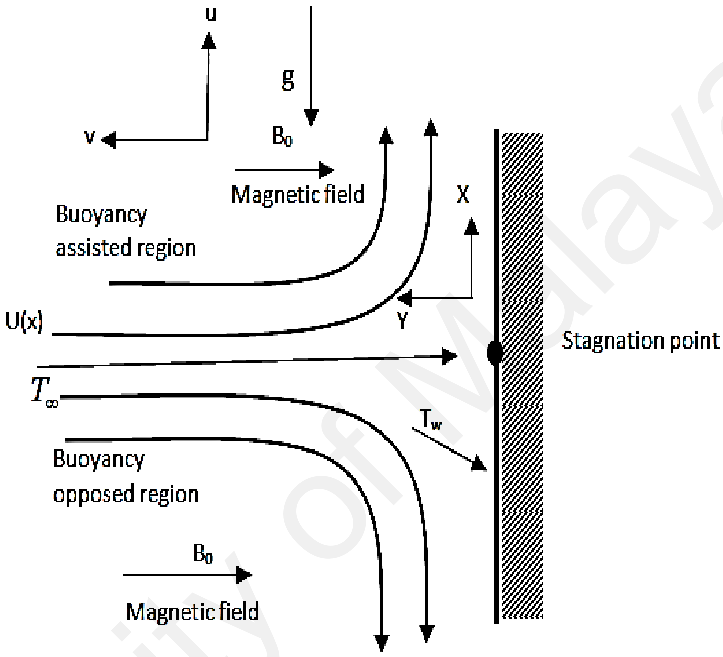

Figure 3.1. Schematic diagram

(i) For the coordinate system, *x*-axis is taken along the plate and *y*-axis is taken normal to the plate, see Fig. 3.1.

(ii) The flow is two-dimensional, steady, laminar and incompressible.

(iii) The potential flow arrives from the *y*-axis and impinges on vertical plate (at *y*=0), which divides at stagnation point into two streams and the viscous flow adheres to the plate. The velocity of the potential flow is given by $U_\infty = cx$, where *c* is a positive constant.

(iv) Fluid has constant properties except the density (ρ) in the body force.

(v) The influence of density variations with temperature and concentration are considered only in the body force in accordance with Boussinesq's approximation $[(\rho_\infty - \rho) \approx \rho\beta(T - T_\infty)]$.

(vi) The pressure gradient in the *x*-direction is negligible. The static pressure in the boundary layer varies only in the direction of *y*-direction.

(vii) Heat due to viscous dissipation in the energy equation is neglected, which is possible in the case of ordinary fluid flow like air or water under usual gravitational force.

(viii) A uniform strength of magnetic field (B_0) is applied transversely. Since the magnetic Reynolds number of the flow is taken to be very small enough, the induced magnetic field can be neglected in comparison with applied magnetic field.

(ix) Fluid considered here is gray, and emitting radiation and heat flux in the equation of energy due to thermal radiation is given by means of the Rosseland approximation.

(x) There is a first order homogeneous chemical reaction between the species and the fluid.

3.1 Continuity Equation

This is the principle of conservation of mass which states that fluid mass can neither create nor destroy. The mathematical form of this law is given by

$$\frac{D\rho}{Dt} + \rho\nabla.\vec{q} = 0, \tag{3.1}$$

where $\vec{q}$ is the velocity vector, the equation (3.1) is known as the equation of continuity. For an incompressible and homogeneous fluid, the density of the fluid is constant and equation of continuity reduces to $\nabla.\vec{q} = 0$. The equation of continuity in a two dimensional Cartesian coordinates is given by

$$\frac{\partial u}{\partial x} + \frac{\partial v}{\partial y} = 0. \tag{3.2}$$

3.2 Momentum Boundary Layer Equation

The flow behavior is governed by the equations of motion which are obtained from the Newton's second law of motion. This states that the time rate of change of the momentum of the fluid element is equal to the total external force exerted on the element and is in the direction of that force.

$$\rho\left[\frac{\partial \vec{q}}{\partial t} + \left(\vec{q}.\vec{\nabla}\right)\vec{q}\right] = -\vec{\nabla}p + \mu\nabla^2\vec{q} + \rho\vec{f}, \tag{3.3}$$

where $\vec{f}$ is the external body forces per unit volume, p is the pressure, ∇^2 is the Laplacian operator, μ is the coefficient of dynamic viscosity and t is the time. By using Newton's law of motion to a different control volume in the fluid by taking body and surface forces in Cartesian co-ordinate system as,

$$\rho\left[\frac{\partial u}{\partial t} + u\frac{\partial u}{\partial x} + v\frac{\partial u}{\partial y}\right] = -\frac{\partial p}{\partial x} + \mu\left(\frac{\partial^2 u}{\partial x^2} + \frac{\partial^2 u}{\partial y^2}\right) + f_x, \tag{3.4}$$

$$\rho\left[\frac{\partial v}{\partial t} + u\frac{\partial v}{\partial x} + v\frac{\partial v}{\partial y}\right] = -\frac{\partial p}{\partial y} + \mu\left(\frac{\partial^2 v}{\partial x^2} + \frac{\partial^2 v}{\partial y^2}\right) + f_y. \tag{3.5}$$

By applying the boundary layer assumptions due to Prandtl, the above x-momentum equation (3.4) is reduced to the boundary layer equation in the steady state condition as

$$\rho\left[u\frac{\partial u}{\partial x} + v\frac{\partial u}{\partial y}\right] = -\frac{\partial p}{\partial x} + \mu\left(\frac{\partial^2 u}{\partial y^2}\right) + f_x. \tag{3.6}$$

The left hand side represents the net rate at which x-momentum leaves the control volume due to fluid motion across its boundaries. The first term in the right hand side represents the net pressure force, and the second term represents the net force due to viscous shear stresses. The pressure does not vary vertically through the boundary layer, the equation (3.6) reduces to

$$u\frac{\partial u}{\partial x}+v\frac{\partial u}{\partial y}=\upsilon\frac{\partial^2 u}{\partial y^2}+f_x. \tag{3.7}$$

By adding the buoyancy force, the momentum equation (3.7) becomes

$$u\frac{\partial u}{\partial x}+v\frac{\partial u}{\partial y}=\upsilon\frac{\partial^2 u}{\partial y^2}+g\beta(T-T_\infty)+g\beta^*(C-C_\infty), \tag{3.8}$$

where β is the thermal expansion coefficient, β^* is the coefficient of expansion with concentration.

3.3 Energy Equation

The equation of energy may be derived by using the first law of thermodynamics. In the vector form, the equation of energy is written as

$$\rho C_p\frac{DT}{Dt}=\nabla.(k\nabla T)+\frac{Dp}{Dt}+\phi, \tag{3.9}$$

where C_p is specific heat at constant pressure, k is thermal conductivity, T is the local temperature and ϕ is the viscous dissipation function (heat generated due to frictional forces). The left hand side of the equation represents the convective terms, and on the right hand side are, respectively, the rate of heat diffusion, the rate of reversible work done on the fluid particles by compression, and the rate of viscous dissipation per unit volume. The work of compression Dp/Dt is usually negligible, except for fluid flows with velocities greater than sonic velocities. The equation of energy becomes

$$\frac{DT}{Dt}=\alpha\nabla^2 T,$$

where $\alpha=\left(\dfrac{k}{\rho c_p}\right)$ is the thermal diffusivity of the fluid. By the boundary layer assumptions, the above equation is reduced as follows:

$$u\frac{\partial T}{\partial x}+v\frac{\partial T}{\partial y}=\alpha\frac{\partial^2 T}{\partial y^2}. \tag{3.10}$$

This is the thermal energy equation for flow in a boundary layer.

3.4 Concentration Equation

The diffusion is the phenomenon of random motion causing a system to decay towards uniform conditions. This equation is derived from Fick's law, which states that the net movement of diffusing substance per unit area of section (the flux) is proportional to the concentration gradient and is toward lower concentration.

$$\frac{\partial C}{\partial t}+\left(\bar{q}.\nabla C\right)=D\nabla^2 C, \tag{3.11}$$

where C is the concentration of the species, D is the mass diffusivity. By the boundary layer assumptions, we get the concentration equation as follows.

$$u\frac{\partial C}{\partial x}+v\frac{\partial C}{\partial y}=D\frac{\partial^2 C}{\partial y^2}. \tag{3.12}$$

3.5 Boundary Conditions

The boundary conditions dictate the particular solutions to be obtained from the governing equations.

1. Velocity Boundary Conditions:

(i) u=0, v=0 (no slip condition) as y=0

(ii) $u=N_1 u_y$ (velocity slip), v=0 as y=0

(iii) $u \to U_\infty = cx$ as $y \to \infty$

2. Temperature Boundary Conditions:

(i) $T=T_w$ as y=0

(ii) $-k\frac{\partial T}{\partial y}=h_f(T_f - T)$ (Convective boundary) as y=0

(iii) $T \to T_\infty$ as $y \to \infty$

3. Concentration Boundary Conditions:

(i) $C = C_w$ as $y=0$

(ii) $C \to C_\infty$ as $y \to \infty$.

3.6 Dimensional Analysis

The mechanical and physical quantities are divided into two classes, depending on the form of measurement. Quantities independent of the scale are called dimensionless or non-dimensional and those depending on some scale are said to be dimensional. Dimensionless parameters give an idea as to which terms are dominant in the governing equations, so that only those terms are retained to find an approximate solution to the governing equations.

Dimensional analysis of any problem enables to know the qualitative behavior of the physical problem. The dimensionless parameters enable to understand the physical significance of a particular phenomenon associated with the problem. There are usually two general methods for obtaining the dimensionless parameters:

(i) The inspection analysis, (ii) The dimensionless analysis

In this thesis, we adopt the dimensional analysis to obtain certain characteristic values in the problem. Consequently, certain non-dimensional numbers appear as the coefficient of various terms in the equations.

3.6.1 Non-dimensional variables

The dimensionless quantity many have dimensionless units, even though it has no physical dimension associated with it. Some of the non-dimensional variables defined below in detail.

$\eta = y\sqrt{\frac{c}{\upsilon}}$, where η is the similarity variable, the stream function $\psi(x,y) = \sqrt{\upsilon c}\, xf(\eta)$, which satisfies $u = -\frac{\partial \psi}{\partial y}$ and $v = \frac{\partial \psi}{\partial x}$, the dimensionless temperature $\theta(\eta) = \frac{T - T_\infty}{T_\omega - T_\infty}$, and the dimensionless concentration is $\phi(\eta) = \frac{C - C_\infty}{C_\omega - C_\infty}$.

3.6.2 Non-dimensional Parameters

Some of the non-dimensional numbers used in this thesis are defined below in detail.

Grashof Number (*Gr*)

It plays a significant role in free convection heat transfer. The Grashof number is the ratio of the buoyancy force to the viscous force in the fluid. The definition of thermal Grashof number (Gr_T) is

$$Gr_T = \frac{g\beta(T_w - T_\infty)x^3}{\upsilon^2},$$

where g is acceleration due to gravity, υ is the kinematic viscosity, $(T_w - T_\infty)$ is the temperature difference and x is the characteristic length. Similarly, we can define the solutal Grashof number (Gr_C) using the concentration difference $(C_w - C_\infty)$. The solutal Grashof number is significant in free convection flows involving with mass transfer. It is defined as

$$Gr_c = \frac{g\beta^*(C_w - C_\infty)x^3}{\upsilon^2}.$$

Internal heat generation (*S*)

Internal heat generation is applied to a part that will either act as a heat source or heat sink throughout the analysis. The internal heat generation is specified on a per volume basis. It is given by

$$S = \frac{Q\upsilon}{\rho C_p c},$$

where Q heat generation/absorption.

Nusselt Number (*Nu*)

The Nusselt number (*Nu*) at the surface defines the rate of heat transfer. It is given by

$$Nu = \frac{-x}{(T_w - T_\infty)}\left(\frac{\partial T}{\partial y}\right)_{y=0},$$

where *y* is the direction of the normal to the surface of the body.

Prandtl Number (*Pr*)

It is an important dimensional parameter dealing with the properties of a fluid. The Prandtl number (*Pr*) is defined as

$$\mathrm{Pr} = \frac{\mu C_p}{k} = \frac{\upsilon}{\alpha}.$$

Reynolds Number (*Re*)

It is defined as the ratio of inertial forces to viscous forces. It is used to help predict similar flow patterns in different fluid flow situations. It is defined as

$$\mathrm{Re}_x = \frac{\rho U_\infty x}{\mu} = \frac{U_\infty x}{\upsilon}.$$

Richardson Number (*Ri*)

It expresses the ratio of the buoyancy term to the flow gradient term. Richardson number represents the importance of natural convection relative to the forced convection. Richardson number can also be expressed by using a combination of the Grashof number and Reynolds number. Thermal Richardson number (Ri_T) can be defined as

$$Ri_T = \frac{Gr_T}{\mathrm{Re}_x^2}.$$

Similarly, the Solutal Richardson number (Ri_c) can be defined as

$$Ri_C = \frac{Gr_c}{\mathrm{Re}_x^2}.$$

Schmidt number (*Sc*)

The ratio of molecular diffusivity of momentum to the mass molecular diffusivity is given by Schmidt number. It plays a major role in convective mass transfer. The definition of Schmidt number is given by

$$Sc = \frac{\upsilon}{D}.$$

Sherwood Number (*Sh*)

The Sherwood number (*Sh*) is a dimensionless number used in mass-transfer operation,

$$Sh = \frac{-x}{(C_w - C_\infty)}\left(\frac{\partial \phi}{\partial y}\right)_{y=0},$$

where $\dfrac{\partial \phi}{\partial y}$ is a mass concentration gradient.

3.7 Skin-friction, Heat and Mass Transfer rates

Skin-friction coefficient

Skin friction arises when a fluid flows over a solid surface. The fluid is in contact with the surface of the body, resulting in a friction force exerted on the surface. The friction force per unit area is called the wall shear stress. The shearing stress for most common fluids, i.e. so-called Newtonian fluids, depends on the dynamic viscosity and the gradient of the velocity:

$$C_f = \frac{\tau_w}{\left(\rho U_\infty{}^2/2\right)},$$ where, $\tau_w = \mu \left.\dfrac{\partial u}{\partial y}\right|_{y=0}$ = local shearing stress on the surface.

$$C_f = \frac{2}{\left(\rho c x^2\right)}\left(\mu \frac{\partial u}{\partial y}\right)_{y=0}, \qquad \because U_\infty = cx.$$

The skin friction coefficient in the non-dimensional form is given below

$$C_f = 2\frac{f''(0)}{\mathrm{Re}_x^{1/2}}, \qquad \text{where} \qquad \mathrm{Re}_x = \frac{U_\infty x}{\upsilon}. \tag{3.13}$$

Heat transfer rate

It is the ratio of heat flow rate by convection to the heat flow rate by conduction processes under unit temperature gradient. The rate of heat transfer in terms of local Nusselt number from the plate to the fluid is given by

$$-k\left.\frac{\partial T}{\partial y}\right|_{y=0} = h(T_w - T_\infty),$$

$$Nu = \frac{h_x x}{k}, \text{ where } h_x = \frac{q_w}{T_w - T_\infty} \text{ (heat transfer rate).}$$

The Nusselt number in the non-dimensional form is given below:

$$Nu = -\theta'(0)\,\mathrm{Re}_x^{1/2}. \tag{3.14}$$

Mass transfer rate

The thermal diffusion effect causes the rate of mass transfer. The local Sherwood number is defined as follows

$$Sh = \frac{x q_m}{D(C_w - C_\infty)},$$

where $$q_m = -D\left.\frac{\partial C}{\partial y}\right|_{y=0} = -D(C_w - C_\infty)\phi'\left.\sqrt{\frac{c}{\upsilon}}\right|_{\eta=0}.$$

The non-dimensional form of Sherwood number is given below

$$Sh = -\phi'(0)\mathrm{Re}_x^{1/2}. \tag{3.15}$$

3.8 Similarity transformation

A similarity solution is one in which the number of independent variables is reduced by at least one, usually by a coordinate transformation. The idea is analogous to dimensional analysis. There are many problems of fluid mechanics in which it plays to recognize on dimensional grounds that the various space and time variables will appear in the solution in certain combinations only and that the governing differential equation may be reduced from one of partial type to one of ordinary type. Such a solution, involving the time only in combination with the space variable is often termed a similarity solution. Since the shape of the velocity distribution with respect to the space variable is similar at all times.

Boundary layer equations are non-linear partial differential equations. We simplify them further by reducing them into ordinary differential equations. To this end, we propose to change, if possible, the independent and dependent variables in such way so as to transform the partial differential equations of the boundary layer equations into an ordinary differential equation. Whenever such a transformation exists, we say that similarity solution exists.

The continuity equation (3.2) is satisfied by using the stream function (ψ) and remaining equations are converted into nonlinear ordinary differential equations using non-dimensional variables and non-dimensional parameters. We get the following ordinary differential equations:

$$f''' + ff'' - f'^2 + Ri_T\theta + Ri_c\phi = 0, \tag{3.16}$$

$$\theta'' + \Pr f\theta' = 0, \tag{3.17}$$

$$\phi'' + Scf\phi' = 0, \tag{3.18}$$

with corresponding boundary conditions are

$$f = 0,\ f' = 0,\ \theta = 1,\ \phi = 1 \text{ as } \eta = 0,$$

$$f' = 1, \theta = 0,\ \phi = 0 \text{ as } \eta \to \infty. \tag{3.19}$$

3.9 Numerical method

Numerical methods are useful to give approximate solutions for the most difficult problems arise in the real life. From the numerical methods available for solving the boundary layer equations, the shooting method and Runge-Kutta fourth-order method are most frequently used and more universally applicable than any other method. Moreover, shooting technique provide numerical solutions in a simple and efficient manner.

The governing equations of fluid flow problems are generally non-linear and boundary value problems type. The set of partial differential equations may be transformed into a set of ordinary differential equations using similarity variables for some special class of flow problem. The final equations can be solved numerically.

Let us consider a nonlinear second-order differential equation $y'' = f(x, y, y')$ with the boundary conditions $y(a)=y_0$ and $y(b)=y_1$. In shooting method the following steps are taken:

i) Transform the given boundary value problem (B.V.P.) into an initial value problem (I.V.P);

ii) Solution of the I.V.P.;

iii) Solution of the given B.V.P.

We write first the second-order differential equation in terms of a system of first-order equation as $y' = z$ and $z' = f(x, y, z)$ with $y(a)=y_0$. Since these equations are non-linear, we cannot get the solution as super position principle. In order to integrate the above system as an initial value problem, we require a value for $z(a)$ that is $y'(a)$. However, if we take a guess for $z(a)$ and use it to compute a numerical solution, we can then compare the calculated value for y at $x = b$ with the given boundary condition $y(b) = y_1$ and adjust the guess value, $z(a)$, to give a better approximation for the solution. This technique is called a shooting method. Basically, we seek a solution which satisfies $y(b) = y_1$. By successively refining the interval, a suitable solution can be found. It is also possible to improve the solution by linear interpolation or other root finding methods. The shooting method depends on the choice of the initial slope, that is, $y'(a)$ which is required to start the integration.

The flow equation (3.16) coupled with the energy and concentration equations. (3.17) and (3.18) constitute a set of nonlinear non-homogeneous differential equation for which closed-form solution cannot be obtained. Hence the problem has been solved numerically using shooting technique along with fourth-order Runge-Kutta integration. The basic idea of shooting method for solving boundary value problem is to try to find appropriate initial condition, so that the boundary conditions at other points are satisfied.

To explain the method, we consider the equation:

$$f''' + ff'' - (f')^2 + Ri_T\theta + Ri_c\phi = 0, \tag{3.20}$$

$$\theta'' + \Pr f\theta' = 0, \tag{3.21}$$

$$\phi'' + Scf\phi' = 0. \tag{3.22}$$

Equations (3.20) to (3.22) must be solved subject to seven boundary conditions:

$$\begin{aligned} &f(\eta=0) = f'\big|_{\eta=0} = 0,\ f'\big|_{\eta\to\infty} = 1, \\ &\theta(\eta=0) = 1 \text{ and } \theta(\eta\to\infty) = 0\ , \\ &\phi(\eta=0) = 1 \text{ and } \phi(\eta\to\infty) = 0. \end{aligned} \tag{3.23}$$

Note that because θ ,ϕ and f' must asymptotically approach zero as η goes to infinity, their derivatives, f'' , θ' and ϕ' also must go to zero. To solve (3.20) to (3.22) numerically, they are first reduced to sets of first-order equations by defining new dependent variables $f^0, f^1, f^2, \theta^0, \theta^1, \phi^0$ and ϕ^1:

$$\begin{aligned} &\frac{df^0}{d\eta} = f^1\ , \\ &\frac{df^1}{d\eta} = f^2\ , \\ &\frac{df^2}{d\eta} = -f^0f^2 + (f^1)^2 - Ri_T\theta^0 - Ri_c\phi^0\ , \\ &\frac{d\theta^0}{d\eta} = \theta^1\ , \\ &\frac{d\theta^1}{d\eta} = -\Pr f^0\theta^1\ , \\ &\frac{d\phi^0}{d\eta} = \phi^1\ , \\ &\frac{d\phi^1}{d\eta} = -Scf^0\phi^1\ . \end{aligned} \tag{3.24}$$

Here f^0 , θ^0 and ϕ^0 are equivalent to f , θ and ϕ in (3.20), and f^1, f^2, θ^1 and ϕ^1 are first and second derivatives of f ,θ and ϕ with respect to η. Note that equation (3.20) is third order and is replaced with three first-order equations, whereas equations (3.21 and 3.22) is second-order and is replaced with two equations. The seven coupled first-order ODEs can be readily solved in Matlab using the built-in ODE45 solver. To solve these coupled ODEs subject to a set of seven initial conditions, over a finite range of η. In this case, the finite range chosen is $0 \le \eta \le 10$. From equation (3.23), only four initial conditions (η=0) are known: $f^0 = 0$, $f^1 = 0$, $\theta^0 = 1$ and $\phi^0 = 1$. The remaining initial conditions must be guessed because f^2, θ^1 and ϕ^1 are proportional to the velocity gradient. In principle, a trial-and-error method can be employed to determine these initial values, but it is tedious. Alternatively, an algorithm to solve two coupled nonlinear equations, such as Newton's method, can be devised to iteratively solve the boundary value problem. Then equations (3.24) are integrated using the 4th order Runge-Kutta method from $\eta = 0$ to $\eta = \eta_{\max}$ over successive steps $\Delta\eta$. The accuracy of the assumed initial values f^2 and θ^1 is then checked by comparing the calculated values of f^2, θ^1 and ϕ^1 at $\eta = \eta_{\max}$ with their given value at $\eta = \eta_{\max}$ in (3.23). If a difference exists, another set of initial values f^2, θ^1 and ϕ^1 must be assumed and the process is repeated. This process is continued until the agreement between the calculated and the given condition at $\eta = \eta_{\max}$ is within the specified degree of accuracy. In the present study, $\eta_{\max}$ has been suitably chosen at each time such that the velocity, temperature and concentration profiles approach zero at the outer edge of the boundary layer.

The accuracy of our numerical procedure is tested by comparing with the previously published work of Singh et al. (2010) and Makinde (2012) for special cases of the problem under consideration. Table 3.1 shows that the good agreement between the comparison results exists. This gives confidence in the numerical results to be reported subsequently.

Table 3.1. Computations showing the comparison with Singh *et al.* (2010) and Makinde (2012) for different values of S when $Ri_T=1$, $Ri_c=0.5$, $Pr=1$, $Sc=0.5$, $M=0$, $K=0$, $Cr=0$, $Rd=0$.

S	$f''(0)$			$-\theta'(0)$			$-\phi'(0)$		
	Singh (2010)	Makinde (2012)	Present	Singh (2010)	Makinde (2012)	Present	Singh (2010)	Makinde (2012)	Present
-1	1.8444	1.8444	1.8501	1.3908	1.3908	1.3897	0.4631	0.4631	0.4618
0	1.9995	1.9995	1.9989	0.6392	0.6932	0.6401	0.4789	0.4789	0.4761
1	2.1342	2.1342	2.1299	-0.0730	-0.0730	-0.0727	0.4917	0.4917	0.4902

CHAPTER 4: EFFECTS OF CHEMICAL REACTION AND RADIATION ON MHD MIXED CONVECTION STAGNATION-POINT FLOW IN A POROUS MEDIUM

4.1 Introduction

The study of combined free and forced convection flow of an incompressible viscous fluid with simultaneous heat and mass transfer past a vertical plate under the influence of a magnetic field and chemical reaction has huge applications in water and air pollutions, several manufacturing processes of industry such as polymers, aerodynamic extrusion of plastic sheets, etc. The research on MHD incompressible viscous flow has many engineering applications such as a power generator, cooling of reactors, design of heat exchangers and MHD accelerators. Makinde (2012) studied the MHD mixed convection stagnation point flow with thermal radiation over a vertical plate in a porous medium with heat generation. The present study extends the work of Makinde (2012) to include chemical reaction effect.

4.2 Mathematical Modeling

Consider the two-dimensional steady stagnation-point flow, heat and mass transfer of an incompressible, electrically conducting fluid through a porous medium along a vertical isothermal plate in the presence magnetic field, volumetric heat generation/absorption and first order homogeneous chemical reaction as shown in Figure 3.1. The magnetic field of constant strength is imposed along the *y*-axis. Since the magnetic Reynolds number of the flow taken to be very small, the induced magnetic field is neglected in comparison with applied magnetic field. As the fluid hits the wall at the stagnation point, the flow divided into two streams and the viscous flow adheres to the plate within the boundary layer. The velocity distribution in the potential flow region is assumed as $U_\infty = cx$, where c is a positive constant. The following equations represent the flow in a porous medium obeying the Darcy law. The substance generated due to chemical reaction is represented as concentration. Thus, the governing equations of continuity of mass, momentum transfer, energy transfer and species concentration are given by

$$\frac{\partial u}{\partial x}+\frac{\partial v}{\partial y}=0, \tag{4.1}$$

$$u\frac{\partial u}{\partial x}+v\frac{\partial u}{\partial y}=\upsilon\frac{\partial^2 u}{\partial y^2}+g\beta(T-T_\infty)+g\beta^*(C-C_\infty)-\left(\frac{\sigma_e B_0{}^2}{\rho}+\frac{\upsilon}{\tilde{K}}\right)(u-U_\infty)+U_\infty\frac{dU_\infty}{dx}, \tag{4.2}$$

$$u\frac{\partial T}{\partial x}+v\frac{\partial T}{\partial y}=\alpha\frac{\partial^2 T}{\partial y^2}-\frac{1}{\rho C_p}\frac{\partial q_r}{\partial y}+\frac{Q(T-T_\infty)}{\rho C_p}, \tag{4.3}$$

$$u\frac{\partial C}{\partial x}+v\frac{\partial C}{\partial y}=D\frac{\partial^2 C}{\partial y^2}-\Gamma_0(C-C_\infty). \tag{4.4}$$

The boundary conditions are

$$u=0, \quad \upsilon=0, \quad T=T_w, \quad C=C_w \quad \text{at} \quad y=0, \tag{4.5a}$$

$$u\to U_\infty=cx, \quad T\to T_\infty, \quad C\to C_\infty \quad \text{as} \quad y\to\infty. \tag{4.5b}$$

The medium is assumed as grey and transparent. It absorbs heat and emits and dispersion of heat are very small. Hence the thermal radiation effect is taken in the medium due to Stefan-Boltzmann's law which states that the radiation is proportional to the 4th power of temperature. The heat flux due to radiation is given by

$$q_r=-\frac{4\sigma^*}{3K'}\frac{\partial T^4}{\partial y}. \tag{4.6}$$

Using the Rosseland approximation, it is assumed that the differences in temperature within the flow are too small, so that, T^4 may be shown as a linear function of temperature T about the free stream temperature T_∞ using Taylor series i.e., $T^4\approx 4T_\infty^3T-3T_\infty^4$. Then we get

$$q_r=-\frac{16\sigma^*T_\infty^3}{3K'}\frac{\partial T}{\partial y}. \tag{4.7}$$

We introduce the following non-dimensional variables:

$$\eta = y\sqrt{\frac{c}{\upsilon}}, \qquad \psi(x,y) = \sqrt{\upsilon c}\, xf(\eta), \qquad Cr = \frac{\Gamma_0}{c}, \qquad \theta(\eta) = \frac{T - T_\infty}{T_\omega - T_\infty}, \qquad \phi(\eta) = \frac{C - C_\infty}{C_\omega - C_\infty},$$

$$Gr_T = \frac{g\beta(T_\omega - T_\infty)x^3}{\upsilon^2}, \qquad Gr_c = \frac{g\beta^*(C_\omega - C_\infty)x^3}{\upsilon^2}, \qquad Ri_T = \frac{Gr_T}{\mathrm{Re}_x^2}, \qquad Ri_C = \frac{Gr_c}{\mathrm{Re}_x^2}, \qquad \mathrm{Re}_x = \frac{U_\infty x}{\upsilon},$$

$$Rd = \frac{4\sigma^* T_\infty^3}{kK'},\ K = \frac{\upsilon}{c\tilde{K}},\ \Pr = \frac{\upsilon}{\alpha},\ Sc = \frac{\upsilon}{D},\ M = \frac{\sigma_e B_0^2}{c\rho},\ S = \frac{Q\upsilon}{\alpha c}. \tag{4.8}$$

where ψ is the stream function which is defined in the usual form as $u = \partial\psi/\partial y$ and $\upsilon = -\partial\psi/\partial x$ so that the continuity equation (4.1) is automatically satisfied. Substituting the expression in (4.7) together with the variables in (4.8) into (4.1)-(4.4), we obtain the following nonlinear ordinary differential equations:

$$f''' + ff'' - f'^2 + Ri_T\theta + Ri_c\phi - (K + M)(f' - 1) + 1 = 0, \tag{4.9}$$

$$\left(1 + \frac{4}{3}Rd\right)\theta'' + \Pr f\theta' + S\theta = 0, \tag{4.10}$$

$$\phi'' + Scf\phi' - ScCr\phi = 0. \tag{4.11}$$

where *Cr* is a chemical reaction parameter, Gr_c is a solutal Grashof number, Gr_T is a thermal Grashof number, *K* is a porous medium permeability parameter, *M* is a magnetic field parameter, *Pr* is a Prandtl number, *Rd* is a thermal radiation parameter, Ri_c is a solutal Richardson number, Ri_T is the thermal Richardson number, *S* is an internal heat generation/absorption parameter, *Sc* is a Schmidt number. The corresponding boundary conditions (4.5 a & b) are

$$f = 0, \quad f' = 0, \quad \theta = 1, \quad \phi = 1, \quad \text{as} \quad \eta = 0$$
$$f' = 1, \quad \theta = 0, \quad \phi = 0, \quad \text{as} \quad \eta \to \infty \tag{4.12}$$

The set of equations (4.9)-(4.11) with boundary conditions (4.12) has been solved numerically by applying the shooting technique along with fourth-order Runge-Kutta integration scheme.

The skin friction (C_f) is the force along the surface, the Nusselt number (Nu) represents heat transfer through a fluid as a result of convection relative to conduction across the fluid layer. The Sherwood number (Sh) is the ratio between the convective to diffusive mass transfer. These non-dimensional numbers Cf, Nu, Sh are defined as follows,

$$\tau_\omega = \mu \left.\frac{\partial u}{\partial y}\right|_{y=0}, \qquad q_\omega = -k\left.\frac{\partial T}{\partial y}\right|_{y=0} - \frac{4\sigma^*}{3K'}\left.\frac{\partial T^4}{\partial y}\right|_{y=0}, \qquad q_m = -D\left.\frac{\partial C}{\partial y}\right|_{y=0}, \tag{4.13}$$

$$C_f = \frac{2\tau_\omega}{\rho U_\infty^2}, \qquad Nu = \frac{xq_\omega}{k(T_\omega - T_\infty)}, \qquad Sh = \frac{xq_m}{D(C_\omega - C_\infty)}. \tag{4.14}$$

Substituting (4.7), (4.8) and (4.13) into (4.14), we obtain the expressions for the skin-friction coefficient, the local Nusselt number and the local Sherwood number as follows.

$$\mathrm{Re}_x^{1/2}\, C_f = f''(0),$$

$$\mathrm{Re}_x^{-1/2}\, Nu = -(1+4Rd/3)\theta'(0), \tag{4.15}$$

$$\mathrm{Re}_x^{-1/2}\, Sh = -\phi'(0).$$

4.3. Results and Discussion

The results are displayed graphically for different values of the parameters (K, M, Ri_T, Ri_C, S, Rd, Cr) with Pr = 0.7 (air) and Sc = 0.5. Table 4.1 illustrates the effect of skin friction, Nusselt number and Sherwood number of different parameters. The skin friction increases on increasing the porous medium permeability parameter, magnetic field parameter and it decreases on increasing the chemical reaction parameter. The local Nusselt number increases with an increasing the value of the permeability parameter, magnetic field parameter and thermal radiation parameter and it decreases on increasing the Richardson number and heat generation parameter. The local Sherwood number increases with an increasing value of the permeability parameter, magnetic field parameter, Richardson number, internal heat generation and chemical reaction parameter.

Table 4.1. Different values of f'', $-\theta'$, $-\phi'$ for Pr=0.7 and Sc=0.5

K	M	Ri_T	Ri_c	S	Rd	Cr	$f''(0)$	$-\theta'(0)$	$-\phi'(0)$
0.5							2.381054	0.131488	0.566446
1.0							2.480144	0.132527	0.567637
2.0							2.658150	0.133415	0.570214
3.0							2.818487	0.134906	0.572237
0.5	0	1	0.5	0.2	0.2	0.2	2.282218	0.129818	0.565269
	2						2.658150	0.133415	0.570214
	4						3.050930	0.139619	0.572251
	6						4.249084	0.157870	0.565790
	8						5.507522	0.135105	0.581117
0.5	0.5	0.1	0.5	0.2	0.2	0.2	1.875287	0.138825	0.546017
		0.5					2.101744	0.135415	0.555178
		1.0					2.381054	0.131488	0.566446
		1.5					2.656359	0.127927	0.577511
		2.0					2.927848	0.124727	0.588375
0.5	0.5	1	0.1	0.2	0.2	0.2	2.203743	0.132965	0.559868
			0.5				2.381054	0.131488	0.566446
			1.0				2.598403	0.129982	0.574389
			1.5				2.811546	0.128839	0.582031
			2.0				3.021085	0.128045	0.589378
0.5	0.5	1	0.5	-1.0	0.2	0.2	2.277775	0.675466	0.561458
				-0.5			2.313538	0.479968	0.563299
				0.0			2.359292	0.242043	0.565472
				0.5			2.418090	-0.054742	0.568029
				1.0			2.493639	-0.432447	0.571028
0.5	0.5	1	0.5	0.2	0	0.2	2.380285	0.11306	0.565899
					0.4		2.380925	0.143412	0.566865
					0.8		2.380485	0.177186	0.567461
					1.0		2.381412	0.27606	0.567670
0.5	0.5	1	0.5	0.2	0.2	-1.0	2.425714	0.130183	0.036520
						-0.5	2.404500	0.130797	0.284168
						0	2.387099	0.131309	0.492312
						0.5	2.372845	0.131731	0.669348
						1.0	2.361162	0.132074	0.822065

Figure 4.1 shows the velocity profiles for different values of K with constant values of Ri_T=1, Ri_c=0.5, M=0.5, Rd=0.2, S=0.2, Cr=0.2. Figure 4.1 shows that the fluid velocity increases gradually from the stationary plate surface to its peak value. It is clear that an overshoot in the fluid velocity near the plate surface is observed. The velocity of the fluid decreases with an increase in the porous medium permeability parameter (K).

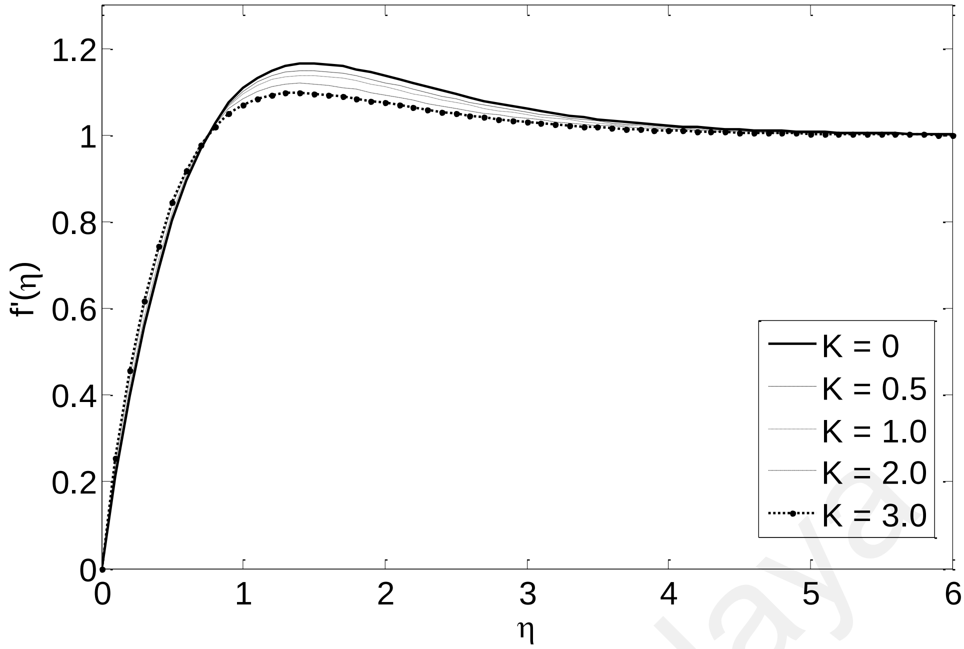

Figure 4.1. Velocity profiles for different K values with Ri_T=1, Ri_C=0.5, M=0.5, Rd=0.2, S=0.2, Cr=0.2.

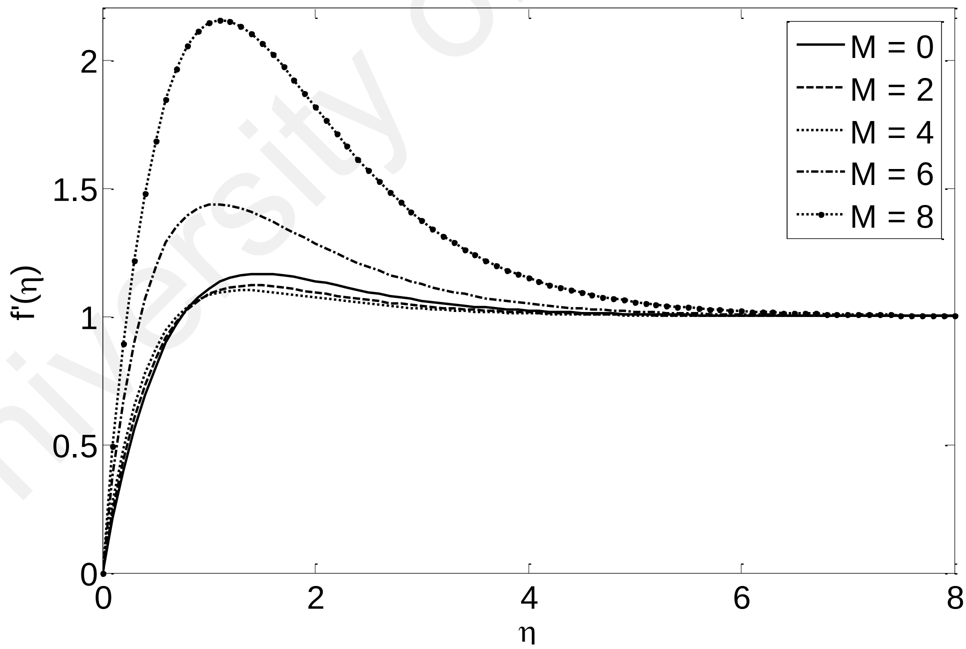

Figure 4.2. Velocity profiles for different M values with Ri_T=1, Ri_C=0.5, K=0.5, Rd=0.2, S=0.2, Cr=0.2.

Figure 4.2 depicts the velocity field against the influence of different magnetic field parameter with constant values of Ri_T=1, Ri_c=0.5, K=0.5, Rd=0.2, S=2, Cr=0.2. It is seen from this figure that the velocity decreases initially and then increases on increasing the magnetic field intensity. It is observed from the Figures 4.3 & 4.4 that velocity increases as the Richardson number increases. The fluid motion is enhanced by buoyancy forces on increasing values of solutal and thermal (Ri_c and Ri_T) Richardson numbers.

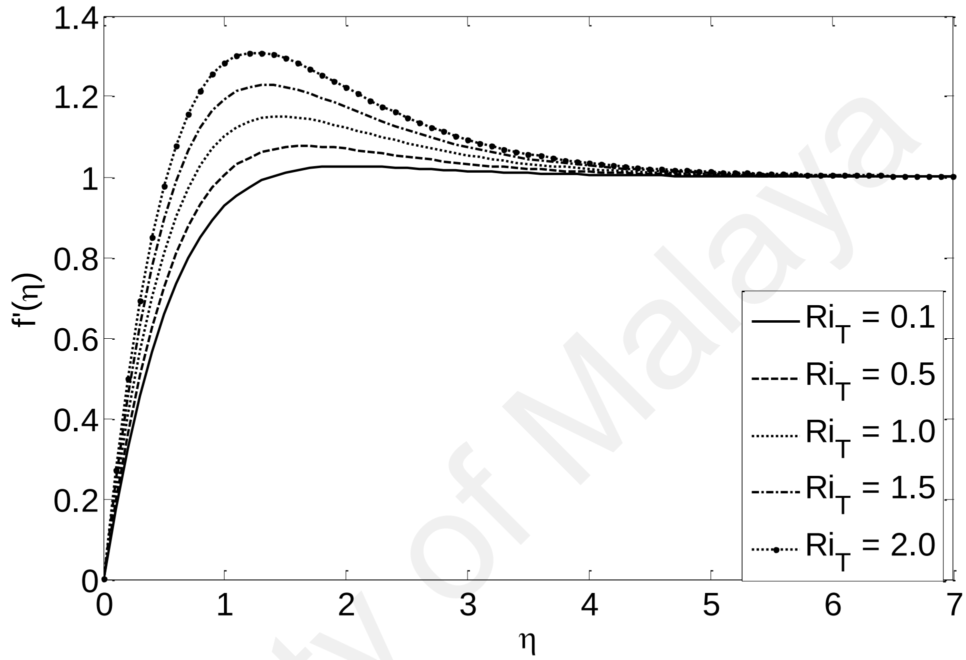

Figure 4.3. Velocity profiles for different Ri_T values with Ri_C=0.5, K=0.5, M=0.5, Rd=0.2, S=0.2, Cr=0.2.

The velocity overshoots near the plate. The fluid velocity increases gradually when increasing the values of heat generation parameter (S) for constant values of Ri_T, Ri_c, K, M, Rd, Cr, see Figure 4.5. Figures 4.6 illustrate the temperature profiles for different values of S. We can observe that thermal boundary layer thickness is more than the momentum boundary layer thickness. The temperature profile overshoot when $S \geq 1$, due to internal heat generation. It is observed from Figure 4.7 that the temperature increases on increasing the thermal radiation parameter. Figure 4.8 illustrates the concentration profiles for different values of chemical reaction parameter with constant values of Ri_T, Ri_c, K, M, S, Rd. We observe that the concentration gradually decreases in the boundary layer on increasing *Cr* values. The plate surface contains high chemical species concentration.

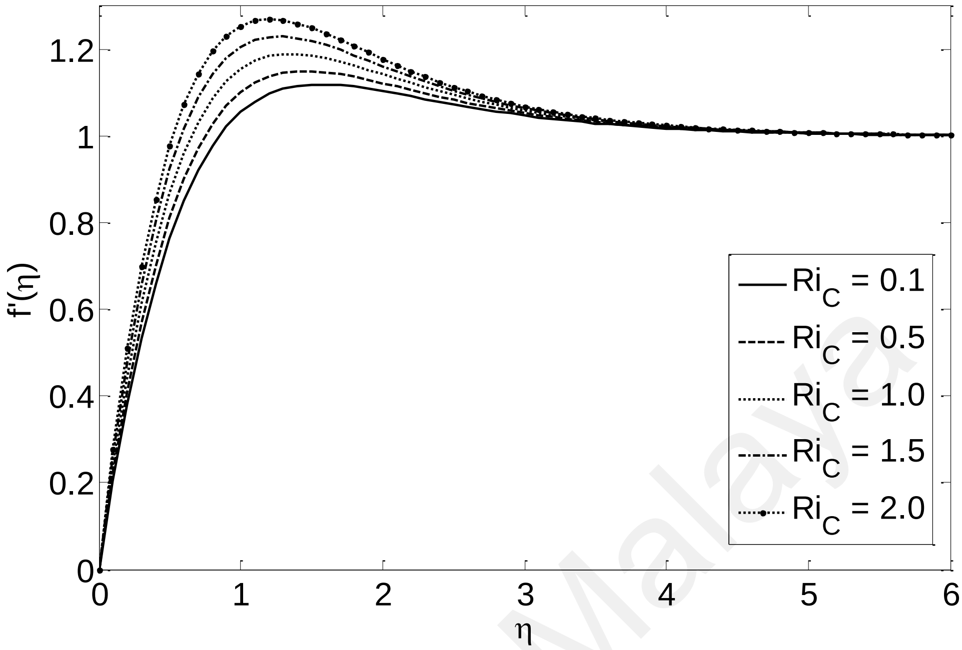

Figure 4.4. Velocity profiles for different Ri_C values with Ri_T=1, K=0.5, M=0.5, Rd=0.2, S=0.2, Cr=0.2.

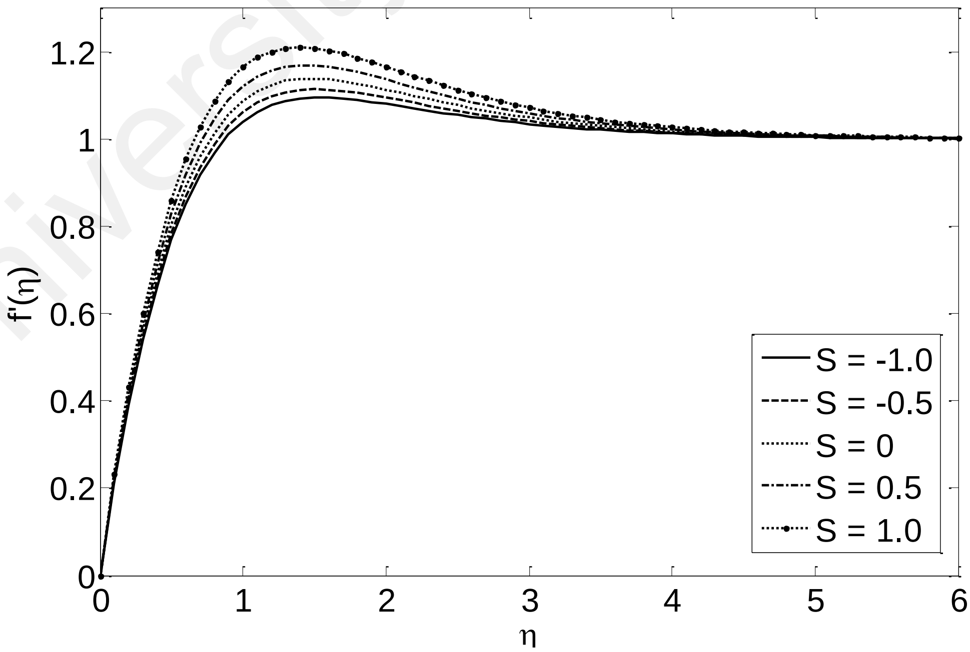

Figure 4.5. Velocity profiles for different S value with Ri_T=1, Ri_C=0.5, K=0.5, M=0.5, Rd=0.2, Cr=0.2.

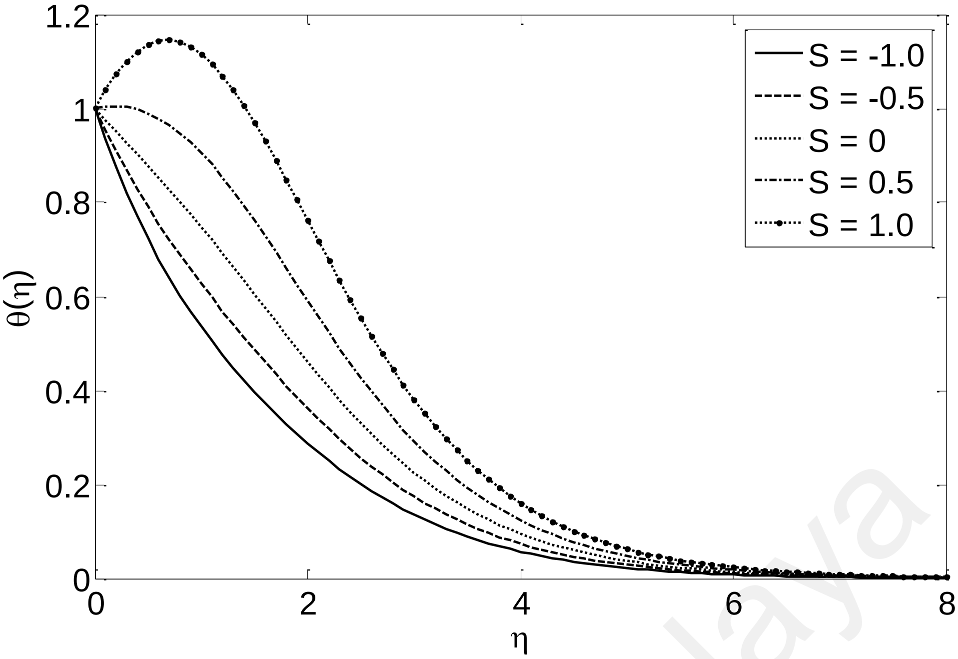

Figure 4.6. Temperature profiles for different S values with Ri_T=1, Ri_C=0.5, K=0.5, M=0.5, Rd=0.2, Cr=0.2.

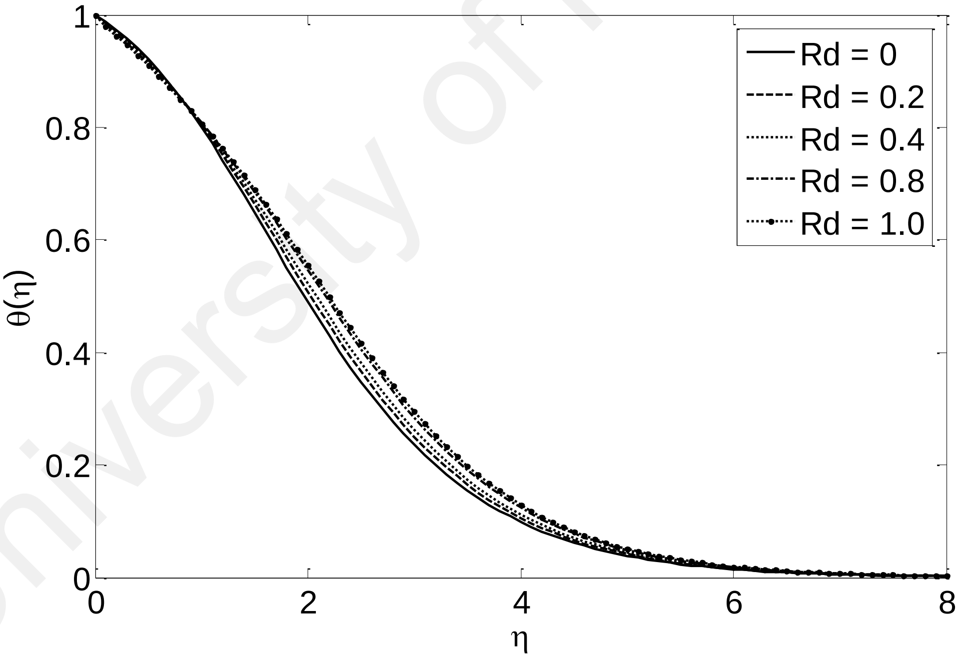

Figure 4.7. Temperature profiles for different Rd values with Ri_T=1, Ri_C=0.5, K=0.5, M=0.5, S=0.2, Cr=0.2.

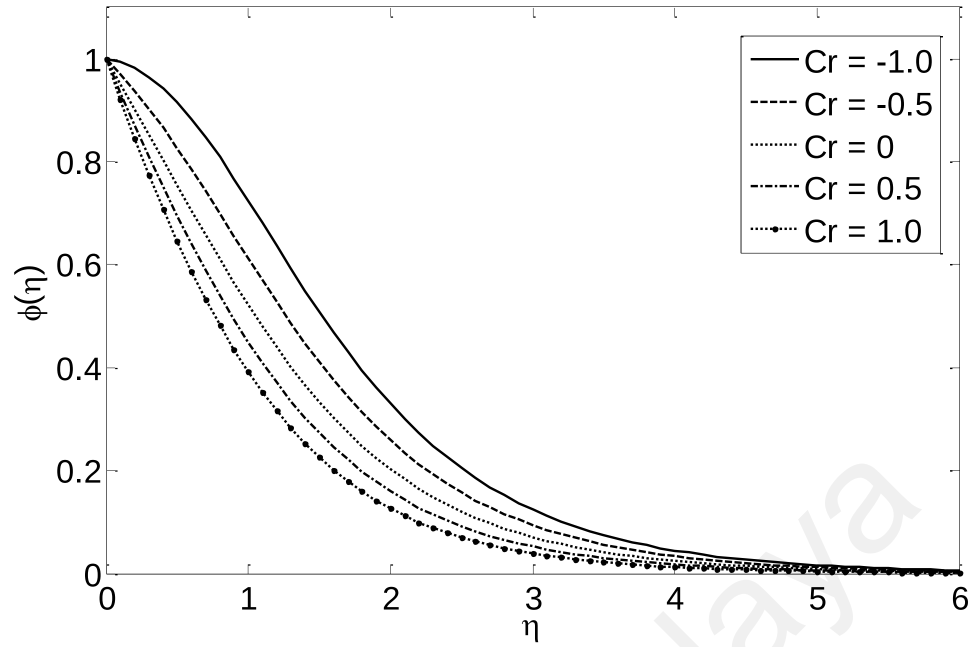

Figure 4.8. Concentration profiles for different Cr values with Ri_T=1, Ri_C=0.5, K = 0.5, M=0.5, S=0.2, Cr=0.2.

CHAPTER 5: EFFECTS OF RADIATION ON MHD MIXED CONVECTION STAGNATION-POINT FLOW OF CHEMICALLY REACTING FLUID IN A POROUS MEDIUM WITH CONVECTIVE BOUNDARY CONDITION

5.1 Introduction

Convection heat transfer and fluid flow are very important in engineering and geophysical fields and its applications. In recent days, the convective heat and mass transfer with chemical reaction play an important role in the metrological, cooling towers, food processing, material processing. Heat generation and thermal radiation appear extensively in various process in astrophysical, electrical power generation. The high temperature may arise the thermal radiation and heat generation. The effect of chemical reaction on heat and mass transfer in polymer production and food processing are important in hydrometallurgical industries and chemical technology. The purpose of the present study to examine the influence of convective boundary condition on MHD mixed convection with heat and mass transfer over a vertical plate embedded in a porous medium near a stagnation point with thermal radiation and chemical reaction. The present study extends the work of chapter 4 to include the convective boundary condition.

5.2 Mathematical Modeling

Consider the two-dimensional steady stagnation-point flow of an electrically conducting incompressible fluid with heat and mass transfer through a porous medium along a vertical plate in the presence of magnetic field as shown in Figure 3.1. The volumetric heat generation/absorption and first-order homogeneous chemical reaction are considered in the study. The magnetic field of constant strength is imposed along the *y*-axis. The induced magnetic field is small compared to the applied magnetic field and the magnetic Reynolds number is very small. So, the induced magnetic field is neglected in this model. As the fluid hits the wall at the stagnation point, the flow divided into two streams and the viscous fluid adheres to the plate within the boundary layer. The velocity distribution in the potential flow region is assumed as $U_\infty = cx$, where c is a positive constant. The porous medium is assumed to be isotropic, homogeneous and in thermodynamic equilibrium with the fluid. The fluid flow in a porous medium obeys the Darcy law with heat transfer due to natural convection. Thus, the governing equations of continuity of mass, momentum transfer, energy transfer and species concentration are given by

$$\frac{\partial u}{\partial x} + \frac{\partial v}{\partial y} = 0, \tag{5.1}$$

$$u\frac{\partial u}{\partial x} + v\frac{\partial u}{\partial y} = \upsilon\frac{\partial^2 u}{\partial y^2} + g\beta(T - T_\infty) + g\beta^*(C - C_\infty) - \left(\frac{\sigma_e B_0{}^2}{\rho} + \frac{\upsilon}{\tilde{K}}\right)(u - U_\infty) + U_\infty\frac{dU_\infty}{dx}, \tag{5.2}$$

$$u\frac{\partial T}{\partial x} + v\frac{\partial T}{\partial y} = \alpha\frac{\partial^2 T}{\partial y^2} - \frac{\alpha}{k}\frac{\partial q_r}{\partial y} + \frac{Q(T - T_\infty)}{\rho c_p}, \tag{5.3}$$

$$u\frac{\partial C}{\partial x} + v\frac{\partial C}{\partial y} = D\frac{\partial^2 C}{\partial y^2} - \Gamma_0(C - C_\infty). \tag{5.4}$$

The boundary conditions are

$$u=0,\ v=0,\ -k\frac{\partial T}{\partial y} = h_f(T_f - T),\ C=C_w \text{ at } y=0,$$

$$u \to U_\infty = cx,\ T \to T_\infty,\ C \to C_\infty \text{ as } y \to \infty. \tag{5.5}$$

where h_f heat transfer coefficient, B_0 strength of magnetic field, C species concentration, D diffusion coefficient, f dimensionless stream function, $\tilde{K}$ porous medium permeability, Re_x Reynolds number, β coefficient of thermal expansion, β^* coefficient of solutal expansion, Γ_0 chemical reaction rate, μ dynamic viscosity, υ kinematic viscosity, σ_e electrical conductivity, respectively.

The heat flux due to radiation is given by

$$q_r = -\frac{4\sigma^*}{3K'}\frac{\partial T^4}{\partial y}, \tag{5.6}$$

where K' mean absorption coefficient, σ^* denotes Stefan-Boltzmann constant.

The medium is assumed to be grey and transparent, i.e., it absorbs heat and emits. Hence, the thermal radiation effect is taken in the medium due to Stefan-Boltzmann's law which states that the radiation is proportional to the fourth power of temperature. Using the Rosseland approximation, it is assumed that the difference in temperature within the flow is too small. Using Taylor series expansion, T^4 is expressed as a linear function of temperature T about the free stream temperature T_∞, i.e., $T^4 = T_\infty^4 + 4T_\infty^3(T - T_\infty) + ...$ then, $T^4 \approx 4T_\infty^3 T - 3T_\infty^4$.

Finally, we get $q_r = -\dfrac{16\sigma^* T_\infty^3}{3K'}\dfrac{\partial T}{\partial y}.$ (5.7)

We introduce the following non-dimensional variables:

$$\eta = y\sqrt{\frac{c}{\upsilon}}, \qquad \psi(x,y) = \sqrt{\upsilon c}\, x f(\eta), \quad \upsilon = \frac{\mu}{\rho}, \quad \theta(\eta) = \frac{T - T_\infty}{T_\omega - T_\infty}, \quad Bi = \frac{h\left(\frac{v}{a}\right)^{\frac{1}{2}}}{k}, \quad Cr = \frac{\Gamma_0}{c},$$

$$Gr_T = \frac{g\beta(T_\omega - T_\infty)x^3}{\upsilon^2}, \quad Gr_c = \frac{g\beta^*(C_\omega - C_\infty)x^3}{\upsilon^2}, \quad Ri_T = \frac{Gr_T}{\mathrm{Re}_x^2}, \quad Ri_C = \frac{Gr_c}{\mathrm{Re}_x^2}, \quad \mathrm{Re}_x = \frac{U_\infty x}{\upsilon},$$

$$Rd = \frac{4\sigma^* T_\infty^3}{kK'}, \; K = \frac{\upsilon}{c\tilde{K}}, \; M = \frac{\sigma_e B_0^2}{c\rho}, \; \Pr = \frac{\upsilon}{\alpha}, \; Sc = \frac{\upsilon}{D}, \; S = \frac{Q\upsilon}{c\alpha}. \tag{5.8}$$

where ψ is the stream function which is defined in the usual form as $u = \partial\psi/\partial y$ and $\upsilon = -\partial\psi/\partial x$ so that the continuity equation (5.1) is automatically satisfied. Substituting the expression in (5.7) together with the variables in (5.8) into (5.1)-(5.4), we obtain the following nonlinear ordinary differential equations:

$$f''' + ff'' - f'^2 + Ri_T\theta + Ri_c\phi - (K + M)(f' - 1) + 1 = 0, \tag{5.9}$$

$$\left(1 + \frac{4}{3}Rd\right)\theta'' + \Pr f\theta' + S\theta = 0, \tag{5.10}$$

$$\phi'' + Scf\phi' - ScCr\phi = 0. \tag{5.11}$$

The corresponding boundary conditions (5.5) are

$$f = 0,\ f' = 0,\ \theta' = Bi[1-\theta(0)],\ \phi = 1 \text{ as } \eta = 0$$

$$f' = 1,\ \theta = 0,\ \phi = 0 \text{ as } \eta \to \infty \tag{5.12}$$

where Bi is the Biot number, Cr is the chemical reaction parameter, Gr_c is the solutal Grashof number, Gr_T is the thermal Grashof number, K is the porous medium permeability parameter, M is the magnetic field parameter, Pr is the Prandtl number, Rd is the thermal radiation parameter, Ri_c is the solutal Richardson number, Ri_T is the thermal Richardson number, S is the internal heat generation/absorption parameter and Sc is the Schmidt number.

The Skin friction (C_f) is the non-dimensional shearing stress on the surface of a body due to the fluid motion and the Nusselt number (Nu) represents the rate of heat transfer at the surface with the fluid. It gives the quantity of heat exchanged between the body (surface) and fluid. The Sherwood number (Sh) is the ratio between the convective to diffusive mass transfer. They are defined as follows,

$$C_f = \frac{2\tau_\omega}{\rho U_\infty^2},\ Nu = \frac{xq_\omega}{k(T_\omega - T_\infty)},\ \ Sh = \frac{xq_m}{D(C_\omega - C_\infty)}, \tag{5.13}$$

where $$\tau_\omega = \mu \left.\frac{\partial u}{\partial y}\right|_{y=0},\ q_\omega = -k\left.\frac{\partial T}{\partial y}\right|_{y=0} - \frac{4\sigma^*}{3K'}\left.\frac{\partial T^4}{\partial y}\right|_{y=0},\ q_m = -D\left.\frac{\partial C}{\partial y}\right|_{y=0}. \tag{5.14}$$

Substituting (5.7), (5.8) and (5.14) into (5.13), we obtain the expressions for the skin-friction coefficient, local Nusselt number and local Sherwood number as follows.

$$\begin{aligned} &\mathrm{Re}_x^{1/2} C_f = f''(0), \\ &\mathrm{Re}_x^{-1/2} Nu = -(1 + 4Rd/3)\theta'(0), \\ &\mathrm{Re}_x^{-1/2} Sh = -\phi'(0). \end{aligned} \tag{5.15}$$

5.3 Results and Discussion

The numerical computation has been carried out for different values of non-dimensional parameters. The Table 5.1 shows that the effect of skin friction gradually increases on increasing *K, M, S, Rd* and *Bi* parameters. The skin friction decreases on increasing chemical reaction parameter (*Cr*). The heat transfer rate increases on increasing the parameters *K, M, Rd, Cr* and *Bi* and decreases on increasing *S*. The mass transfer rate increases on increasing *S, Rd, Cr, Bi*. It increases and suddenly decreases on increasing *K* and *M*.

Table 5.1. Different values of $f''(0)$, $-\theta'(0)$, $-\phi'(0)$ for Pr=0.7 and Sc=0.5

K	*M*	*S*	*Rd*	*Cr*	*Bi*	$f''(0)$	$-\theta'(0)$	$-\phi'(0)$
0	0.1	0.1	0.1	0.1	1.0	2.13284	0.09186	0.52357
2						2.54635	0.09372	0.53004
4						2.90619	0.09520	0.53424
6						3.90180	0.10370	0.52916
8						5.55318	0.10339	0.53390
1.0	0	0.1	0.1	0.1	1.0	2.32394	0.09321	0.52660
	1					2.52791	0.09371	0.52972
	3					2.88236	0.09498	0.53422
	5					3.82295	0.10318	0.52956
	7					5.51097	0.10442	0.53241
1.0	0.1	-2.0	0.1	0.1	1.0	2.27333	0.51846	0.52316
		-1.0				2.29870	0.35488	0.52462
		0.0				2.34004	0.12246	0.52667
		1.0				2.40903	-0.24331	0.52951
		2.0				2.52276	-0.85669	0.53339
1.0	0.1	0.1	0	0.1	1.0	2.34490	0.09112	0.52676
			0.3			2.34608	0.09612	0.52716
			0.6			2.34656	0.09889	0.52744
			0.9			2.34724	0.12383	0.52764
			1.2			2.34994	0.31652	0.52778
1.0	0.1	0.1	0.1	-2.0	1.0	2.53748	0.09030	-0.61903
				-1.0		2.42662	0.09200	0.03503
				0.0		2.35146	0.09321	0.48934
				1.0		2.30081	0.09405	0.81858
				2.0		2.26623	0.09460	1.07161
1.0	0.1	0.1	0.1	0.1	0	2.07691	0	0.51600
					1	2.34545	0.09331	0.52691
					2	2.43429	0.12349	0.53051
					3	2.47858	0.13842	0.53230
					5	2.52279	0.15325	0.53409

Figure 5.1 depicts the velocity for different values of *K* with constant values of *M*=0.1, *Rd*=0.1, *S*=0.1, *Cr*=0.1 and *Bi*=1. Figure 5.2 depicts the velocity for different values of *M* with constant values of *K*=1.0, *Rd*=0.1, *S*=0.1, *Cr*=0.1 and *Bi*=1. Figures 5.1 & 5.2 show that the velocity of the fluid initially decreases and then increases on increasing the porous medium permeability parameter (*K*) and magnetic field parameter (*M*). It is observed that the velocity profile overshoots near the plate when porous medium permeability parameter (*K*) and magnetic field parameter (*M*) is high. Figure 5.3 illustrated the velocity of the fluid increases on increasing the internal heat generation parameter (*S*). It is observed that overshoot in the fluid velocity is observed near the plate surface. Figure 5.4 shows that the influences of chemical reaction parameter on the velocity field. It is seen that, the velocity decreases on increasing the chemical reaction parameter within the boundary layer. Figure 5.5 displays the influence of the Biot number on the velocity profiles. It is clearly observed from this figure that, increasing the values of the Biot number produces an increase in the velocity profiles. The temperature of the fluid increases on increasing internal heat generation parameter, see Figure 5.6. The temperature gradient between the fluid and the surface of the plate increases steeply.

Figure 5.7 showed the temperature profiles for different thermal radiation parameters for constant values of *K, M, S, Cr, Bi* parameters. It is observed that an increase in the thermal radiation parameter causes an increase in the temperature within the boundary layer. Figure 5.8 shows the variations of the Biot number effect on the thermal boundary layer. The temperature increases on increasing the Biot number. Figure 5.9 illustrate the concentration profiles for different values of chemical reaction parameter. The fluid concentration decreases on increasing the chemical reaction parameter. The concentration profiles overshoot near the plate in the case of generative chemical reaction ($Cr < 0$).

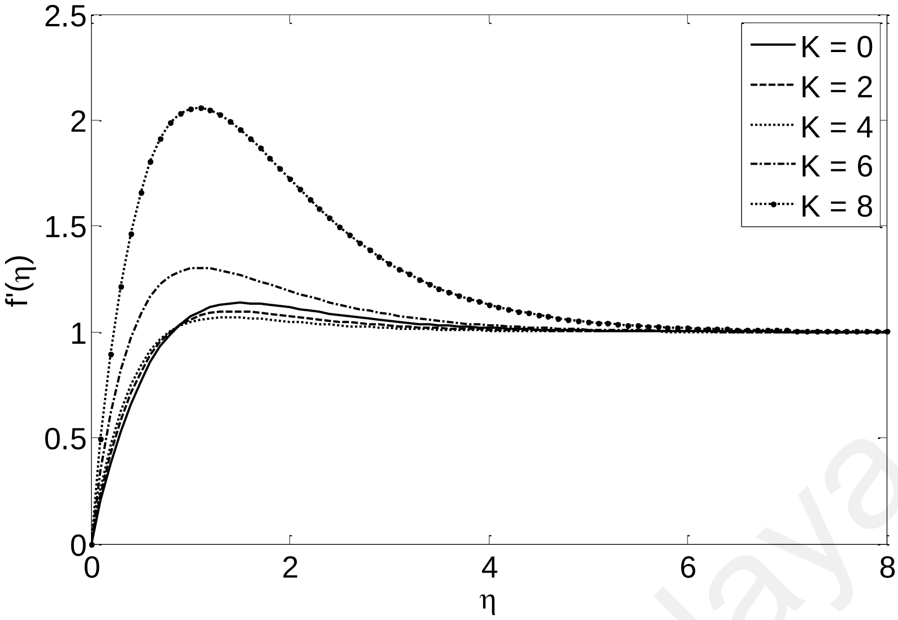

Figure. 5.1. Velocity profiles for different permeability parameter (K) with M=0.1, Rd=0.1, S=0.1, Cr=0.1, Bi=1.

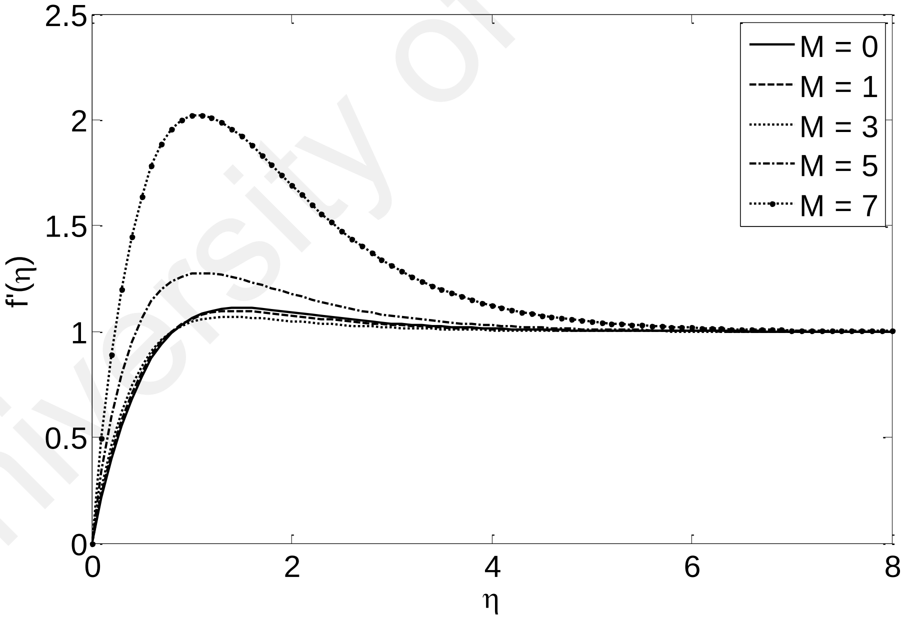

Figure. 5.2. Velocity profiles for different magnetic parameters (M) with K=1.0, Rd=0.1, S=0.1, Cr=0.1, Bi=1.

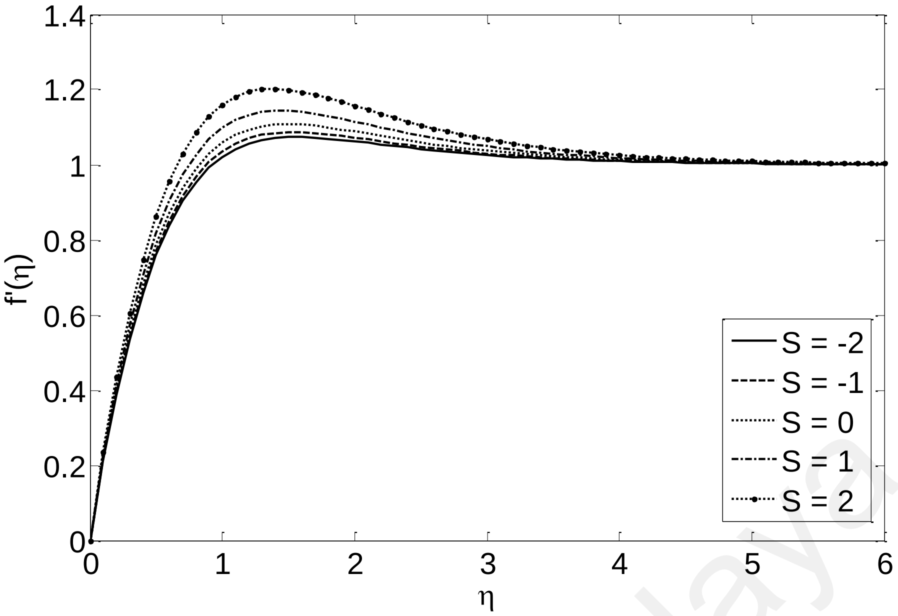

Figure. 5.3. Velocity profiles for different heat generation parameters (S) with K=1.0, M=0.1, Rd=0.1, Cr=0.1, Bi=1.

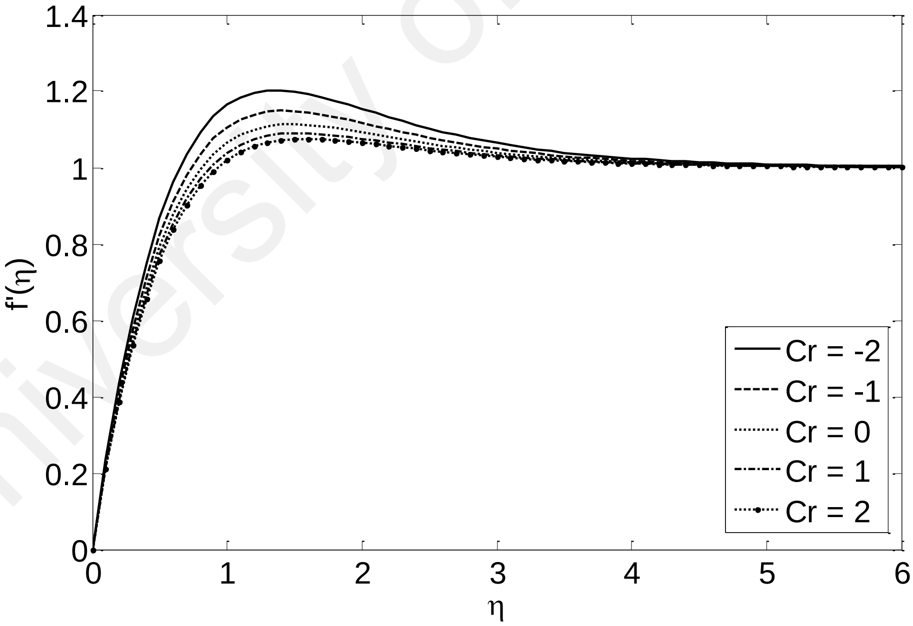

Figure. 5.4. Velocity profiles for different chemical reaction parameters (Cr) with K=1.0, M=0.1, Rd=0.1, S=0.1, Bi=1.

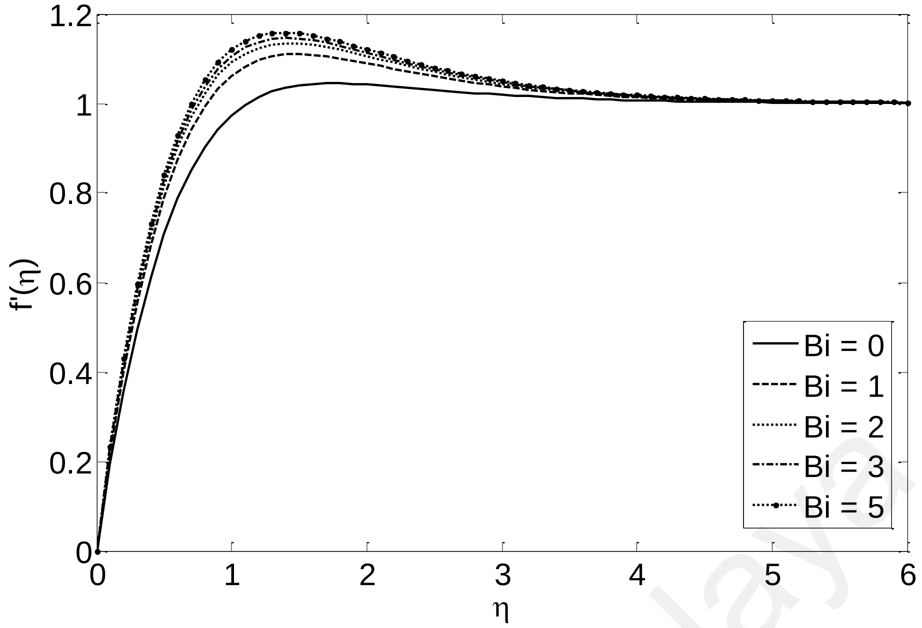

Figure. 5.5. Velocity profiles for different Biot numbers (Bi) with K=1.0, M=0.1, Rd=0.1, S=0.1, Cr=0.1.

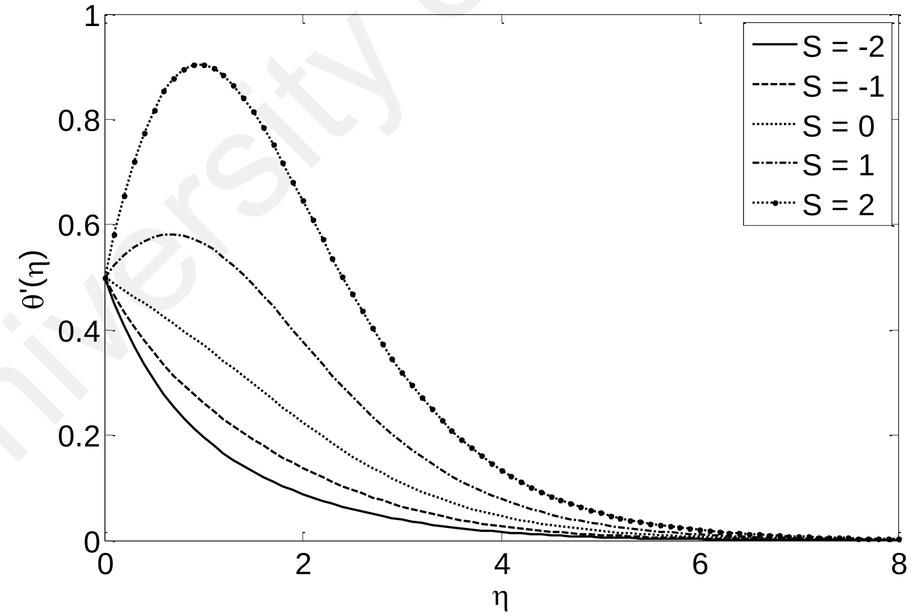

Figure. 5.6. Temperature profiles for different heat generation parameters (S) with K=1.0, M=0.1, Rd=0.1, Cr=0.1, Bi=1.

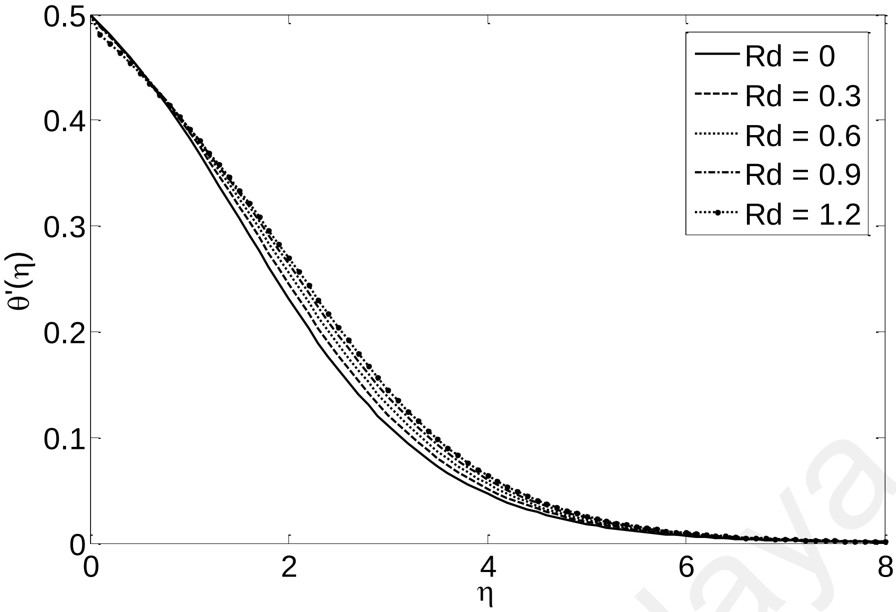

Figure 5.7. Temperature profiles for different radiation parameters (Rd) with K=1.0, M=0.1, S=0.1, Cr=0.1, Bi=1.

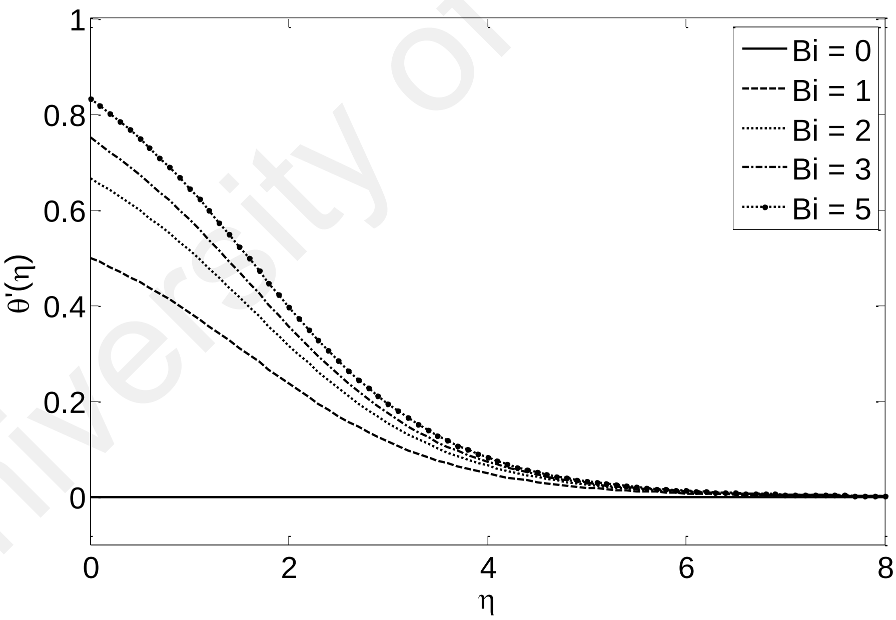

Figure. 5.8. Temperature profiles for different Biot numbers (Bi) with K=1.0, M=0.1, R=0.1, S=0.1, Cr=0.1.

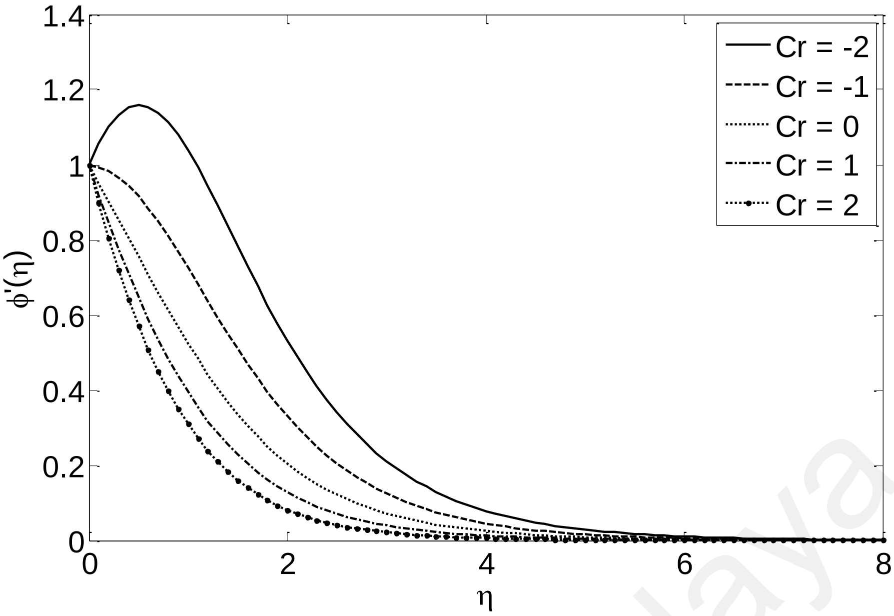

Figure. 5.9. Concentration profiles for different chemical reaction parameters (Cr) with K=1.0, M=0.1, R=0.1, S=0.1, Bi=1.

CHAPTER 6: SLIP, SORET AND DUFOUR EFFECTS ON MHD MIXED CONVECTION STAGNATION-POINT FLOW OF A CHEMICALLY REACTING FLUID IN A POROUS MEDIUM WITH RADIATION

6.1 Introduction

Mixed convection flow over a vertical plate of an incompressible fluid embedded in a porous medium have extensively encountered in chemical and metallurgical industries, such as in drying devices, energy related engineering problems. Since the stagnation area meets the zero velocity, highest pressure, maximum rate of mass deposition and highest heat transfer. In general, many researchers are having interest in computational numerical studies with heat transfer of stagnation flow in the existence of chemical reaction and magnetic field areas. Thermal radiation effect on fluid flow plays vital role in heat controlling factor over a vertical plate, such as polymer processing industries and several progressions in engineering areas arise at high temperature. The diffusion of species boundary layer fluid flow with chemical reaction has various uses in water and air pollutions, atmospheric flows, fibrous separation and technological processes.

The effects of thermal-diffusion & diffusion-thermo are normally ignored by reason of negligible order of intensities in comparison with the effects defined by Fick’s law of diffusion and Fourier’s law of conduction. Motivated by the above revealed literature review, the author explored the Soret and Dufour effects on MHD stagnation point flow over a surface in a porous medium in the presence of chemical reaction, slip and thermal radiation. No effort has been made until now to study this problem. The present study extends the work of chapter 4 to include the slip, Soret and Dufour effects.

6.2 Mathematical Modeling

The steady, laminar, 2-D boundary layer mixed convective electrically conducting flow, heat & mass transfer of an incompressible viscous fluid over a vertical plate in a porous medium near the stagnation-point in the existence of magnetic field, radiation and slip effects are considered. In addition, chemical reaction with first order, Soret & Dufour effects are deliberated. Fig. 3.1 describes the coordinate system and physical model of the problem. The x-axis along the surface and y-axis perpendicular to the plate are considered. Then, u and v are taken as the velocity components along x and y directions, respectively. It is supposed that the distribution of velocity of the potential flow is occupied as $U_\infty=cx$ along the y-axis at time t=0, where c is a constant. The magnetic field is executed along the y direction. We have neglected induced magnetic field owing to assumption of insignificant magnetic Reynolds number of the flow. The governing equations are given by

$$u_x + u_y = 0, \tag{6.1}$$

$$uu_x + vu_y = \upsilon u_{yy} + U_\infty (U_\infty)_x - \left(\frac{\sigma_e B_0{}^2}{\rho} + \frac{\upsilon}{\tilde{K}} \right)(u - U_\infty) + g\beta(T - T_\infty) + g\beta^*(C - C_\infty), \tag{6.2}$$

$$uT_x + vT_y = \alpha T_{yy} + \frac{Q(T - T_\infty)}{\rho c_p} - \frac{1}{\rho c_p}(q_r)_y + \frac{D_m K_T}{c_s c_p} C_{yy}, \tag{6.3}$$

$$uC_x + vC_y = DC_{yy} - \Gamma_0 (C - C_\infty) + \frac{D_m K_T}{T_m} T_{yy}, \tag{6.4}$$

subject to the boundary conditions

$$u = N_1 u_y,\ v=0,\ C=C_w,\ T=T_w \text{ as } y=0,$$

$$u \to U_\infty = cx, \quad C = C_\infty, \ T = T_\infty \text{ as } \quad y \to \infty. \tag{6.5}$$

Thus, the heat flux (q_r) radiative term in the energy equation is simplified by employing the approximation of Rosseland diffusion

$$q_r = -\frac{4\sigma^*}{3K'}(T^4)_y. \tag{6.6}$$

We assume that the temperature differences are too small and T^4 can be accepted as a linear combination of the temperature by Taylor's series about free stream temperature. Ignoring the higher order expressions, we get, $T^4 \approx 4T_\infty^3 T - 3T_\infty^4$ then equation (6.6) reduces to

$$q_r = -\frac{16\sigma^* T_\infty^3}{3K'} T_y. \tag{6.7}$$

The non-dimensional variables are introduced as follows:

$$\eta = y\sqrt{\frac{c}{\upsilon}},\quad \psi(x,y) = \sqrt{\upsilon c}\, xf(\eta),\quad b = N_1\left(\frac{c}{\upsilon}\right)^{1/2},\ Cr = \frac{\Gamma_0}{c},\ Df = \frac{D_m K_T (C_w - C_\infty)}{c_s c_p (T_w - T_\infty)\alpha},\ \theta(\eta) = \frac{T - T_\infty}{T_\omega - T_\infty},$$

$$\phi(\eta) = \frac{C - C_\infty}{C_\omega - C_\infty},\quad Gr_T = \frac{g\beta(T_\omega - T_\infty)x^3}{\upsilon^2},\quad Gr_c = \frac{g\beta^*(C_\omega - C_\infty)x^3}{\upsilon^2},\quad Ri_T = \frac{Gr_T}{\mathrm{Re}_x^2},\quad Ri_C = \frac{Gr_c}{\mathrm{Re}_x^2},$$

$$\mathrm{Re}_x = \frac{U_\infty x}{\upsilon},\quad Rd = \frac{4\sigma^* T_\infty^3}{kK'},\quad K = \frac{\upsilon}{c\tilde{K}},\quad \Pr = \frac{\upsilon}{\alpha},\quad Sc = \frac{\upsilon}{D},\quad M = \frac{\sigma_e B_0^2}{c\rho},\quad S = \frac{Q\upsilon}{\rho c_p c},$$

$$Sr = \frac{D_m K_T (T_w - T_\infty)}{T_m \alpha (C_w - C_\infty)}, \tag{6.8}$$

where the stream function represented as ψ, well-defined as $u = \partial\psi/\partial y$ and $\upsilon = -\partial\psi/\partial x$. Substituting (6.7&6.8) into (6.1)-(6.4) equations, we obtain the ensuing coupled ordinary differential equations with boundary conditions:

$$f''' + ff'' - f'^2 - (K+M)(f'-1) + Ri_T\theta + Ri_c\phi + 1 = 0, \tag{6.9}$$

$$\left(1 + \frac{4}{3}Rd\right)\theta'' + S\theta + \Pr f\theta' + D_f\phi'' = 0, \tag{6.10}$$

$$\phi'' + Scf\phi' + SrSc\theta'' - ScCr\phi = 0, \tag{6.11}$$

$$f=0,\ f' = bf''(0),\ \phi = 1,\ \theta = 1 \text{ as } \eta = 0,$$

$$f' = 1,\ \phi = 0,\ \theta = 0 \text{ as } \eta \to \infty. \tag{6.12}$$

The coupled Eqns. (6.9-6.11) cannot result in a closed form solution. Therefore, the problem solved numerically using shooting method along with Runge-Kutta 4th order integration. From the process of numerical computation, the physical quantities describing the local skin-friction coefficient, local Nusselt number and local Sherwood number interest for the present problem, which designate physical wall shear stress, rates of heat transfer and mass transfer. They are given by the expressions

$$C_f = \frac{2\tau_\omega}{\rho U_\infty^2},\ Nu = \frac{xq_\omega}{k(T_\omega - T_\infty)},\ \ Sh = \frac{xq_m}{D(C_\omega - C_\infty)}, \tag{6.13}$$

where $$\tau_\omega = \mu u_y\big|_{y=0},\ \ q_\omega = -kT_y\big|_{y=0} - \frac{4\sigma^*}{3K'}T_y^4\big|_{y=0},\ \ q_m = -DC_y\big|_{y=0}. \tag{6.14}$$

Finally, we get the non-dimensional local skin friction (C_f), Nusselt (Nu) and Sherwood (Sh) numbers as follows.

$$\begin{aligned} &\mathrm{Re}_x^{1/2} C_f = f''(0), \\ &\frac{\mathrm{Re}_x^{-1/2} Nu}{(1+\frac{4}{3}Rd)} = -\theta'(0), \\ &\mathrm{Re}_x^{-1/2} Sh = -\phi'(0). \end{aligned} \tag{6.15}$$

6.3 Results and Discussion

The authors performed the computation to understand the effects of Soret & Dufour on MHD heat transfer and mixed convective flow characteristics of viscous fluid near a stagnation-point flow for various values of the pertinent parameter elaborated in the study. The local skin friction coefficient dissimilarities, the rates of heat & mass transfer are presented in Table 6.1 for various values of the parameters *S, Rd, Cr, Df, Sr, b* with fixed values of Ri_T=1, Ri_c=1, *Pr*=0.7, *Sc*=0.5, *K*=2, *M*=2. The skin friction increases at the plate on increasing the values of the parameters *S, Rd, Df*. The rate of heat transfer decreases on increasing the *S, Cr, Df, Sr* parameters. The heat transfer rate increases on increasing the thermal radiation and slip parameters. By increasing the *S, Cr, Df, Sr, b* parameters the rate of mass transfer increases.

Figure 6.1 (a-c) shows the distributions of velocity, temperature and concentration for numerous values of heat generation parameter. The Fig. 6.1(a) illustrated that the fluid gets more heat energy due to internal heat generation/absorption, and it results higher buoyancy force. Hence, the velocity of fluid particle is increasing inside the boundary layer on increasing heat generation parameter.

Table 6.1. Computations showing $f''(0), -\theta'(0)$ and $-\phi'(0)$ for various values of *S*, *Rd*, *Cr*, *Df*, *Sr*, *b* when Ri_T =1, Ri_c=1, *Pr*=0.7, *Sc*=0.5, *K*=2, *M*=2.

S	*Rd*	*Cr*	*Df*	*Sr*	*b*	$f''(0)$	$-\theta'(0)$	$-\phi'(0)$
-1	0.5	0.5	0.5	0.5	0.5	1.38850	0.84319	0.62070
-0.5						1.39513	0.64589	0.66274
0						1.40450	0.39454	0.71482
0.5						1.41979	0.03009	0.78737
1						1.45297	-0.67018	0.91922
0.5	0.5	0.5	0.5	0.5	0.5	1.41979	0.03009	0.78737
	1					1.42146	0.05236	0.77764
	2					1.42361	0.06610	0.76872
	3					1.42482	0.07087	0.76427
	4					1.42551	0.07438	0.76141
0.5	0.5	-1	0.5	0.5	0.5	1.44627	0.26153	0.01226
		-0.5				1.43351	0.15800	0.36017
		0				1.42549	0.08608	0.60064
		0.5				1.41979	0.03009	0.78737
		1				1.41542	-0.01650	0.94258
0.5	0.5	0.5	0	0.5	0.5	1.41113	0.21681	0.75162
			0.5			1.41979	0.03009	0.78737
			1			1.42907	-0.17802	0.82782
			2			1.44998	-0.68065	0.92795
			3			1.47526	-1.36131	1.06831
0.5	0.5	0.5	0.5	0	0.5	1.42026	0.04312	0.74316
				0.5		1.41979	0.03009	0.78737
				1		1.41928	0.01473	0.83932
				2		1.41764	-0.02580	0.97585
				3		1.41516	-0.08776	1.18367
0.5	0.5	0.5	0.5	0.5	0	3.08303	-0.03381	0.74502
					0.3	1.82129	0.01590	0.77782
					0.5	1.41979	0.03009	0.78737
					0.8	1.06408	0.04212	0.79554
					1	0.91111	0.04715	0.79897

The velocity profile overshoot for heat generation (*S*>0) case. The velocity of the fluid increases on increasing the internal heat generation parameter (*S*). There is less effect observed in the case of heat absorption (*S*<0). Fig. 6.1(b) depicts the different values of temperature for *S* with constant parameters of *K, M, Rd, Df, Sr, Cr, b*. The temperature profiles overshoots on increasing the heat generation (*S*>0.5) parameter. This effect occurs due to buoyancy force is larger when fluid gets large quantity of heat energy because of internal heat energy. It is detected that the profiles of temperature increases on increasing the heat generation parameter. When *S*<1, the influence of heat generation is less on temperature distribution inside the thermal boundary layer. Fig 6.1(c) shows the profiles of concentration with constant values of *K, M, Rd, Df, Sr, Cr, b*. The concentration decreases on increasing the *S*.

Figure 6.2(a-b) shows the different values of the radiation parameter (*Rd*) on dimensionless profiles of velocity and temperature. The radiation parameter increases on increasing the temperature of the fluid and decreasing the value of mean absorption coefficient. The radiation parameter increases then, the boundary layer thickness decreases. The momentum and thermal boundary layer thicknesses increase on increasing the radiation parameter. Figures 6.3(a-c) illustrate the profiles of velocity, temperature and concentration for different values of Dufour parameter with fixed values of *K, M, Rd, S, Sr, Cr, b*. It is perceived that the velocity of the fluid increases on increasing the Dufour number. Since, the Dufour parameter is in energy equation, it affects mainly the temperature distribution. The higher temperature difference reduces the value of Dufour effect on thermal flow. Fig. 6.3(b) displays the temperature of the fluid near the plate surface overshoots with increasing the Dufour number values. The thickness of thermal boundary layer increases on increasing the Dufour number. It is detected from the Fig. 6.3(c) that the fluid concentration profile decreases on increasing the Dufour number.

The Soret effect on the velocity and concentration profiles is illustrated in Figures 6.4(a-b). Fig. 6.4(a) shows the velocity increases on increasing the Soret number. The soret number increases on increasing the temperature of the fluid.

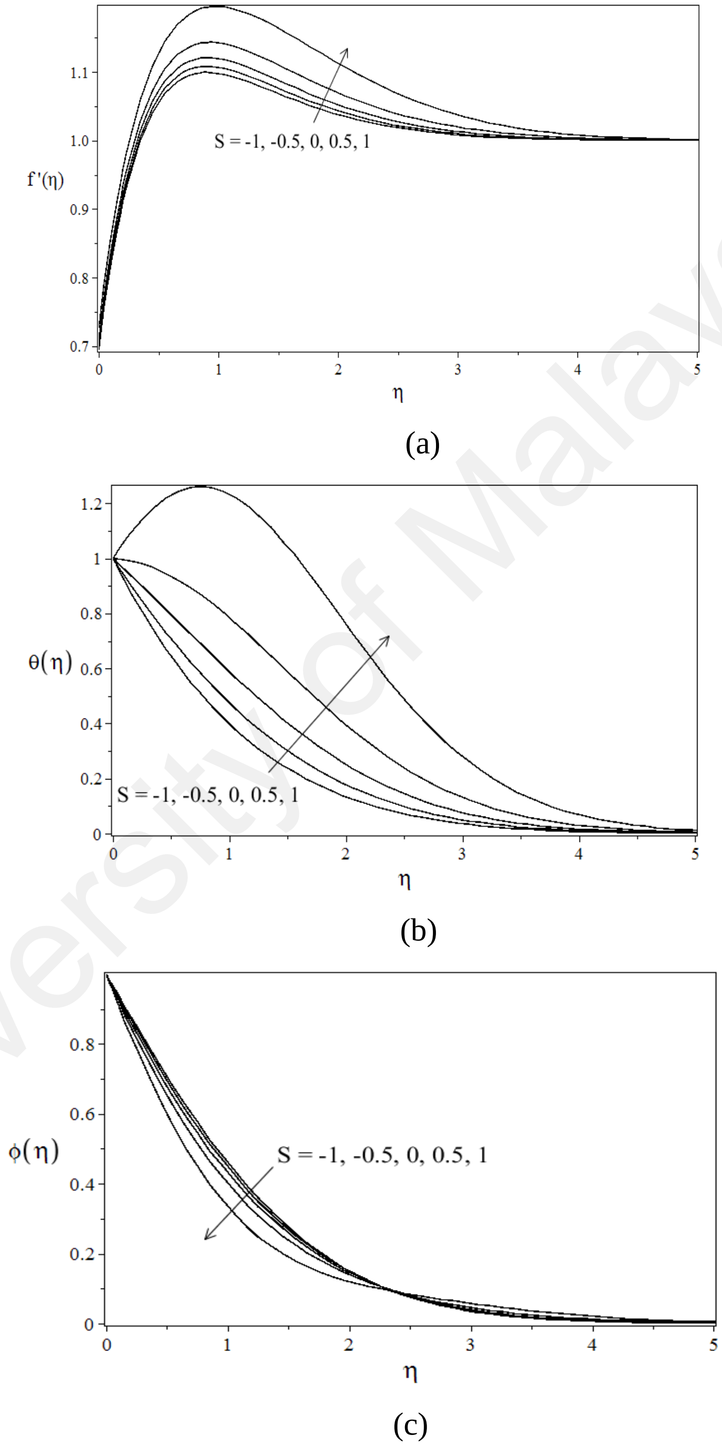

Figure 6.1. (a) Velocity, (b) Temperature, (c) Concentration profiles for different heat generation parameters S with K=2, M=2, Rd=0.5, Df=0.5, Sr=0.5, Cr=0.5, b=0.5.

The larger Soret number views for a larger temperature variance and hasty gradient. Thus, the fluid velocity increases due to greater Soret effect. The effects of Soret number are clearly playing a significant role in concentration profile, See Fig. 6.4(b). The concentration increases on raising the Soret number. Therefore, we can understand that the effects of Soret and Dufour are generally more enthusiastic in the study of mixed convection problems. The effects of Dufour and Soret are apparently acting a vital role in combined convection in a porous medium in the occurrence of radiation, chemical reaction and slip parameter.

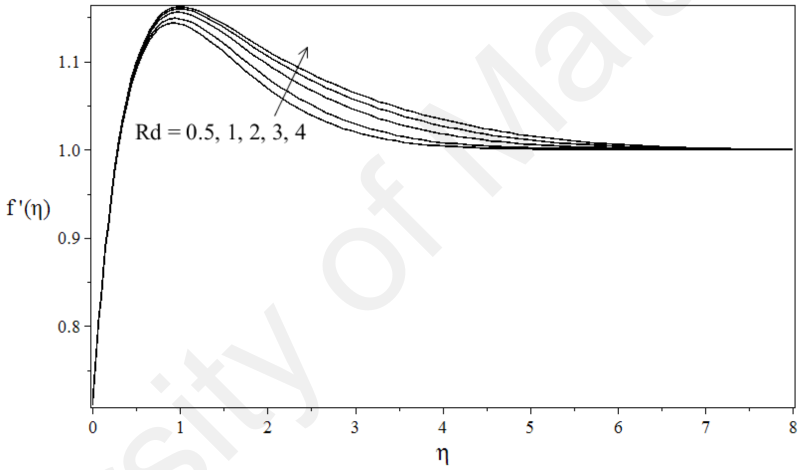

(a)

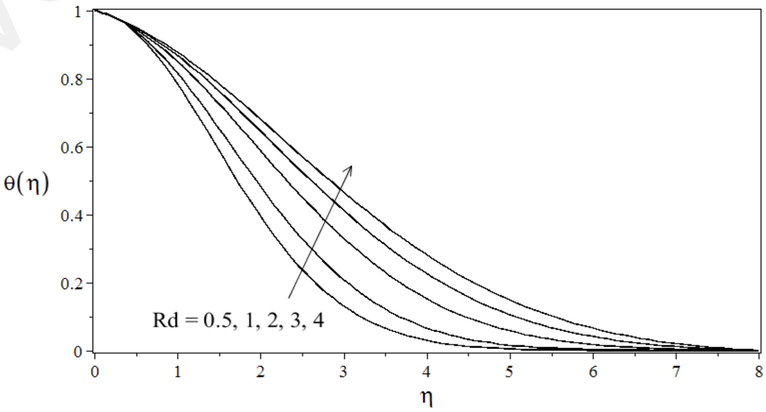

(b)

Figure 6.2. (a) Velocity, (b) Temperature profiles for different radiation parameters Rd with K=2, M=2, S=0.5, Df=0.5, Sr=0.5, Cr=0.5, b=0.5.

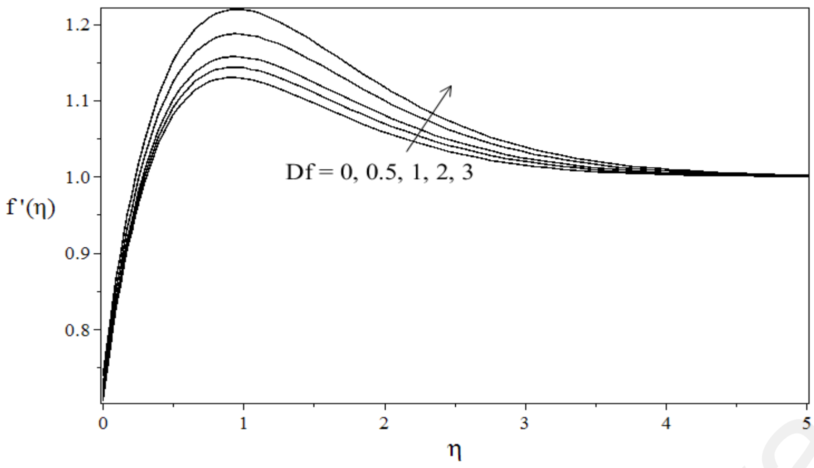

(a)

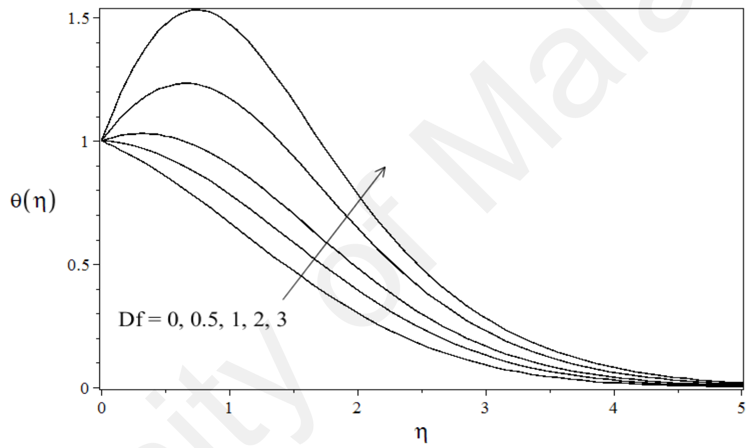

(b)

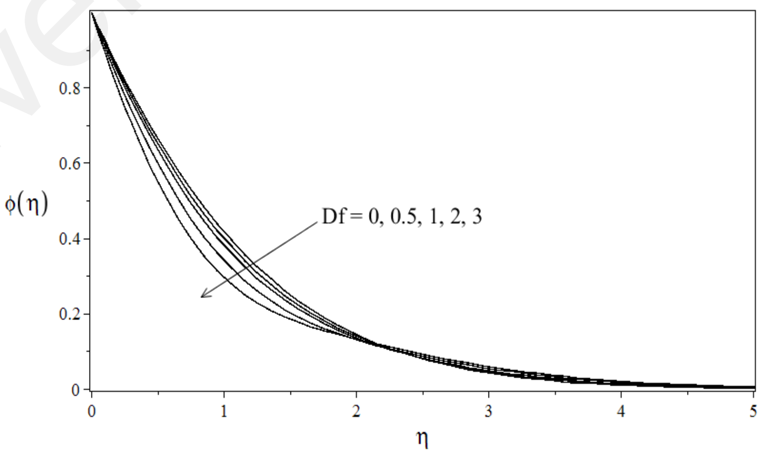

(c)

Figure 6.3. (a) Velocity, (b) Temperature, (c) Concentration profiles for different Dufour parameters Df with K=2, M=2, Rd=0.5, S=0.5, Sr=0.5, Cr=0.5, b=0.5.

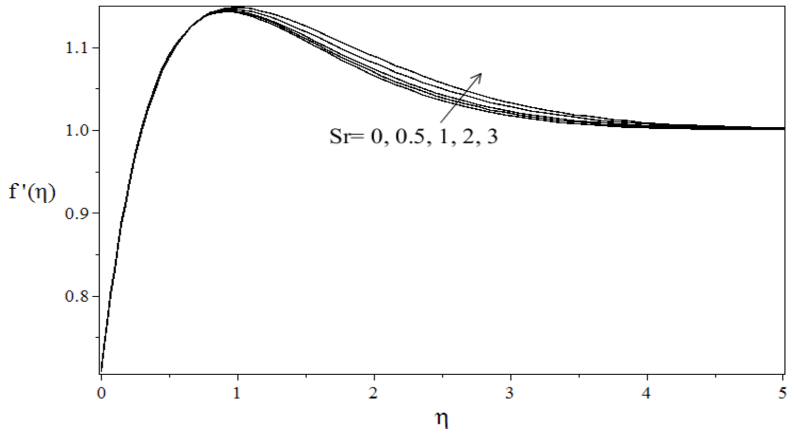

(a)

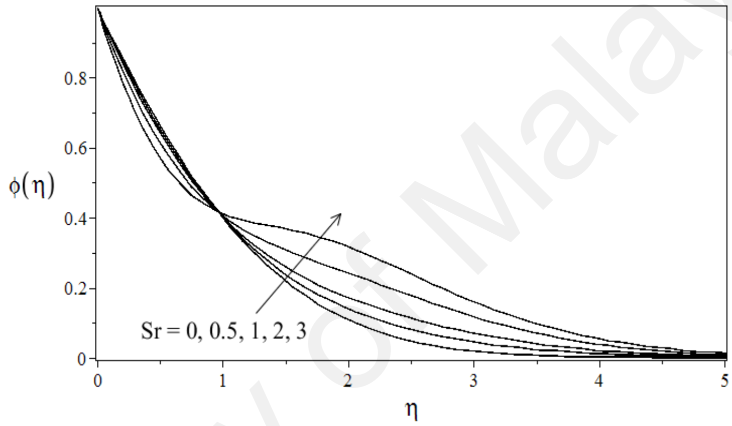

(b)

Figure 6.4. (a) Velocity, (b) Concentration profiles for different Soret parameters Sr with K=2, M=2, Rd=0.5, S=0.5, Df=0.5, Cr=0.5, b=0.5.

So, we can appreciate that the effects of diffusion-thermal greatly genuine in the mixed convection problems study.

Figure 6.5(a-c) displays the effect of chemical reaction (*Cr*) on various boundary layer profiles. It is openly grasped from these figures that increasing the *Cr* values produces a decrease in the velocity profiles (Fig. 6.5(a)). The temperature profiles increases on increasing the *Cr* parameter which is observed in Fig. 6.5(b). There is no high significant in temperature profiles on increasing the *Cr* parameter. The concentration profiles (Fig. 6.5(c)) of the species decreases on increasing the chemical reaction parameter (*Cr*) for destructive and generative cases. The boundary layer thickness is very high and overshoot in generative case (*Cr<0*). We observed that the concentration boundary layer thickness is very less in destructive case (*Cr*>0).

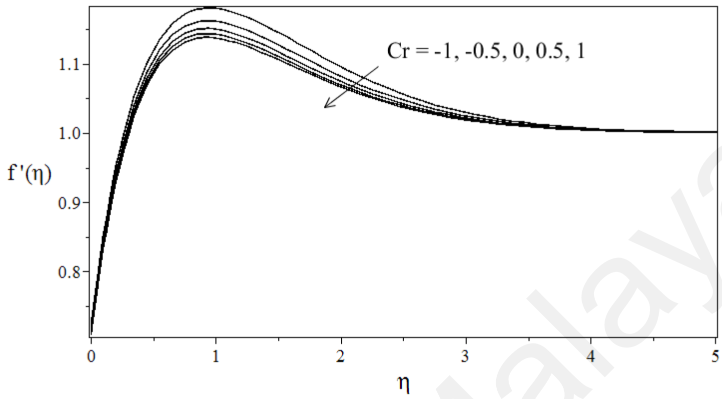

(a)

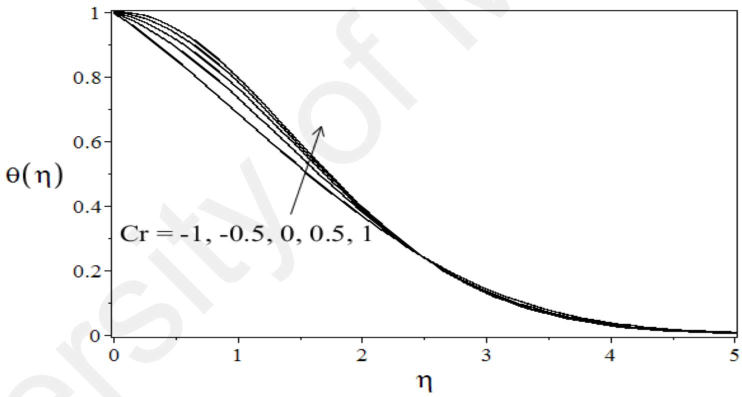

(b)

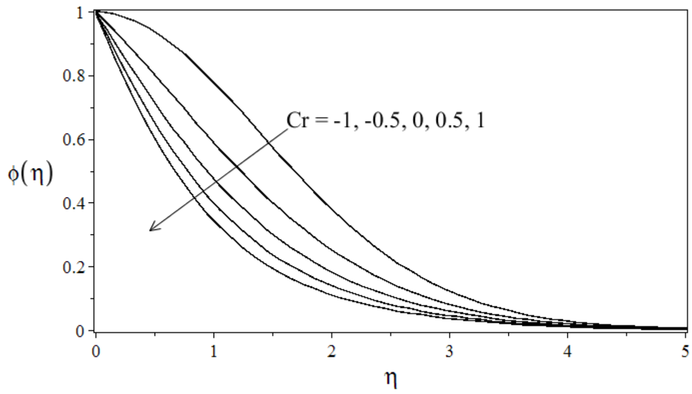

(c)

Figure 6.5. (a) Velocity, (b) Temperature, (c) Concentration profiles for different chemical reaction parameters Cr with K=2, M=2, Rd=0.5, S=0.5, Df=0.5, Sr=0.5, b=0.5.

Figures 6.6(a-b) illustrate the slip parameter effect on the profiles of velocity and temperature. It is perceived from the Fig. 6.6(a) that the profiles of velocity increase on increasing the slip parameter. Fig. 6.6(b) shows the distribution of temperature increases on decreasing the slip parameter. It is readily seen that slip parameter has substantial effect.

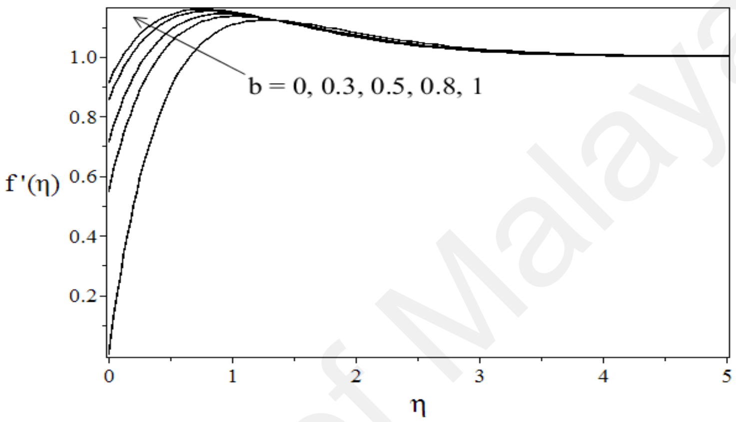

(a)

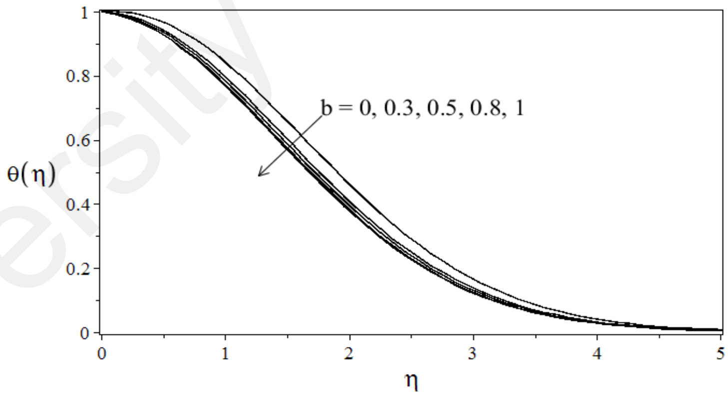

(b)

Figure 6.6. (a) Velocity, (b) Temperature profiles for different slip parameter b with K=2, M=2, Rd=0.5, S=0.5, Df =0.5, Sr=0.5, Cr=0.5.

CHAPTER 7: EFFECT OF SLIP ON MHD MIXED CONVECTION STAGNATION-POINT FLOW OF CHEMICALLY REACTING FLUID IN A POROUS MEDIUM WITH RADIATION

7.1 Introduction

The study of convective heat transfer through a porous medium for an incompressible fluid on the heated surface has attached major attention because of its diverse uses in the insulation of nuclear reactors, petroleum industry, storage of nuclear waste and several other areas. The study of slip condition on convective boundary layer flow beside a vertical plate embedded in a porous medium has accepted considerable practical and theoretical awareness. The research has been maintained out in this area to analyze the heat and mass transfer characteristics within the boundary layer flow.

The research on MHD flow and heat transfer has several applications in engineering fields such as design of MHD accelerators, cooling of nuclear reactors and heat exchangers. The effect of radiation on heat and mass transfer is essential in some applications, such as hydrometallurgical industries and solar power technology. The study of chemical reaction on heat and mass transfer is very significant in chemical technology, food processing. Inspired the above applications and surveys explained, the purpose of this present study is to explore the effects of chemical reaction and velocity slip on mixed convection stagnation-point flow over a vertical plate embedded in a porous medium in the presence of external magnetic field and thermal radiation. The present study extends the work of chapter 4 to include the velocity slip effect.

7.2 Mathematical Modeling

Consider a steady, 2D laminar, mixed convection boundary layer flow of an incompressible viscous fluid near a stagnation-point along a vertical plate in the presence of magnetic field through a porous medium as shown in Figure 3.1. It is presumed that the chemical reaction is considered as homogeneous and first order. It is assumed that the porous medium is a heat generating or absorbing internally at a fixed rate. Constant strength is enforced on unvarying magnetic field along the y-axis. The induced magnetic field is negligible due to small magnetic Reynolds number. As the fluid hits the wall at the stagnation point, the flow is divided into two equal and opposite forces. In the potential flow region, the velocity distribution is assumed as $U_\infty = cx$, where c is a positive constant. The porous medium is isotropic, homogeneous and in thermodynamic equilibrium with local fluid. Therefore, the governing equations are given by

$$u_x + v_y = 0, \tag{7.1}$$

$$uu_x + vu_y = \upsilon u_{yy} + g\beta(T - T_\infty) + g\beta^*(C - C_\infty) - (u - U_\infty)\left(\frac{\sigma_e B_0{}^2}{\rho} + \frac{\upsilon}{\tilde{K}}\right) + U_\infty \frac{dU_\infty}{dx}, \tag{7.2}$$

$$uT_x + vT_y = \alpha T_{yy} - \frac{\alpha}{k}\frac{\partial q_r}{\partial y} + \frac{Q(T - T_\infty)}{\rho c_p}, \tag{7.3}$$

$$uC_x + vC_y = DC_{yy} - \Gamma_0(C - C_\infty), \tag{7.4}$$

subject to the boundary conditions

$$u = N_1 u_y,\ v = 0\ ,\ C = C_w,\ T = T_w \ \text{ at } \ y = 0,$$

$$u \to U_\infty = cx,\ C \to C_\infty,\ T \to T_\infty \text{ as } \ y \to \infty. \tag{7.5}$$

The medium is taken to be a gray, absorbing and emitting radiation and heat flux in the equation of energy due to thermal radiation is given by means of the Rosseland approximation,

$$q_r = -\frac{4\sigma^*}{3K'}\frac{\partial T^4}{\partial y}. \tag{7.6}$$

It is presumed that the change in temperature within the flow is too small, so that the temperature term T^4 might be stated as a linear combination of temperature (T) about free stream temperature (T_∞) using Taylor series and ignoring higher terms, we may expressed as i.e., $T^4 \approx 4T_\infty^3 T - 3T_\infty^4$. Then we get,

$$q_r = -\frac{16\sigma^* T_\infty^3}{3K'} T_y. \tag{7.7}$$

we use the following variables to non-dimensionalise the governing equations:

$$b = N_1\left(\frac{c}{\nu}\right)^{1/2}, \quad Cr = \frac{\Gamma_0}{c}, \quad Gr_c = \frac{g\beta^*(C_\omega - C_\infty)x^3}{\upsilon^2}, \quad Gr_T = \frac{g\beta(T_\omega - T_\infty)x^3}{\upsilon^2}, \quad K = \frac{\upsilon}{c\tilde{K}},$$

$$M = \frac{\sigma_e B_0^2}{c\rho}, \ \Pr = \frac{\upsilon}{\alpha}, \ Rd = \frac{4\sigma^* T_\infty^3}{kK'}, \ \mathrm{Re}_x = \frac{U_\infty x}{\upsilon}, \ Ri_C = \frac{Gr_c}{\mathrm{Re}_x^2}, \ Ri_T = \frac{Gr_T}{\mathrm{Re}_x^2}, \ S = \frac{Q\upsilon}{\alpha c}, \ Sc = \frac{\upsilon}{D},$$

$$\eta = y\sqrt{\frac{c}{\upsilon}}, \theta(\eta) = \frac{T - T_\infty}{T_\omega - T_\infty}, \quad \phi(\eta) = \frac{C - C_\infty}{C_\omega - C_\infty}, \quad \psi(x, y) = \sqrt{\upsilon c}\, x f(\eta). \tag{7.8}$$

Wherever the stream function (ψ), defined in the normal notation as $u = \psi_y$ and $\upsilon = -\psi_x$, then the continuity equation (7.1) is satisfied. Replacing the expression in (7.7) together with (7.8) into equations (7.1)-(7.4), we obtain the nonlinear ordinary differential equations:

$$f''' + ff'' - f'^2 + Ri_T\theta + Ri_c\phi - (K + M)(f' - 1) + 1 = 0, \tag{7.9a}$$

$$\left(1 + \frac{4}{3}Rd\right)\theta'' + \Pr f\theta' + S\theta = 0, \tag{7.10a}$$

$$\phi'' + Scf\phi' - ScCr\phi = 0. \tag{7.11a}$$

By taking $(K+M) = M_p$=Porous magnetic parameter and also consider $\left(1 + \frac{4}{3}Rd\right) = RD$, the equations (7.9a) to (7.11a) modified as follows:

$$f''' + ff'' - f'^2 + Ri_T\theta + Ri_c\phi - M_p(f' - 1) + 1 = 0, \tag{7.9b}$$

$$RD\theta'' + \Pr f\theta' + S\theta = 0, \tag{7.10b}$$

$$\phi'' + Scf\phi' - ScCr\phi = 0. \tag{7.11b}$$

The corresponding boundary conditions are:

$$f=0, \ f' = bf''(0), \ \theta = 1, \ \phi = 1 \ \text{ as } \eta = 0,$$

$$f' = 1, \ \theta = 0, \ \phi = 0, \ \text{ as } \eta \to \infty. \tag{7.12}$$

The set of equations (7.9b) to (7.11b) with boundary conditions (7.12) has been solved analytically by homotopy analysis method (HAM) and numerically by applying the shooting technique along with fourth-order Runge-Kutta integration scheme.

The non-dimensional numbers C_f, Nu, Sh are defined as follows:

$$C_f = \frac{2\tau_\omega}{\rho U_\infty^2},\ Nu = \frac{xq_\omega}{k(T_\omega - T_\infty)},\ Sh = \frac{xq_m}{D(C_\omega - C_\infty)}, \tag{7.13}$$

$$\tau_\omega = \mu \left.\frac{\partial u}{\partial y}\right|_{y=0},\ q_\omega = -k\left.\frac{\partial T}{\partial y}\right|_{y=0} - \frac{4\sigma^*}{3K'}\left.\frac{\partial T^4}{\partial y}\right|_{y=0},\ q_m = -D\left.\frac{\partial C}{\partial y}\right|_{y=0}. \tag{7.14}$$

Substituting (7.7), (7.8) and (7.14) into (7.13), we obtain the terms for the skin-friction, local Nusselt and Sherwood numbers as follows:

$$\mathrm{Re}_x^{1/2}\, C_f = f''(0),$$

$$\mathrm{Re}_x^{-1/2}\, Nu = -(1 + 4Rd/3)\theta'(0), \tag{7.15}$$

$$\mathrm{Re}_x^{-1/2}\, Sh = -\phi'(0).$$

7.3 Method of solution

7.3.1 Analytical Solution by HAM

The analytical solutions of the equations (7.9b)-(7.11b) along with the boundary conditions (7.12) are obtained by homotopy analysis method (HAM). The initial approximations for homotopy analysis solutions are chosen as

$$f_0(\eta) = \eta + \frac{e^{-\eta}}{1+b} - \frac{1}{1+b},$$

$$\theta_0(\eta) = e^{-\eta},$$

$$\phi_0(\eta) = e^{-\eta},$$

the auxiliary linear operators L_f, L_θ and L_ϕ as

$$L_f = f''' - f',$$

$$L_\theta = \theta'' - \theta,$$

$$L_\phi = \phi'' - \phi,$$

satisfying the following properties

$$L_f\left[C_1 + C_2 e^{\eta} + C_3 e^{-\eta}\right] = 0,$$

$$L_\theta\left[C_4 e^{\eta} + C_5 e^{-\eta}\right] = 0,$$

$$L_\phi\left[C_6 e^{\eta} + C_7 e^{-\eta}\right] = 0,$$

where $C_i, (i = 1 - 7)$ denote the arbitrary constants.

The zeroth order deformation problems are

$$(1-p)L_f\left[\bar{f}(\eta,p) - f_0(\eta)\right] = p h_f N_f\left[\bar{f}(\eta,p), \bar{\theta}(\eta,p), \bar{\phi}(\eta,p)\right],$$

$$(1-p)L_\theta\left[\bar{\theta}(\eta,p) - \theta_0(\eta)\right] = p h_\theta N_\theta\left[\bar{f}(\eta,p), \bar{\theta}(\eta,p), \bar{\phi}(\eta,p)\right],$$

$$(1-p)L_\phi\left[\bar{\phi}(\eta,p) - \phi(\eta)\right] = p h_\phi N_\phi\left[\bar{f}(\eta,p), \bar{\theta}(\eta,p), \bar{\phi}(\eta,p)\right],$$

$$\bar{f}(0,p) = 0,\ \bar{f}'(0,p) = b\bar{f}''(0,p),\ \bar{f}'(\infty,p) = 1,$$

$$\bar{\theta}(0,p) = 1,\ \bar{\theta}(\infty,p) = 0,\ \bar{\phi}(0,p) = 1,\ \bar{\phi}(\infty,p) = 0.$$

The m^{th}-order deformation problem is of the form

$$L_f\left[f_m(\eta) - \chi_m f_{m-1}(\eta)\right] = h_f R_m^f(\eta), \tag{7.16}$$

$$L_\theta\left[\theta_m(\eta) - \chi_m \theta_{m-1}(\eta)\right] = h_\theta R_m^\theta(\eta), \tag{7.17}$$

$$L_\phi\left[\phi_m(\eta) - \chi_m \phi_{m-1}(\eta)\right] = h_\phi R_m^\phi(\eta), \tag{7.18}$$

and

$$f_m(0) = 0,\ f_m'(0) = b f_m''(0), \theta_m(0) = 0, \phi_m(0) = 0,\ f_m'(\infty) = 0, \theta_m(\infty) = 0, \phi_m(\infty) = 0.$$

where

$$R_m^f(\eta) = f_{m-1}'''(\eta) + \sum_{k=0}^{m-1}\left(f_{m-1-k}(\eta) f_k''(\eta) - f_{m-1-k}'(\eta) f_k'(\eta)\right) + Ri_T\theta + Ri_C\phi$$
$$-(K+M) f_{m-1}'(\eta) + (K+M+1)(1-\chi_m),$$

$$R_m^\theta(\eta) = \left(1 + \frac{4}{3}Rd\right)\theta_{m-1}''(\eta) + \Pr\sum_{k=0}^{m-1} f_{m-1-k}(\eta)\theta_k'(\eta) + S\theta_{m-1}(\eta),$$

$$R_m^\phi(\eta) = \phi_{m-1}''(\eta) + \Pr\sum_{k=0}^{m-1} f_{m-1-k}(\eta)\phi_k'(\eta) - ScCr\phi,$$

and

$$\chi_m = \begin{cases} 0, & m \le 1 \\ 1, & m > 1. \end{cases}$$

The general solution of Equations (8.16)-(8.18) is

$$f_m(\eta) = f_m^*(\eta) + C_1 + C_2\eta + C_3 e^{-\eta},$$

$$\theta_m(\eta) = \theta_m^*(\eta) + C_4 e^{\eta} + C_5 e^{-\eta},$$

$$\phi_m(\eta) = \phi_m^*(\eta) + C_6 e^{\eta} + C_7 e^{-\eta},$$

where $f_m^*(\eta)$, $\theta_m^*(\eta)$ and $\phi_m^*(\eta)$ are the special solutions. The numerical calculations are obtained by MATLAB. Figure 7.1 indicates that the respective admissible values of h_f, h_θ and h_ϕ are $-0.5 \le h_f \le -0.2$ and $-0.6 \le h_\theta, h_\phi \le -0.2$. We choose the values of auxiliary parameter (h=-0.35) from this range, we will get the more accurate results.

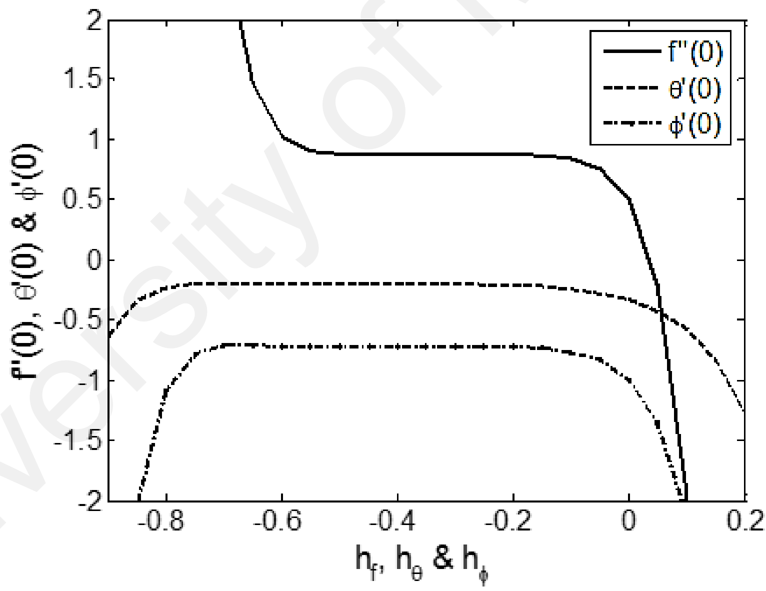

Figure 7.1. h curves for $f''(0), \theta'(0)$ and $\phi'(0)$

7.3.2 Numerical solution

The coupled equations (7.9b)-(7.11b) along with the boundary conditions (7.12) are transformed into the differential equations of linear by significant dependent variables of first order. Using shooting method by reasonable initial predict values for $f''(0), \theta'(0)$ and $\phi'(0)$ to gratify at $f'(\infty), \theta(\infty)$ and $\phi(\infty)$ with the boundary conditions respectively. The standards of f'', θ' and ϕ' are not cited in the boundary conditions (7.12). The coupled linear differential equations of first-order system are integrated using Runge–Kutta–Fehlberg method from η =0 to $\eta = \eta_{max}$ by taking consecutive steps $\Delta\eta$. The presumed initial values of $f''(0), \theta'(0)$ and $\phi'(0)$ are compared with measured values of $f''(0), \theta'(0)$ and $\phi'(0)$ at $\eta = \eta_{max}$. If a difference exists, assume another set of primary values for $f''(0), \theta'(0), \phi'(0)$ and the procedure is repeated. This process is repeated until the agreement between value obtained and the measured values at $\eta=\eta_{max}$ is within the set tolerance.

Therefore, it can be concluded that the present numerical study results can be used with great confidence and stable to study the problem discussed in this paper. The analytical and numerical procedure exactness of our work is directly matching with the earlier circulated data as shown in Table 3.1. This affords confidence on our numerical results to be reported subsequently.

7.4 Results and Discussion

Analytical solution by using HAM and numerical solution by using shooting method were obtained for different values of radiation, chemical reaction and velocity slip parameters. The values of the parameters Ri_T=0.2, Ri_c=0.2, Mp=2.0, Pr=7.2 and Sc=1 are fixed throughout the study.

Tables 7.1-7.3 depict the values of $f''(0), -\theta'(0)$ and $-\phi'(0)$ from the analytical and numerical methods. Table 7.1 depicts that skin friction increases on increasing the internal heat generation (S) and radiation (Rd) parameters. It is inferred that the skin friction decreases on increasing the chemical reaction (Cr) and slip (b) parameters. Tables 7.2 and 7.3 show that the heat transfer rate decreases and the mass transfer rate increases on increasing S, Rd and Cr parameters. It is noticed that the mass and heat transfer rates increase on increasing the slip parameter (b).

Table 7.1. Analytical and numerical solutions for various values of $f''(0)$ when Ri_T=2.0, Ri_c=2.0, K=1, M=1, Pr=7.2 and Sc=1.0.

S	*Rd*	*Cr*	*b*	*f″(0)*		*Error* (%)
				HAM	*RK4*	
-1.5	1.0	0.5	0.4	1.741935	1.742816	0.05055
-1.0				1.745303	1.746196	0.05114
0.0				1.748974	1.749733	0.04338
1.0				1.752804	1.753440	0.03627
1.5				1.756711	1.757330	0.03522
0.5	0.0	0.5	0.4	1.696237	1.697773	0.09047
	0.3			1.718371	1.719537	0.06780
	0.5			1.731982	1.731025	0.05528
	0.8			1.744971	1.745330	0.02057
	1.5			1.770112	1.770255	0.08078
	2.0			1.782315	1.783635	0.07400
0.5	1.0	-2.0	0.4	2.061214	2.060439	0.03761
		-1.5		1.925079	1.924475	0.03139
		-0.5		1.805891	1.805358	0.02952
		0		1.774912	1.775401	0.02754
		0.5		1.752906	1.753440	0.03045
		1.5		1.723012	1.722443	0.03303
		2.0		1.711073	1.710801	0.01589
0.5	1.0	0.5	0.0	3.158507	3.157450	0.03347
			0.2	2.273258	2.272768	0.02156
			0.6	1.422014	1.421517	0.03496
			0.8	1.194172	1.193269	0.07567
			1.0	1.028569	1.027359	0.11777

Figure 7.2(a) illustrates that profiles of velocity along the boundary layer for Rd=0.3, S=1.5, Cr=0.3 and different values of slip parameter. The velocity increases as the slip parameter is increased. The boundary layer thickness increases when the slip parameter is increased. Figures 7.2 (b&c) show the influence of slip parameter on temperature as well as concentration, respectively. These two profiles decrease on increasing the slip parameter. This is the reason that the viscosity decreases in the medium or the free stream velocity increases, and it results the thermal and solutal boundary layer thickness decrease.

The velocity and temperature profiles for various values of radiation parameter (Rd) are illustrated in Figures 7.3 (a&b). As the radiation increases, the velocity as well as temperature increase significantly. The thickness of the thermal boundary layer increase on increasing the radiation parameter because the intensity of the electro-magnetic radiation in the medium decreases as well as the Stefan-Boltzmann constant of the medium increases.

Table 7.2. Analytical and numerical solutions for various values of $-\theta'(0)$ when K=1, M=1, Pr=7.2 and Sc=1.0.

S	*Rd*	*Cr*	*b*	$-\theta'(0)$		*Error* (%)
				HAM	*RK4*	
-1.5	1.0	0.5	0.4	1.503127	1.502298	0.05518
-1.0				1.439975	1.439975	0.00000
0.0				1.375810	1.375810	0.00000
1.0				1.309663	1.309663	0.00000
1.5				1.241382	1.241382	0.00000
0.5	0.0	0.5	0.4	1.912091	1.911775	0.01653
	0.3			1.646183	1.645690	0.02995
	0.5			1.523071	1.522510	0.03684
	0.8			1.383101	1.382877	0.01619
	1.5			1.169021	1.169727	0.06035
	2.0			1.068943	1.068377	0.05297
0.5	1.0	-2.0	0.4	1.445169	1.444713	0.03156
		-1.5		1.387088	1.386636	0.03259
		-0.5		1.334001	1.333199	0.06015
		0		1.319987	1.319596	0.02963
		0.5		1.309897	1.309663	0.01786
		1.5		1.296015	1.295783	0.01790
		2.0		1.291136	1.290635	0.03881
0.5	1.0	0.5	0.0	1.018166	1.017375	0.07775
			0.2	1.209972	1.209753	0.01810
			0.6	1.370195	1.369418	0.05673
			0.8	1.409185	1.408859	0.02313
			1.0	1.437043	1.436746	0.02067

Figures 7.4 (a&b) depicts the chemical reaction effect on both the velocity and concentration profiles along the surface for constant values of radiation (Rd=1.0), internal heat generation (S=1.0), and the slip parameter (b=0.4). The velocity and concentration increase on increasing the chemical reaction parameter. The concentration profile

overshoots in the generative chemical reaction case, that is, the negative values of the chemical reaction parameter.

Table 7.3. Analytical and numerical solutions for various values of $-\phi'(0)$ when K=1, M=1, Pr=7.2 and Sc=1.0.

S	Rd	Cr	b	$-\phi'(0)$		*Error* (%)
				HAM	*RK4*	
-1.5	1.0	0.5	0.4	1.044089	1.043630	0.04398
-1.0				1.045321	1.044155	0.11166
0.0				1.045172	1.044706	0.04460
1.0				1.046004	1.045285	0.06878
1.5				1.046148	1.045894	0.02428
0.5	0.0	0.5	0.4	1.036874	1.036006	0.08378
	0.3			1.039876	1.039445	0.04146
	0.5			1.042083	1.041357	0.06971
	0.8			1.044115	1.043834	0.02692
	1.5			1.049270	1.048402	0.08279
	2.0			1.051298	1.050986	0.02968
0.5	1.0	-2.0	0.4	-1.559173	-1.564133	0.31710
		-1.5		-0.489101	-0.490619	0.30940
		-0.5		0.513916	0.514218	0.05872
		0		0.808952	0.808147	0.09961
		0.5		1.046013	1.045285	0.06964
		1.5		1.425416	1.424446	0.06809
		2.0		1.585091	1.584309	0.04935
0.5	1	0.5	0.0	0.949062	0.948406	0.06916
			0.2	1.012067	1.011676	0.03864
			0.6	1.066135	1.065652	0.04532
			0.8	1.079006	1.079208	0.01871
			1.0	1.089222	1.088848	0.03434

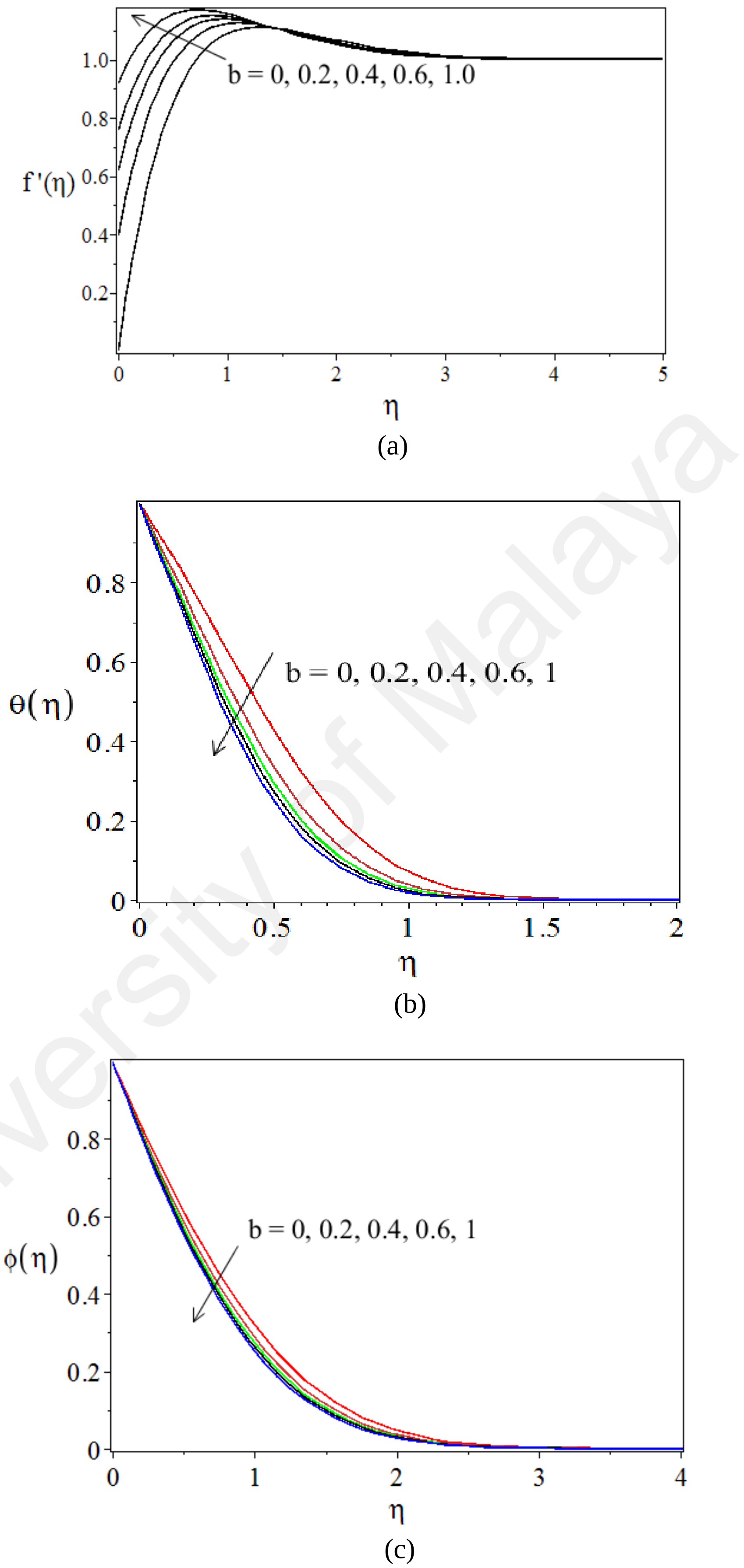

Figure 7.2. Velocity (a), Temperature (b) and Concentration (c) profiles for different values of slip parameters (b) with S= 1.5; Rd=0.3; Cr=0.3.

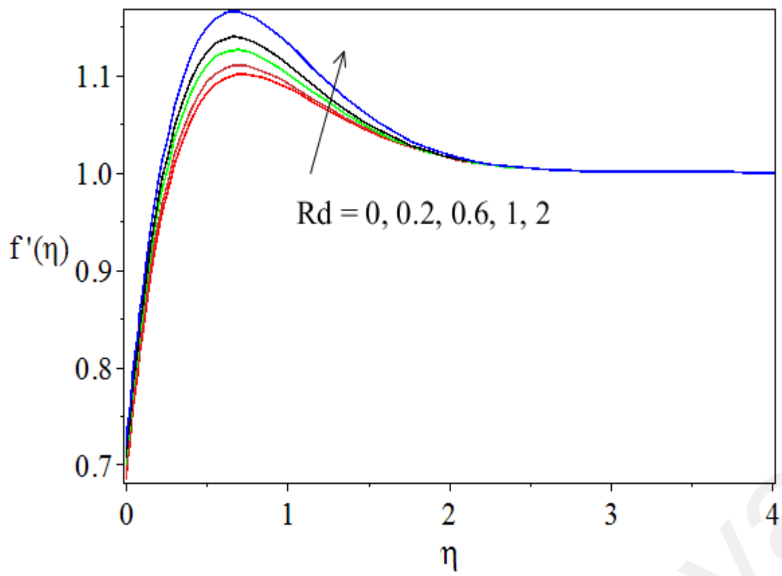

(a)

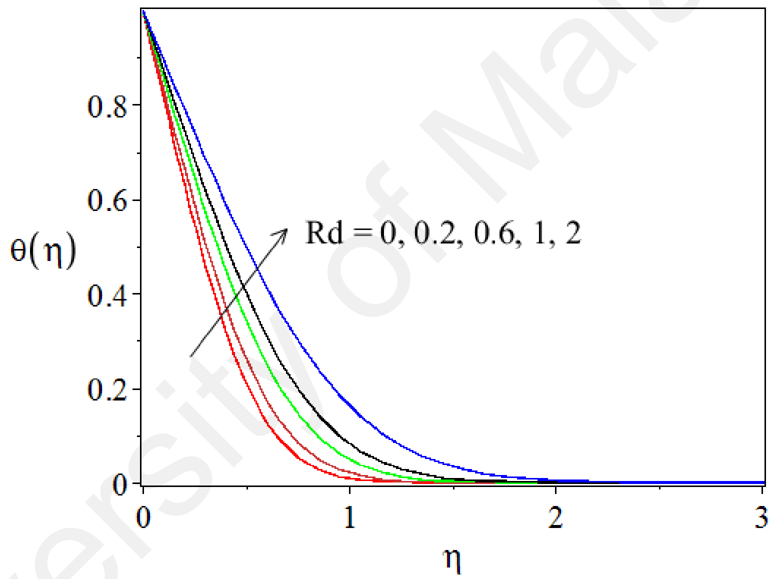

(b)

Figure 7.3. Velocity (a) and Temperature (b) profiles for different values of radiation parameters (*Rd*) with S=1.0, Cr=0.3, b=0.4.

It can observed from Figure 7.5 (a-c) that the local skin friction decreases on increasing the chemical reaction parameter and slip parameter. As the radiation increases, local skin friction increases due to temperature gradient causes in the fluid. In Figure 7.6 (a-c), it is interesting to note that Nusselt number increases on increasing the slip and radiation parameters. However, as the chemical reaction parameter increases, the local Nusselt number decreases. It is interesting to note that the local heat transfer rate decreases on increasing the internal heat generation parameter. Figure 7.7 (a-c) shows that the local Sherwood number increases on increasing the chemical reaction, radiation and slip parameters. Further scrutinizing these figures, it is found that the local mass transfer rate increases with slip parameter. However, the effect of internal heat generation on local mass transfer rate is negligible.

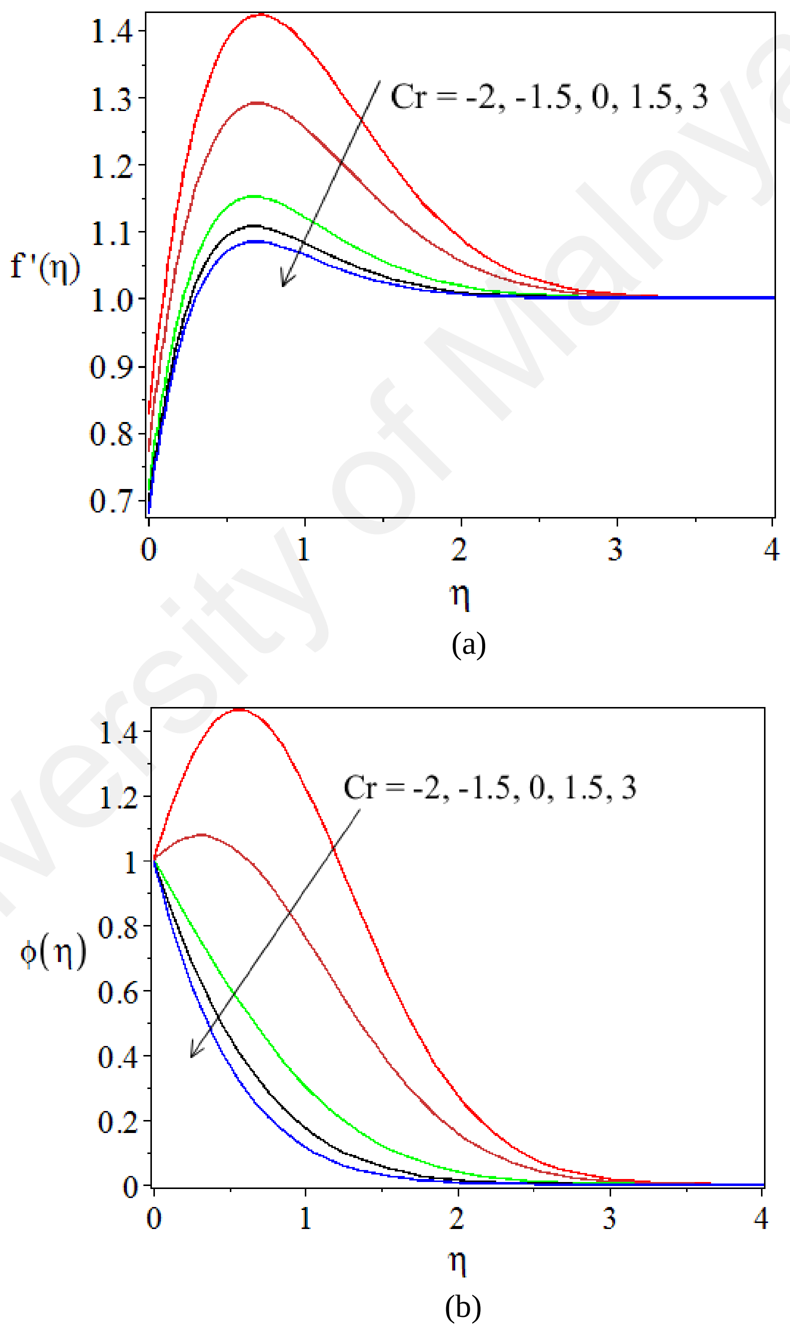

Figure 7.4. Velocity (a) and Concentration (b) profiles for different values of chemical reaction parameters (*Cr*) with S= 1.0, Rd= 1.0, b=0.4.

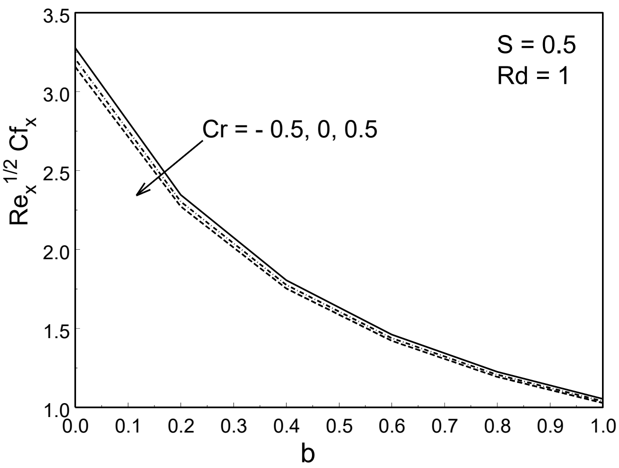

(a)

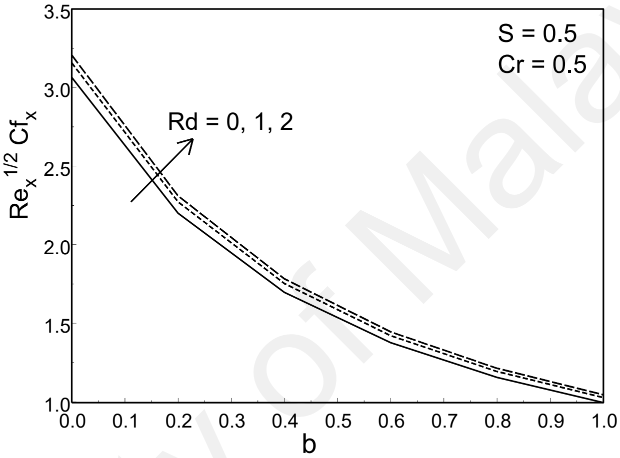

(b)

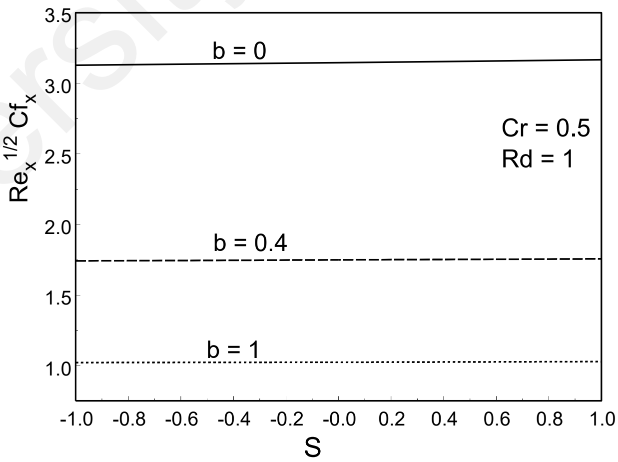

(c)

Figure 7.5. Local Skin friction for different (a) chemical reaction parameters (Cr) with S=0.5, Rd=1.0, (b) radiation parameters (Rd) with S=0.5, Cr=0.5 and (c) slip parameters (b) with Cr=0.5, Rd=1.0.

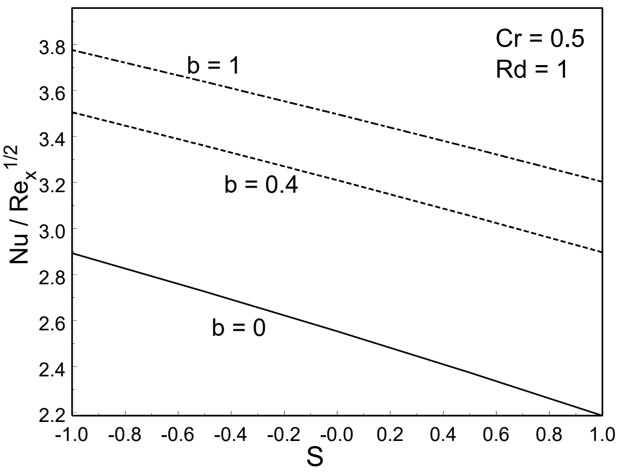

(a)

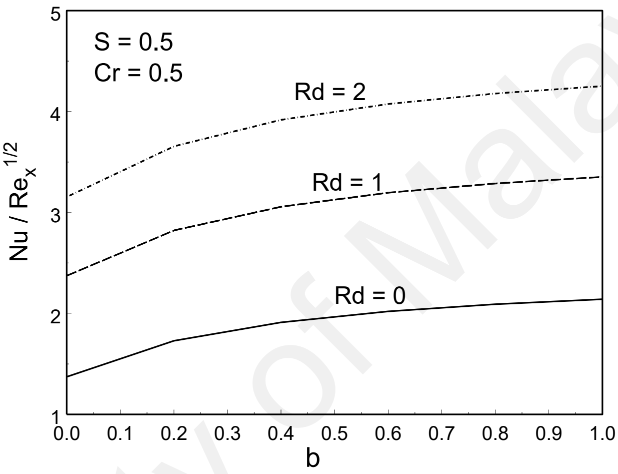

(b)

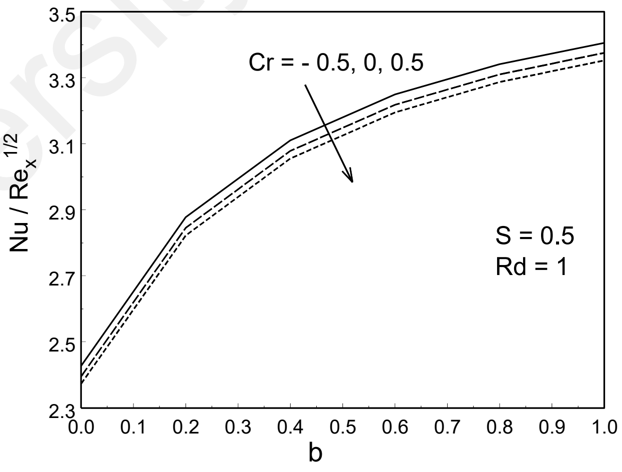

(c)

Figure 7.6. Local Nusselt numbers for different (a) slip parameters (b) with Cr=0.5, Rd=1.0, (b) radiation parameters (Rd) with S=0.5, Cr=0.5 and (c) chemical reaction parameters (Cr) with S=0.5, Rd=1.0.

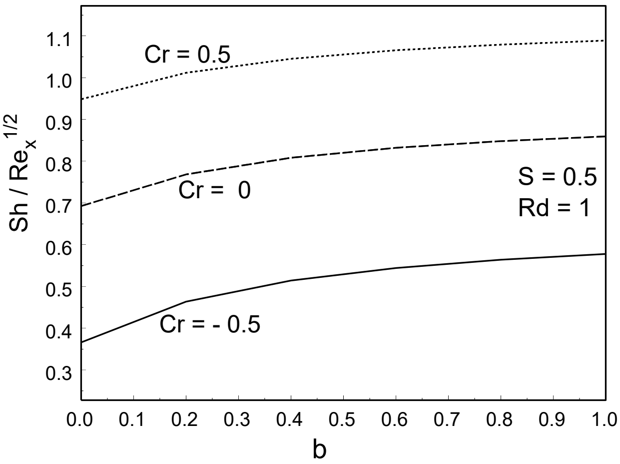

(a)

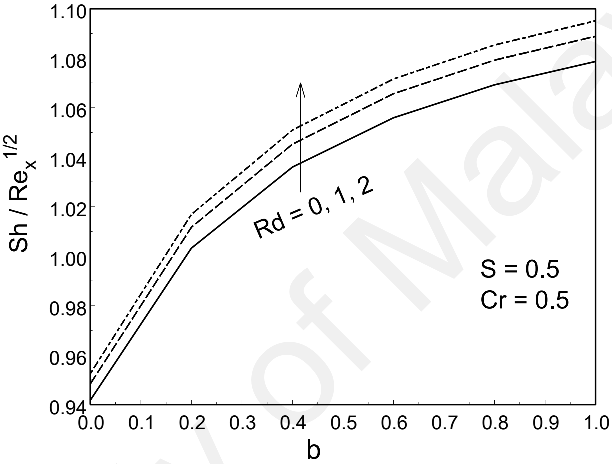

(b)

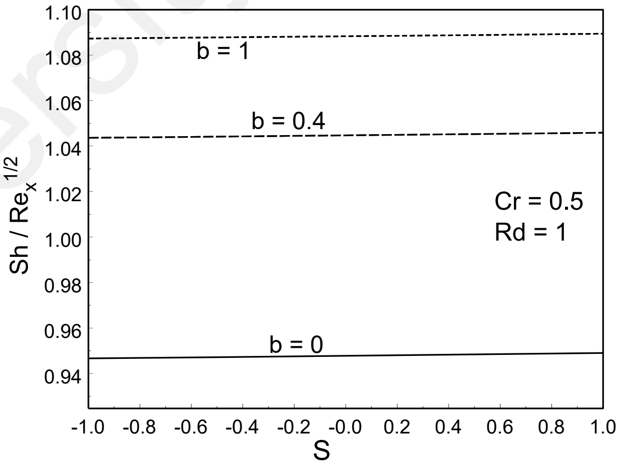

(c)

Figure 7.7. Local Sherwood numbers for different (a) chemical reaction parameters (Cr) with S=0.5, Rd=1.0, (b) radiation parameters (Rd) with S=0.5, Cr=0.5 and (c) slip parameters (b) with Cr=0.5, Rd=1.0.

CHAPTER 8: EFFECTS OF SLIP AND NEWTONIAN HEATING ON MHD MIXED CONVECTION STAGNATION-POINT FLOW OF CHEMICALLY REACTING FLUID IN A POROUS MEDIUM WITH RADIATION

8.1 Introduction

The role of magneto-convection stagnation-point flow is significant due to enormous applications in engineering fields such as industrial manufacturing, geothermal, transpiration cooling and thermal oil recovery. MHD and radiation are important in various fields of engineering, industrial, plasma, power generators and control of boundary layer flow. The chemical reaction effects on heat and mass transfer have widespread applications in chemical technology industries such as food processing, production of polymers, hydrometallurgical industries and enhanced oil recovery. Many researchers have done a large amount of research work on the effect of chemical reaction on convective flow over a vertical plate. Much research has been investigating the effects of different boundary conditions under the influence of several effects.

Motivated by the work of Makinde and Aziz (2010) and others, we have attempted here to present a numerical study with including by all these above mentioned effects. The main objective of this paper is to analyze the effects of slip, convective boundary conditions, chemical reaction and radiation on mixed convection flow of a viscous fluid near a stagnation point towards a vertical plate in a porous medium. The present study extends the work of chapter 5 and 7 to include the convective boundary condition.

8.2 Mathematical Modeling

Consider a steady, laminar, two-dimensional boundary layer flow of an incompressible electrically conducting viscous fluid in a stagnation point along a vertical plate in the presence of magnetic field using slip and convective boundary conditions. Chemically reactive species undergoing chemical reaction with first order is considered. Along the y-axis the magnetic field of constant strength is imposed. The induced magnetic field is negligible as the magnetic Reynolds number is assumed to be small. The physical model and coordinate systems are shown in Figure 3.1. It assumed that the velocity distribution in the viscous flow region is $U_\infty = cx$, where c is a positive constant. The fluid is assumed to be homogeneous in porous medium, isotropic and in thermodynamic equilibrium. We consider Darcy's law for fluid flow with heat transfer due to natural convection in a porous medium. Thus, the governing equations of continuity, momentum, energy and species concentration are expressed by

$$\frac{\partial u}{\partial x}+\frac{\partial v}{\partial y}=0, \tag{8.1}$$

$$u\frac{\partial u}{\partial x}+v\frac{\partial u}{\partial y}=\upsilon\frac{\partial^2 u}{\partial y^2}+g\beta(T-T_\infty)+g\beta^*(C-C_\infty)-\left(\frac{\sigma_e B_0{}^2}{\rho}+\frac{\upsilon}{\tilde{K}}\right)(u-U_\infty)+U_\infty\frac{dU_\infty}{dx}, \tag{8.2}$$

$$u\frac{\partial T}{\partial x}+v\frac{\partial T}{\partial y}=\alpha\frac{\partial^2 T}{\partial y^2}-\frac{\alpha}{k}\frac{\partial q_r}{\partial y}+\frac{Q(T-T_\infty)}{\rho c_p}, \tag{8.3}$$

$$u\frac{\partial C}{\partial x}+v\frac{\partial C}{\partial y}=D\frac{\partial^2 C}{\partial y^2}-\Gamma_0(C-C_\infty), \tag{8.4}$$

subject to the boundary conditions

$$u=N_1\frac{\partial u}{\partial y},\ v=0,\ -k\frac{\partial T}{\partial y}=h_f(T_f-T),\ C=C_w \text{ at } y=0,$$

$$u\to U_\infty=cx,\ T\to T_\infty,\ C\to C_\infty \text{ as } y\to\infty. \tag{8.5}$$

where u and v are the velocity components in the x and y axes. We take the x-axis along the surface and the y-axis is normal to it. T is the temperature of the fluid, υ (=μ/ρ) kinematic viscosity of fluid, k is the thermal conductivity, respectively. The heat flux due to radiation is given by

$$q_r=-\frac{4\sigma^*\partial T^4}{3K'\partial y}. \tag{8.6}$$

The differences in temperature within the flow are assumed to be too small by the Rosseland approximation for radiation. We can express the term T^4 as a linear function of temperature using Taylor's series. Then, T^4 expanded about T_∞ and neglecting higher order terms, it may be shown as a linear function of temperature T,

i.e., $T^4 = T_\infty^4 + 4T_\infty^3(T - T_\infty) + ...$ then $T^4 \approx 4T_\infty^3 T - 3T_\infty^4$.

Finally, we get

$$q_r = -\frac{16\sigma^* T_\infty^3}{3K'}\frac{\partial T}{\partial y}. \tag{8.7}$$

We introduce the following non-dimensional variables:

$$\eta = y\sqrt{\frac{c}{\upsilon}},\quad \psi(x,y) = \sqrt{\upsilon c}\,x f(\eta),\quad b = N_1\left(\frac{c}{\upsilon}\right)^{1/2},\quad Bi = \frac{h\left(\frac{\nu}{a}\right)^{\frac{1}{2}}}{k},\quad Cr = \frac{\Gamma_0}{c},\quad \theta(\eta) = \frac{T - T_\infty}{T_\omega - T_\infty},$$

$$\phi(\eta) = \frac{C - C_\infty}{C_\omega - C_\infty},\quad Gr_T = \frac{g\beta(T_\omega - T_\infty)x^3}{\upsilon^2},\quad Gr_c = \frac{g\beta^*(C_\omega - C_\infty)x^3}{\upsilon^2},\quad Ri_T = \frac{Gr_T}{\mathrm{Re}_x^2},\quad Ri_C = \frac{Gr_c}{\mathrm{Re}_x^2},$$

$$\mathrm{Re}_x = \frac{U_\infty x}{\upsilon},\ Rd = \frac{4\sigma^* T_\infty^3}{kK'},\ K = \frac{\upsilon}{c\tilde{K}},\ \Pr = \frac{\upsilon}{\alpha},\ Sc = \frac{\upsilon}{D},\ M = \frac{\sigma_e B_0^2}{c\rho},\ S = \frac{Q\upsilon}{\alpha c}. \tag{8.8}$$

We define the stream function (ψ) as $u = \partial\psi/\partial y$ and $\upsilon = -\partial\psi/\partial x$, so that the continuity equation (8.1) is identically satisfied. η is the similarity variable. Substituting the expression in (8.7) together with the variables in (8.8) into (8.1)-(8.4), we obtain the following ordinary differential equations:

$$f''' + ff'' - f'^2 + Ri_T\theta + Ri_c\phi - (K + M)(f' - 1) + 1 = 0, \tag{8.9}$$

$$\left(1 + \frac{4}{3}Rd\right)\theta'' + \Pr f\theta' + S\theta = 0, \tag{8.10}$$

$$\phi'' + Scf\phi' - ScCr\phi = 0. \tag{8.11}$$

The corresponding boundary conditions (8.5) are

$$f=0,\quad f' = bf''(0),\quad \theta' = Bi[1 - \theta(0)],\ \phi = 1 \ \text{as}\ \eta = 0,$$

$$f' = 1,\quad \theta = 0,\quad \phi = 0,\ \text{as}\quad \eta \to \infty. \tag{8.12}$$

The system of coupled non-linear ordinary differential equations (8.9)-(8.11) along with boundary conditions (8.12) was solved by analytically HAM and numerically using shooting technique along with Runge–Kutta method. The physical quantities describing the skin friction (C_f), heat transfer (Nu) and mass transfer rates (Sh) are shown below,

$$C_f = \frac{2\tau_\omega}{\rho U_\infty^2}, \qquad Nu = \frac{xq_\omega}{k(T_\omega - T_\infty)}, \qquad Sh = \frac{xq_m}{D(C_\omega - C_\infty)}, \tag{8.13}$$

where,

$$\tau_\omega = \mu \left.\frac{\partial u}{\partial y}\right|_{y=0}, \; q_\omega = -k\left.\frac{\partial T}{\partial y}\right|_{y=0} - \frac{4\sigma^*}{3K'}\left.\frac{\partial T^4}{\partial y}\right|_{y=0}, \; q_m = -D\left.\frac{\partial C}{\partial y}\right|_{y=0}. \tag{8.14}$$

Substituting (8.7), (8.8) and (8.14) into (8.13), we obtain the expressions for drag force on the plate in terms of skin-friction coefficient, the rate of heat transfer in terms of local Nusselt number and the rate of mass transfer in terms of Sherwood number as follows:

$$\mathrm{Re}_x^{1/2} C_f = f''(0),$$

$$\mathrm{Re}_x^{-1/2} Nu = -(1 + 4Rd/3)\theta'(0), \tag{8.15}$$

$$\mathrm{Re}_x^{-1/2} Sh = -\phi'(0).$$

8.3 Method of solution

8.3.1 Analytical Solution by HAM

The analytical solutions of the equations (8.9)-(8.11) along with the boundary conditions (8.12) are obtained by homotopy analysis method (HAM). The initial approximations for homotopy analysis solutions are chosen as

$$f_0(\eta) = \eta + \frac{e^{-\eta}}{1+b} - \frac{1}{1+b},$$

$$\theta_0(\eta) = e^{-\eta},$$

$$\phi_0(\eta) = e^{-\eta}.$$

the auxiliary linear operators L_f, L_θ and L_ϕ as

$$L_f = f''' - f',$$

$$L_\theta = \theta'' - \theta,$$

$$L_\phi = \phi'' - \phi.$$

with satisfying the following properties

$$L_f\left[C_1 + C_2 e^{\eta} + C_3 e^{-\eta}\right] = 0,$$

$$L_\theta\left[C_4 e^{\eta} + C_5 e^{-\eta}\right] = 0,$$

$$L_\phi\left[C_6 e^{\eta} + C_7 e^{-\eta}\right] = 0.$$

where $C_i, (i = 1 - 7)$ denote the arbitrary constants.

The zero[th] order deformation problems are

$$(1-p)L_f\left[\bar{f}(\eta,p) - f_0(\eta)\right] = p h_f N_f\left[\bar{f}(\eta,p), \bar{\theta}(\eta,p), \bar{\phi}(\eta,p)\right],$$

$$(1-p)L_\theta\left[\bar{\theta}(\eta,p) - \theta_0(\eta)\right] = p h_\theta N_\theta\left[\bar{f}(\eta,p), \bar{\theta}(\eta,p), \bar{\phi}(\eta,p)\right],$$

$$(1-p)L_\phi\left[\bar{\phi}(\eta,p) - \phi(\eta)\right] = p h_\phi N_\phi\left[\bar{f}(\eta,p), \bar{\theta}(\eta,p), \bar{\phi}(\eta,p)\right],$$

$$\bar{f}(0,p) = 0,\ \bar{f}'(0,p) = b\bar{f}''(0,p),\ \bar{f}'(\infty,p) = 1,$$

$$\bar{\theta}(0,p) = 1,\ \bar{\theta}(\infty,p) = 0,\ \bar{\phi}(0,p) = 1,\ \bar{\phi}(\infty,p) = 0,$$

The m^{th}-order deformation problem is of the form

$$L_f\left[f_m(\eta) - \chi_m f_{m-1}(\eta)\right] = h_f R_m^f(\eta), \tag{8.16}$$

$$L_\theta\left[\theta_m(\eta) - \chi_m \theta_{m-1}(\eta)\right] = h_\theta R_m^\theta(\eta), \tag{8.17}$$

$$L_\phi\left[\phi_m(\eta) - \chi_m \phi_{m-1}(\eta)\right] = h_\phi R_m^\phi(\eta). \tag{8.18}$$

$$f_m(0) = 0,\ f_m'(0) = b f_m''(0), \theta_m(0) = 0, \phi_m(0) = 0,\ f_m'(\infty) = 0, \theta_m(\infty) = 0, \phi_m(\infty) = 0,$$

where

$$R_m^f(\eta) = f_{m-1}'''(\eta) + \sum_{k=0}^{m-1}\left(f_{m-1-k}(\eta) f_k''(\eta) - f_{m-1-k}'(\eta) f_k'(\eta)\right) + Ri_T\theta + Ri_C\phi$$
$$-(K+M) f_{m-1}'(\eta) + (K+M+1)(1-\chi_m),$$

$$R_m^\theta(\eta) = \left(1 + \frac{4}{3}Rd\right)\theta_{m-1}''(\eta) + \Pr\sum_{k=0}^{m-1} f_{m-1-k}(\eta)\theta_k'(\eta) + S\theta_{m-1}(\eta),$$

$$R_m^\phi(\eta) = \phi_{m-1}''(\eta) + \Pr\sum_{k=0}^{m-1} f_{m-1-k}(\eta)\phi_k'(\eta) - ScCr\phi,$$

and

$$\chi_m = \begin{cases} 0, & m \leq 1 \\ 1, & m > 1. \end{cases}$$

The general solution of Equations (8.16)-(8.18) is

$$f_m(\eta) = f_m^*(\eta) + C_1 + C_2\eta + C_3 e^{-\eta},$$

$$\theta_m(\eta) = \theta_m^*(\eta) + C_4 e^{\eta} + C_5 e^{-\eta},$$

$$\phi_m(\eta) = \phi_m^*(\eta) + C_6 e^{\eta} + C_7 e^{-\eta},$$

where $f_m^*(\eta)$, $\theta_m^*(\eta)$ and $\phi_m^*(\eta)$ are the special solutions. The numerical calculations are obtained by MATLAB. Figure 8.1 indicates that the respective admissible values of h_f, h_θ and h_ϕ are $-0.5 \leq h_f \leq -0.2$ and $-0.6 \leq h_\theta, h_\phi \leq -0.2$. We choose the values of auxiliary parameter (h=-0.35) from this range, we will get the more accurate results.

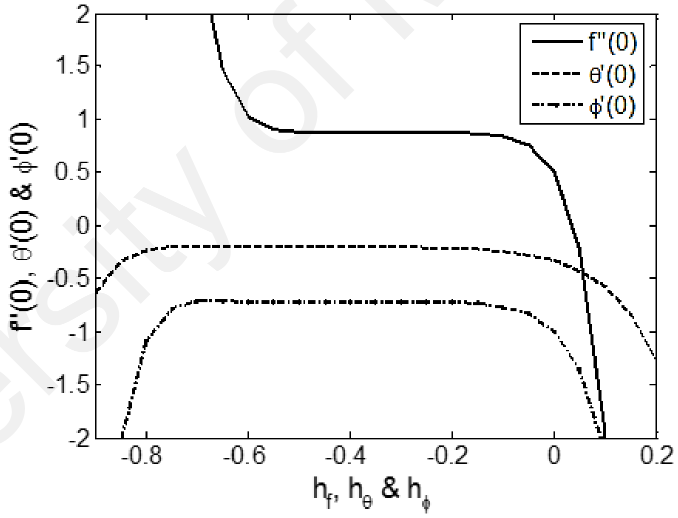

Figure 8.1. h curves for $f''(0), \theta'(0)$ and $\phi'(0)$

8.3.2 Numerical solution

The coupled equations (8.9)-(8.11) along with the boundary conditions (8.12) are transformed into the differential equations of linear by significant dependent variables of first order. Using shooting method by reasonable initial predict values for $f''(0), \theta'(0)$ and $\phi'(0)$ to gratify at $f'(\infty), \theta(\infty)$ and $\phi(\infty)$ with the boundary conditions, respectively. The standards of f'', θ' and ϕ' are not cited in the boundary conditions (8.12). The coupled linear differential equations of first order system are integrated using Runge–Kutta–Fehlberg method from η =0 to $\eta = \eta_{max}$ by taking consecutive steps $\Delta\eta$. The presumed initial values of $f''(0), \theta'(0)$ and $\phi'(0)$ are compared with measured values of $f''(0), \theta'(0)$ and $\phi'(0)$ at $\eta=\eta_{max}$. If the dissimilarity be present, assume another set of primary values for $f''(0), \theta'(0), \phi'(0)$ and the procedure is repeated. This process is continual up to the arrangement between considered value and the agreed condition at $\eta=\eta_{max}$ with in the degree of exactness.

Therefore, it can be concluded that the present numerical study results can be used with great confidence and stable to study the problem discussed in this paper. The analytical and numerical procedure exactness of our work is directly matching with the earlier circulated data as shown in Table 3.1. This affords confidence on our numerical results to be reported subsequently.

8.4 Results and Discussion

This section describes the analytical and numerical scheme obtained results of some interesting parameters for velocity, temperature and concentration profiles. The skin friction, local heat and mass transfer rates for various values of non-dimensional parameters as shown in Table 8.1, 8.2 and 8.3. The skin friction increases on increasing the radiation, internal heat generation, Biot number. The skin friction decreases on increasing the values of slip, chemical reaction parameters. The heat transfer rate decreases on increasing the *S, Rd* and *Cr* parameters and it increases on increasing *b, Bi* parameters. The effect of mass transfer rate increases on increasing *S, Rd, Cr, b, Bi* parameters.

Table 8.1. Numerical and analytical (HAM) results for ($f''(0)$) different parameters with Pr =0.7, Sc=0.5, K=0.4, M=0.4 and h=–0.35.

S	*Rd*	*Cr*	*b*	*Bi*	*f''(0)*		*Error (%)*
					RK4	*HAM*	
-1.2	0.4	0.4	1.0	0.5	0.82645	0.82645	0.00
-0.6					0.83648	0.83648	0.00
0.0					0.85549	0.85552	0.00
0.6					0.90962	0.90771	0.21
1.2					1.21815	1.21360	0.37
0.4	0	0.4	1.0	0.5	0.87016	0.86939	0.09
	0.2				0.87728	0.87676	0.06
	0.5				0.88546	0.88541	0.01
	0.7				0.88970	0.89007	0.04
	1.0				0.89474	0.89593	0.13
0.4	0.4	-1.5	1.0	0.5	0.94253	0.94404	0.16
		-0.5			0.89987	0.90021	0.04
		0			0.88937	0.88930	0.01
		0.5			0.88162	0.88136	0.03
		1.5			0.87056	0.87014	0.05
0.4	0.4	0.4	0	0.5	2.34676	2.33677	0.43
			0.3		1.60255	1.60106	0.09
			0.5		1.30538	1.30472	0.05
			0.7		1.09722	1.09684	0.03
			1.0		0.88301	0.88278	0.03
0.4	0.4	0.4	1.0	0.2	0.84893	0.84724	0.20
				0.4	0.87488	0.87436	0.06
				0.6	0.88936	0.88930	0.01
				0.8	0.89866	0.89877	0.01
				1.0	0.90517	0.90533	0.02

Figure 8.2(a) depicts the velocity behavior along the boundary layer for different values of heat generation parameter with constant values of *K, M, Rd, Cr, b, Bi*. It is observed that the fluid velocity is increased with increase in the values of internal heat generation parameter. In the case of heat absorption (S<0), the effect of this parameter on velocity of fluid and thickness of boundary layer are very less. The effect of heat generation parameter on velocity of the fluid is very high in the case of heat generation S>0. When S>1, the velocity profile overshoots near the boundary layer. Figure 8.2(b) shows the distribution of temperature for various values of heat generation parameter with

constant value of *K, M, Rd, Cr, b, Bi* parameter. The fluid temperature is high for internal generation parameter due to generation of thermal energy inside the boundary layer. The temperature profile overshoots when $S>1$. The effect of heat absorption on temperature is less in the case $S<0$. The effect of different values of radiation parameter (*Rd*) on velocity and temperature profiles are illustrated in Figures 8.3(a) and 8.3(b) (*K, M, S, Cr, b, Bi* are constants).

Table 8.2. Numerical and analytical (HAM) results for ($-\theta'(0)$) different parameters with Pr=0.7, Sc=0.5, K=0.4, M=0.4 and h=–0.35

S	*Rd*	*Cr*	*b*	*Bi*	$-\theta'(0)$		*Error* (%)
					RK4	*HAM*	
-1.2	0.4	0.4	1.0	0.5	0.33521	0.33521	0.00
-0.6					0.30954	0.30954	0.00
0.0					0.26262	0.26257	0.02
0.6					0.13221	0.13661	3.22
1.2					-0.68917	-0.68443	0.69
0.4	0	0.4	1.0	0.5	0.21915	0.22104	0.86
	0.2				0.20637	0.20755	0.57
	0.5				0.19201	0.19219	0.09
	0.7				0.18470	0.18405	0.35
	1.0				0.17616	0.17393	1.28
0.4	0.4	-1.5	1.0	0.5	0.20813	0.20519	1.43
		-0.5			0.19962	0.19958	0.02
		0			0.19753	0.19788	0.18
		0.5			0.19601	0.19658	0.29
		1.5			0.19392	0.19471	0.41
0.4	0.4	0.4	0	0.5	0.14959	0.15325	2.39
			0.3		0.17752	0.17852	0.56
			0.5		0.18597	0.18667	0.37
			0.7		0.19127	0.19186	0.31
			1.0		0.19628	0.19681	0.27
0.4	0.4	0.4	1.0	0.2	0.12179	0.12325	1.18
				0.4	0.17790	0.17879	0.50
				0.6	0.21092	0.21115	0.11
				0.8	0.23281	0.23261	0.09
				1.0	0.24842	0.24797	0.18

Table 8.3. Numerical and analytical (HAM) results for ($-\phi'(0)$) different parameters with Pr=0.7, Sc=0.5, K=0.4, M=0.4 and h=–0.35

S	*Rd*	*Cr*	*b*	*Bi*	$-\phi'(0)$		*Error (%)*
					RK4	*HAM*	
-1.2	0.4	0.4	1.0	0.5	0.71087	0.71090	0.00
-0.6					0.71308	0.71308	0.00
0.0					0.71739	0.71727	0.02
0.6					0.72992	0.72777	0.30
1.2					0.79782	0.79625	0.20
0.4	0	0.4	1.0	0.5	0.72018	0.71946	0.10
	0.2				0.72213	0.72135	0.11
	0.5				0.72445	0.72370	0.10
	0.7				0.72568	0.72503	0.09
	1.0				0.72717	0.72675	0.06
0.4	0.4	-1.5	1.0	0.5	-0.33571	-0.33588	0.05
		-0.5			0.38275	0.38093	0.48
		0			0.58858	0.58744	0.19
		0.5			0.75464	0.75393	0.09
		1.5			1.02053	1.02002	0.05
0.4	0.4	0.4	0	0.5	0.64440	0.64273	0.26
			0.3		0.68860	0.68743	0.17
			0.5		0.70381	0.70283	0.14
			0.7		0.71386	0.71299	0.12
			1.0		0.72375	0.72297	0.11
0.4	0.4	0.4	1.0	0.2	0.71670	0.71544	0.18
				0.4	0.72207	0.72116	0.13
				0.6	0.72505	0.72439	0.09
				0.8	0.72695	0.72645	0.07
				1.0	0.72828	0.72788	0.05

As the velocity and temperature profiles increase significantly on increasing the radiation parameter (*Rd*). With the increase of radiation parameter, the thermal boundary layer thickness also increases, which is acceptable because the Stefan Boltzmann constant increases and also the intensity of the electro-magnetic radiation also decrease in the medium. Figures 8.4(a) and 8.4(b) depict the velocity and concentration distribution for various values of chemical reaction parameter (*Cr*) (*K*, *M*, *Rd*, *S*, *b*, *Bi* are constants).

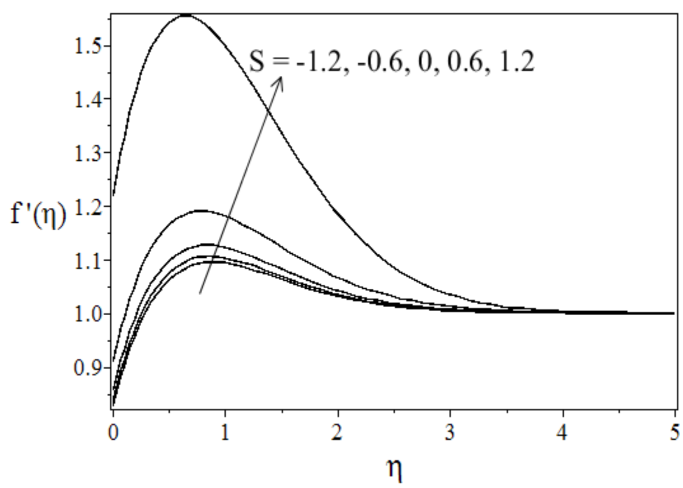

(a)

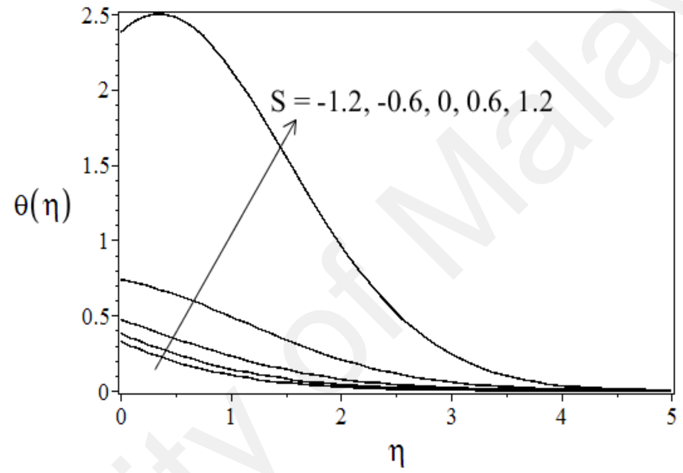

(b)

Figure 8.2. (a) Velocity and (b) Temperature profiles for different heat generation parameters S with K=0.4, M=0.4, Rd=0.4, Cr=0.4, b=1.0, Bi=0.5.

The velocity and concentration profiles increase on decreasing the chemical reaction parameter. The concentration profile overshoot in the case of generative chemical reaction (*Cr*<0) along the boundary layer. Figure 8.5(a) shows that the velocity profile along the boundary layer for various values of slip parameter (*b*) with constant values of *K, M, Rd, S, Cr, Bi.* The velocity increases on increasing the slip parameter (*b*). In the viscous region the thickness of the boundary layer decreases on increasing the slip parameter.

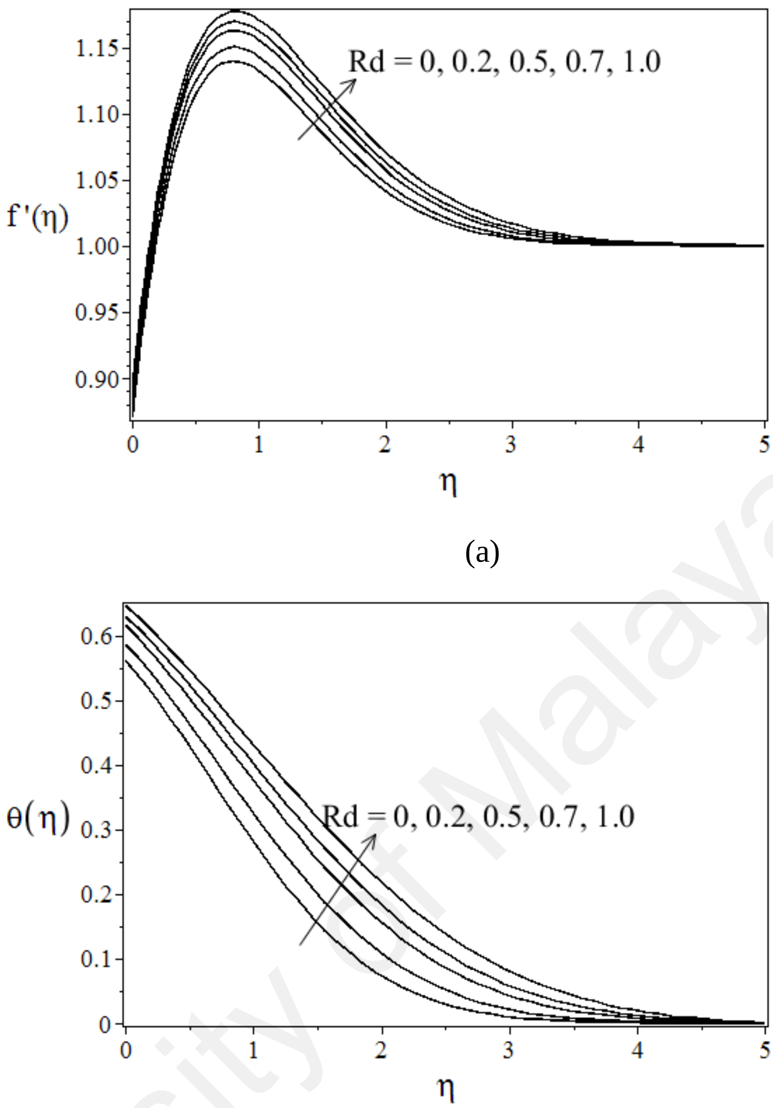

(a)

(b)

Figure 8.3. (a) Velocity and (b) Temperature profiles for different radiation parameters Rd with K=0.4, M=0.4, S=0.4, Cr=0.4, b=1.0, Bi=0.5.

It is observed from the Figures 8.5(b) and 8.5(c) that the influence of different velocity slip parameters on temperature and concentration profiles with constant values of *K, M, Rd*, *S*, *Cr* and *Bi* respectively. The results indicate that increasing the slip parameter (*b*) decreases both temperature and concentration profiles at the surface of the boundary layer. The thermal and solutal boundary layer thickness decreases due to decrease in the viscosity or increase in the free stream velocity in the medium. Figure 8.6(a) exhibits an increase in the velocity profile on increasing the values Biot number with constant values of other parameters (*K*, *M*, *Rd*, *S*, *Cr*, *b*). Figure 8.6(b) shows the effect of various values of Biot number on temperature. The temperature increases on increasing the Biot number in the thermal boundary layer.

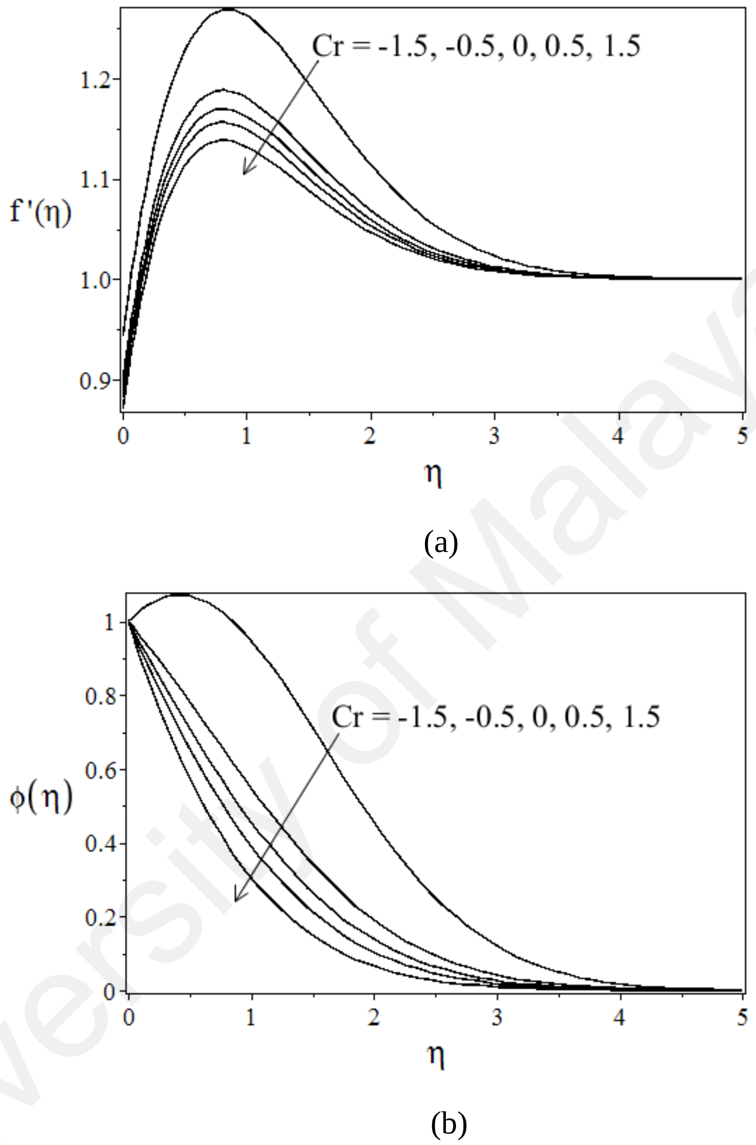

Figure 8.4. (a) Velocity and (b) Concentration profiles for different chemical reaction parameters Cr values with K=0.4, M=0.4, Rd=0.4, S=0.4, b=1.0, Bi=0.5.

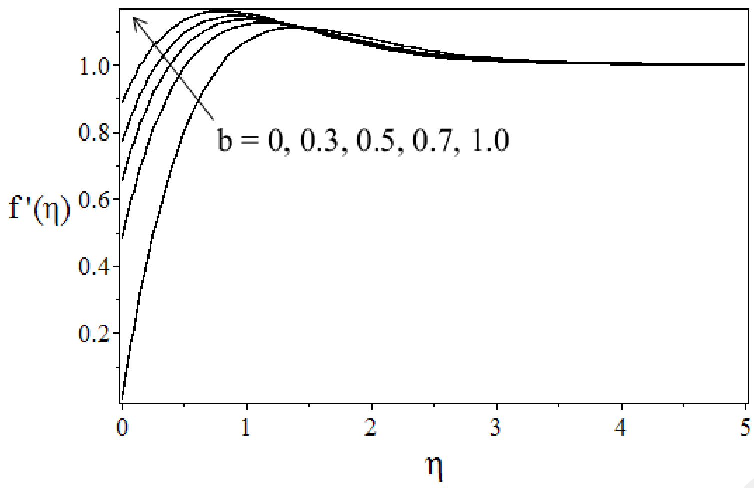

(a)

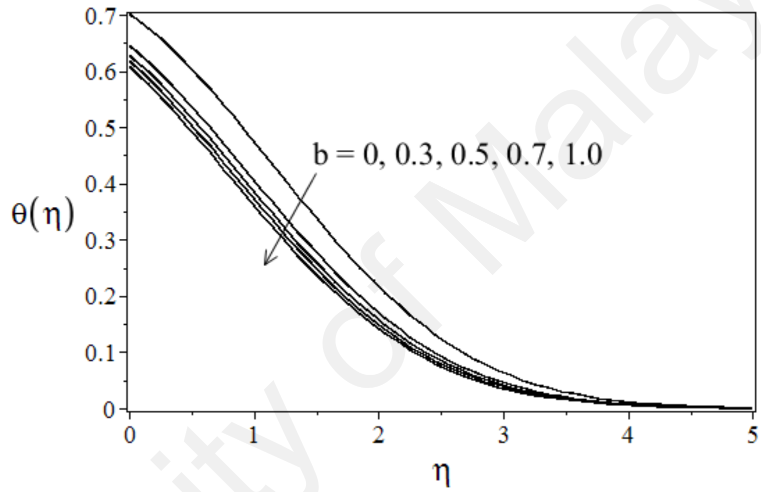

(b)

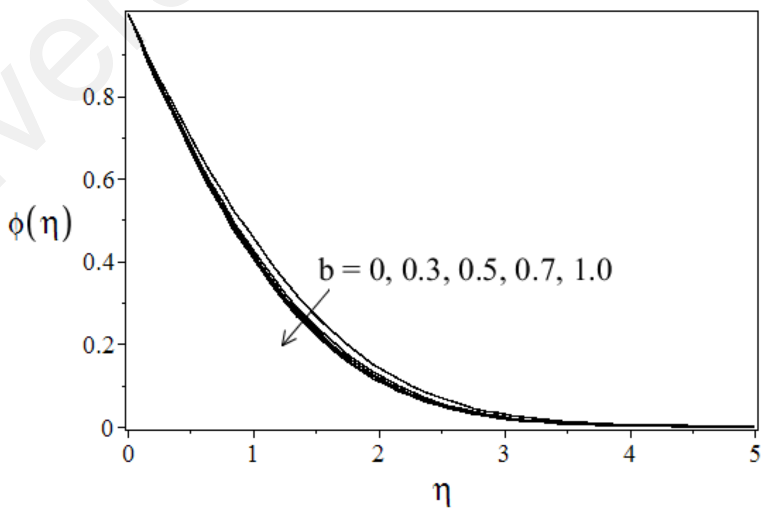

(c)

Figure 8.5. (a) Velocity, (b) Temperature and (c) Concentration profiles for different slip parameter b with K=0.4, M=0.4, Rd=0.4, S=0.4, Cr=0.4, Bi=0.5.

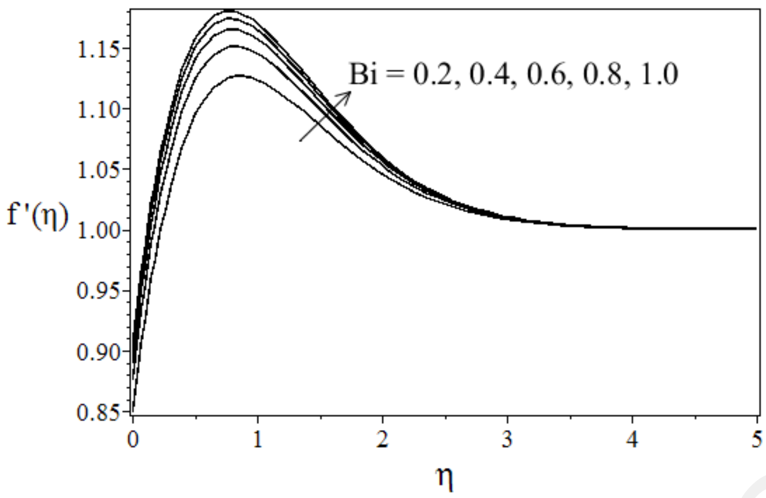

(a)

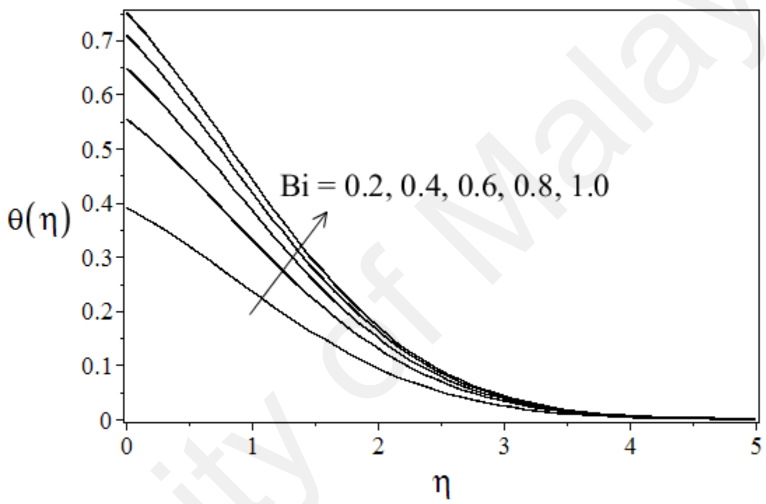

(b)

Figure 8.6. (a) Velocity and (b) Temperature profiles for different Biot number Bi with K=0.4, M=0.4, Rd=0.4, S=0.4, Cr=0.4, b=1.0.

CHAPTER 9: CONCLUSIONS

The present work is to investigate the interaction of mixed convection with thermal radiation, chemical reaction, slip, convective boundary condition and soret and dufour effects on viscous incompressible flow over a vertical plate in a porous medium near a stagnation point in the presence of magnetic field.

From this study it is concluded that the velocity profiles increases on decreasing the chemical reaction parameter and increasing the magnetic field, slip, thermal radiation, permeability parameters, biot number and soret and dufour numbers. The temperature profiles of the fluid increases on decreasing the slip parameter and increasing the heat generation, thermal radiation, chemical reaction parameters, Biot number and dufour number. The concentration profiles increases on increasing the soret number and decreasing the chemical reaction, slip parameters and dufour number.

The effect of local skin friction increases on increasing the permeability, magnetic field, internal heat generation, thermal radiation parameters and dufour number and the skin friction decreases on increasing the slip, chemical reaction parameters and soret number. The local heat transfer rate increases on increasing the slip, thermal radiation parameters and biot number, decreasing the internal heat generation and chemical reaction parameters. The local mass transfer rate increases on increasing the permeability, slip, chemical reaction, internal heat generation parameters, Soret and Dufour numbers, decreasing the magnetic field parameter.

REFERENCES

Abdelkhalek, M.M. (2006). The skin friction in the MHD mixed convection stagnation point with mass transfer. *International Communications in Heat and Mass Transfer*, *33*: 249–258.

Adeniyan, A., Adigun, J. A. (2013). Effects of chemical reaction on stagnation point MHD flow over a vertical plane with convective boundary conditions in the presence of a transverse uniform magnetic field. *The International Journal of Engineering and Science*, *2*(4): 14-18.

Afify, A.A., Elgazery, N.S. (2012). Lie group analysis for the effects of chemical reaction on MHD stagnation-point flow of heat and mass transfer towards a heated porous stretching sheet with suction or injection. *Nonlinear Analysis: Modelling and Control*, *17*(1): 1–15.

Akbar, N.S., Khan, Z.H., and Nadeem, S. (2014). The combined effects of slip and convective boundary conditions on stagnation-point flow of CNT suspended nanofluid over a stretching sheet. *Journal of Molecular Liquids*, *196*: 21–25.

Akeem B.D., Toyin, O., and Christie Y.I. (2014). Effects of variable viscousity on boundary layer flow with convective surface boundary condition. *IOSR Journal of Applied Physics*, *6*(4): 35-38.

Alam, M.S., and Rahman, M.M. (2006). Dufour and Soret effects on mixed convection flow past a vertical porous flat plate with variable suction. *Nonlinear Analysis: Modelling and Control*, *11*(1): 3–12.

Al-Odat, M.Q., and Al-Ghamdi, A.(2012). Numerical investigation of Dufour and Soret effects on unsteady MHD natural convection flow past vertical plate embedded in non-Darcy porous medium. *Applied Mathematics and Mechanics*, *33*(2): 195–210.

Alsaedi, A., Awais, M., and Hayat, T. (2012). Effects of heat generation/absorption on stagnation point flow of nanofluid over a surface with convective boundary conditions. *Communications in Nonlinear Science and Numerical Simulation*, *17*: 4210–4223.

Ashraf, M., and Ahmad, S. (2012). Radiation effects on MHD axisymmetric stagnation point flow towards a heated shrinking sheet. *Chemical Engineering Communications*, *199*(7): 823-837.

Attia, H.A. (2007). On the effectiveness of porosity on stagnation point flow towards a stretching surface with heat generation. *Computational Materials Science, 38*: 741–745.

Baag, S., Mishra, S.R., Dash, G.C., and Acharya, M.R. (2014). Numerical investigation on MHD micropolar fluid flow toward a stagnation point on a vertical surface with heat source and chemical reaction. *Journal of King Saud University–Engineering Sciences*.

Bachok, N., Ishak, A., and Pop, I. (2010). Melting heat transfer in boundary layer stagnation-point flow towards a stretching/shrinking sheet. *Physics Letters A, 374:* 4075–4079.

Bachok, N., Ishak, A., and Pop, I. (2013). Stagnation point flow toward a stretching/shrinking sheet with a convective surface boundary condition. *Journal of the Franklin Institute, 350*: 2736–2744.

Bhattacharyya, K. (2013). Heat transfer analysis in unsteady boundary layer stagnation-point flow towards a shrinking/stretching sheet. *Ain Shams Engineering Journal*, *4*: 259–264.

Bhattacharyya, K., Layek, G.C., and Seth, G.S. (2014). Soret and Dufour effects on convective heat and mass transfer in stagnation-point flow towards a shrinking surface. *Physica Scripta*, *89*(9): 095203-095213.

Bhattacharyya, K., Mukhopadhyay, S., and Layek, G.C. (2011). Slip effects on boundary layer stagnation-point flow and heat transfer towards a shrinking sheet. *International Journal of Heat and Mass Transfer*, *54*: 308–313.

Bhattacharyya, K., Mukhopadhyay, S., and Layek, G.C. (2012). Reactive solute transfer in magnetohydrodynamic boundary layer stagnation-point flow over a stretching sheet with suction/blowing. *Chemical Engineering Communications*, *199*: 368–383.

Bhutani, O.P., Chandran, P., and Kumar, P. (1984). Quasilinearized solution of axisymmetric hydromagnetic stagnation-point flow and heat transfer, *Journal of Mathematical Analysis and Applications*, *98*: 458-469.

Bhuvaneswari, M., Sivasankaran, S., and Ferdows, M. (2009) Lie group analysis of natural convection heat and mass transfer in an inclined surface with chemical reaction, *Nonlinear Analysis: Hybrid Systems*, *3*: 536-542.

Bhuvaneswari, M., Sivasankaran, S., and Kim, Y.J. (2012). Lie group analysis of radiation natural convection flow over an inclined surface in a porous medium with internal heat generation. *Journal of Porous Media*, *15*: 1155–1164.

Boutros, Y.Z., Abd-el-Malek, M.B., Badran, N.A., and Hassan, H.S. (2006). Lie-group method of solution for steady two-dimensional boundary-layer stagnation-point flow towards a heated stretching sheet placed in a porous medium. *Meccanica*, *41*: 681–691.

Chamkha, A.J., Aly, A.M., and Mansour, M.A. (2010). Similarity solution for unsteady heat and mass transfer from a stretching surface embedded in a porous medium with suction/injection and chemical reaction effects. *Chemical Engineering Communications*, *197*(6): 846-858.

Chamkha, A.J., and Ahmed, S.E. (2011). Similarity solution for unsteady MHD flow near a stagnation point of a three-dimensional porous body with heat and mass transfer, heat generation/absorption and chemical reaction. *Journal of Applied Fluid Mechanics*, *4* (2): 87-94.

Chao, B.H., Wang, H., and Cheng, P. (1996). Stagnation point flow of a chemically reactive fluid in a catalytic porous bed. *International Communications in Heat and Mass Transfer*, *39*(14): 3003-3019.

Cheng, J., Liao, S., and Pop, I. (2005). Analytic series solution for unsteady mixed convection boundary layer flow near the stagnation point on a vertical surface in a porous medium. *Transport in Porous Media*, *61*: 365–379.

Chiam, T.C. (1994). Stagnation-point flow towards a stretching plate. *Journal of the Physical Society of Japan*, *63*(6): 2443-2444.

Cortell, R. (2008). Effects of viscous dissipation and radiation on the thermal boundary layer over a nonlinearly stretching sheet. *Physics Letters A*, *372*: 631–636.

Daba, M., Devaraj, P., Subhashini, S.V.(2015). Mixed convection on boundary layer flow over a vertically stretching sheet with convective boundary condition and effect of partial slip. *Frontiers in Heat and Mass Transfer*, *6*(3): 1-6.

Das, K. (2014). Influence of chemical reaction and viscous dissipation on MHD mixed convection flow. *Journal of Mechanical Science and Technology*, *28* (5): 1881-1885.

Fang, T. (2008). A note on the unsteady boundary layers over a flat plate. *International Journal of Non-Linear Mechanics*, *43*: 1007–1011.

Fang, T., Zhang, J., and Yao, S. (2010). A new family of unsteady boundary layers over a stretching surface. *Applied Mathematics and Computation*, *217*: 3747–3755.

Fang, T., Lee, C.F., and Zhang, J. (2011). The boundary layers of an unsteady incompressible stagnation-point flow with mass transfer. *International Journal of Non-Linear Mechanics*, *46*: 942–948.

Geindreau, C., and Auriault, J.L. (2002). Magnetohydrodynamic flows in porous media. *Journal of Fluid Mechanics*, *466*: 343-363.

Hamad, M.A.A., Uddin, Md. J., Ismail, A.I. Md. (2012). Radiation effects on heat and mass transfer in MHD stagnation-point flow over a permeable flat plate with thermal convective surface boundary condition, temperature dependent viscosity and thermal conductivity. *Nuclear Engineering and Design*, *242*: 194–200.

Harris, S.D., Ingham, D.B., and Pop, I. (2009). Mixed convection boundary-layer flow near the stagnation point on a vertical surface in a porous medium: Brinkman model with slip. *Transport in Porous Media*, *77*: 267–285.

Hayat, T., Abbas, Z., Pop, I., and Asghar, S. (2010). Effects of radiation and magnetic field on the mixed convection stagnation-point flow over a vertical stretching sheet in a porous medium. *International Journal of Heat and Mass Transfer*, *53*: 466–474.

Hayat, T., Mustafa, M., and Obaidat, S. (2011). Simultaneous effects of MHD and thermal radiation on the mixed convection stagnation-point flow of a power-law fluid. *Chinese Physics Letters*, *28*(7): 074702-705.

Ishak, A., Jafar, K., Nazar, R., and Pop, I. (2009). MHD stagnation point flow towards a stretching sheet. *Physica A*, *388*: 3377-3383.

Ishak, A., Nazar, R., and Pop, I. (2006). Mixed convection boundary layers in the stagnation-point flow toward a stretching vertical sheet. *Meccanica*, *41*: 509–518.

Ishak, A., Yacob, N.A., and Bachok, N. (2011). Radiation effects on the thermal boundary layer flow over a moving plate with convective boundary condition. *Meccanica*, *46*: 795–801.

Jat, R.N., and Chaudhary, S. (2010). Radiation effects on the MHD flow near the stagnation point of a stretching sheet. *Zeitschrift fur Angewandte Mathematik und Physik*, *61*: 1151–1154.

Kafoussias, N.G., Rees, D.A.S., and Daskalakis, J.E. (1998). Numerical study of the combined free-forced convective laminar boundary layer flow past a vertical isothermal flat plate with temperature-dependent viscosity. *Acta Mechanica*, *127*: 39-50.

Kandasamy, R., Hayat, T., and Obaidat, S. (2011). Group theory transformation for Soret and Dufour effects on free convective heat and mass transfer with thermophoresis and chemical reaction over a porous stretching surface in the presence of heat source/sink. *Nuclear Engineering and Design*, *241*: 2155–2161.

Kumari, M., and Nath, G. (1999). Flow and heat transfer in a stagnation-point flow over a stretching sheet with a magnetic field. *Mechanics Research Communications*, *26*(4): 469-478.

Lakshmisha, K.N., Venkateshwaran, S., and Nath, G. (1988). Three dimensional unsteady flow with heat and mass transfer over a continuous stretching surface. *Journal of Heat Transfer*, *115*: 590.

Layek, G.C., Mukhopadhyay, S., and Samad, Sk. A. (2007). Heat and mass transfer analysis for boundary layer stagnation-point flow towards a heated porous stretching sheet with heat absorption/generation and suction/blowing. *International Communications in Heat and Mass Transfer*, *34*: 347–356.

Lee, J., Kandaswamy, P., Bhuvaneswari, M., and Sivasankaran, S. (2008). Lie group analysis of radiation natural convection heat transfer past an inclined porous surface. *Journal of Mechanical Science and Technology*, *22*: 1779-1784.

Lok, Y.Y., Ishak, A., and Pop, I. (2011). MHD stagnation-point flow towards a shrinking sheet. *International Journal of Numerical Methods for Heat & Fluid Flow***,** *21*(1): 61 – 72.

Lok, Y.Y., and Pop, I. (2014). Stretching or shrinking sheet problem for unsteady separated stagnation-point flow. *Meccanica*, *49*: 1479–1492.

Magyari, E., and Aly, E.H. (2006a). Exact analytical solution for a thermal boundary layer in a saturated porous medium. *Applied Mathematics Letters*, *19*: 1351–1355.

Magyari, E., and Aly, E.H. (2006b). Mechanical and thermal characteristics of a mixed convection boundary-layer flow in a saturated porous medium. *International Journal of Heat and Mass Transfer*, *49*: 3855–3865.

Mahapatra, T.R., and Gupta, A.S. (2001). Magnetohydrodynamic stagnation-point flow towards a stretching sheet. *Acta Mechanica*, *152*: 191–196.

Mahapatra, T.R., and Gupta, A.S. (2002). Heat transfer in stagnation-point flow towards a stretching sheet. *Heat and Mass Transfer*, *38*: 517-521.

Mahapatra, T.R., and Nandy, S.K. (2013). Momentum and heat transfer in MHD axisymmetric stagnation-point flow over a shrinking sheet. *Journal of Applied Fluid Mechanics*, *6* (1): 121-129.

Makinde, O.D. (2012). Heat and mass transfer by MHD mixed convection stagnation point flow toward a vertical plate embedded in a highly porous medium with radiation and internal heat generation. *Meccanica*, *47*: 1173–1184.

Makinde, O.D., and Aziz, A. (2010). MHD mixed convection from a vertical plate embedded in a porous medium with a convective boundary condition. *International Journal of Thermal Sciences*, *49*: 1813-1820.

Makinde, O.D., and Sibanda, P.(2011). Effects of chemical reaction on boundary layer flow past a vertical stretching surface in the presence of internal heat generation. *International Journal of Numerical Methods for Heat & Fluid Flow*, *21*(6): 779–792.

Merkin, J.H. (2013). Unsteady free convective boundary-layer flow near a stagnation point in a heat-generating porous medium. *Journal of Engineering Mathematics*, *79*: 73–89.

Merkin, J.H., Nazar, R., and Pop, I. (2012). The development of forced convection heat transfer near a forward stagnation point with Newtonian heating. *Journal of Engineering* Mathematics, *74*: 53–60.

Mohamed, M.K.A., Salleh, M.Z., Nazar, R., and Ishak, A. (2013). Numerical investigation of stagnation point flow over a stretching sheet with convective boundary conditions. *Boundary value Problems*, 2013:4.

Mukhopadhyay, S. (2013). Effects of thermal radiation and variable fluid viscosity on stagnation point flow past a porous stretching sheet. *Meccanica*, *48*: 1717–1730.

Nandeppanavar, M.M., Vajravelu, K., and Abel, M.S. (2011). Heat transfer in MHD viscoelastic boundary layer flow over a stretching sheet with thermal radiation and non-uniform heat source/sink. *Communications in Nonlinear Science and Numerical Simulation*, *16*: 3578–3590.

Nazar, R., Amin, N., and Pop, I. (2004a). Unsteady mixed convection boundary layer flow near the stagnation point on a vertical surface in a porous medium. *International Journal of Heat and Mass Transfer*, *47*: 2681–2688.

Nazar, R., Amin, N., Filip, D., and Pop, I. (2004b). Unsteady boundary layer flow in the region of the stagnation point on a stretching sheet. *International Journal of Engineering Science*, *42*: 1241–1253.

Nield, D.A. and Bejan, A. (2006). *Convection in Porous Media*, 3rd Ed., Springer, New York, USA.

Pal, D. (2009). Heat and mass transfer in stagnation-point flow towards a stretching surface in the presence of buoyancy force and thermal radiation. *Meccanica*, *44*: 145–158.

Pal, D., and Mondal, H. (2011). Effects of Soret Dufour, chemical reaction and thermal radiation on MHD non-Darcy unsteady mixed convective heat and mass transfer over a stretching sheet. *Communications in Nonlinear Science and Numerical Simulation*, 16: 1942–1958.

Phillips, C.G., and Kaye, S.R. (1999). The influence of the viscous boundary layer on the critical stokes number for particle impaction near a stagnation point. *Journal of Aerosol Science*, *30* (6): 709-718.

Pop, I., Ishak, A., and Aman, F. (2011). Radiation effects on the MHD flow near the stagnation point of a stretching sheet: revisited. *Zeitschrift fur Angewandte Mathematik und Physik*, *62*: 953–956.

Pop, S.R., Grosan, T., and Pop, I. (2004). Radiation effects on the flow near the stagnation point of a stretching sheet. *Technische Mechanik*, *25*(2): 100-106.

Postelnicu, A. (2007). Influence of chemical reaction on heat and mass transfer by natural convection from vertical surfaces in porous media considering Soret and Dufour effects. *Heat Mass Transfer*, *43*: 595–602.

Postelnicu, A. (2010). Heat and mass transfer by natural convection at a stagnation point in a porous medium considering Soret and Dufour effects. *Heat Mass Transfer*, *46*: 831–840.

Raju, M.C., Ananda Reddy, N., and Varma, S.V.K. (2014). Analytical study of MHD free convective, dissipative boundary layer flow past a porous vertical surface in the presence of thermal radiation, chemical reaction and constant suction. *Ain Shams Engineering Journal*, *5*: 1361–1369.

Ramesh, B.K. (2012). A new exact solution for boundary layer flow over a stretching plate. *International Journal of Non-Linear Mechanics*, *47*: 727–733.

Rohni, A.M., Ahmad, S., and Pop, I. (2014). Flow and heat transfer at a stagnation-point over an exponentially shrinking vertical sheet with suction. *International Journal of Thermal Sciences*, *75*: 164-170.

Rohni, A.M., Ahmad, S., Pop, I., and Merkin, J.H. (2012). Unsteady mixed convection boundary-layer flow with suction and temperature slip effects near the stagnation point on a vertical permeable surface embedded in a porous medium. *Transport in Porous Media*, *92*: 1–14.

Rosali, H., Ishak, A., and Pop, I. (2011). Stagnation point flow and heat transfer over a stretching/shrinking sheet in a porous medium. *International Communications in Heat and Mass Transfer*, *38*: 1029–1032.

Saleh, S.H.M., Arifin, N.M., Nazar, R., Ali, F.M., and Pop, I. (2014). Mixed convection stagnation flow towards a vertical shrinking sheet. *International Journal of Heat and Mass Transfer*, *73*: 839–848.

Salleh, M.Z., Nazar, R., and Pop, I. (2010). Boundary layer flow and heat transfer over a stretching sheet with Newtonian heating. *Journal of the Taiwan Institute of Chemical Engineers*, *41*: 651–655.

Santra, B., Dandapat, B. S., and Andersson, H.I. (2007). Axisymmetric stagnation-point flow over a lubricated surface. *Acta Mechanicca*, *194*: 1–10.

Seini, I.Y., and Makinde, O.D. (2014). Boundary layer flow near stagnation-points on a vertical surface with slip in the presence of transverse magnetic field. *International Journal of Numerical Methods for Heat & Fluid Flow*, *24*(3): 643–653.

Sharma, P.R., and Singh, G. (2009). Effects of variable thermal conductivity and heat source / sink on MHD flow near a stagnation point on a linearly stretching sheet. *Journal of Applied Fluid Mechanics*, *2* (1): 13-21.

Shateyi, S., and Marewo, G.T. (2014). Numerical analysis of unsteady MHD flow near a stagnation point of a two-dimensional porous body with heat and mass transfer, thermal radiation, and chemical reaction. *Boundary Value Problems*, *2014*: 2014:218.

Shehzad, S.A., Hayat, T., Asghar, S., and Alsaedi, A. (2015). Stagnation point flow of thixotropic fluid over a stretching sheet with mass transfer and chemical reaction. *Journal of Applied Fluid Mechanics*, *8*(3): 465- 471.

Singh, G., and Makinde, O.D. (2015). Mixed convection slip flow with temperature jump along a moving plate in presence of free stream. *Thermal Science*, *19*(1): 119-128.

Singh, G., and Sharma, P.R. (2014). Heat and mass transfer in the boundary layer flow along a vertical isothermal reactive plate near stagnation point: Existence of dual solution. *Journal of Applied Fluid Mechanics*, *7*(1): 25-33.

Singh, G., Sharma, P.R., and Chamkha, A.J. (2010). Effect of volumetric heat generation/absorption on mixed convection stagnation point flow on an iso-thermal vertical plate in porous media. *International Journal of Industrial Mathematics*, *2* (2): 59-71.

Sinha, A. (2014). Steady stagnation point flow and heat transfer over a shrinking sheet with induced magnetic field. *Journal of Applied Fluid Mechanics*, *7*(4): 703-710.

Sparrow, E.M., and Cess, R.D. (1978). *Radiation Heat Transfer*, Hemisphere public. Corp., Washington, DC, USA.

Surma Devi, C.D., Takhar, H.S., and Nath, G. (1986). Unsteady three dimensional boundary layer flow due to a stretching surface. *International Journal of Heat and Mass Transfer*, *29*: 1996.

Takhar, H.S., Chamkha, A. J., and Nath, G. (2005). Unsteady mixed convection on the stagnation-point flow adjacent to a vertical plate with a magnetic field. *Heat Mass Transfer*, *41*: 387–398.

Vafai, K. (2005), *Handbook of Porous Media*, Taylor & Francis, 2nd Ed, New York, USA.

Van Gorder, R.A., Vajravelu, K., Pop, I. (2012). Hydromagnetic stagnation point flow of a viscous fluid over a stretching or shrinking sheet. *Meccanica*, *47*: 31–50.

Vedavathi, N., Ramakrishna, K., and Jayarami Reddy, K. (2015). Radiation and mass transfer effects on unsteady MHD convective flow past an infinite vertical plate with Dufour and Soret effects. *Ain Shams Engineering Journal*, *6*: 363–371.

Wang, C.Y. (1984). The three-dimensional flow due to a stretching at surface. *Physics of Fluids*, 27: 1915.

Wang, J., Pan, C., Choi, K.S., Gao, L., and Lian, Q.X. (2013). Formation, growth and instability of vortex pairs in an axisymmetric stagnation flow. *Journal of Fluid Mechanics*, *725*: 681-708.

Weidman, P.D., and Sprague, M.A. (2011). Flows induced by a plate moving normal to stagnation-point flow. *Acta Mechanica*, *219*: 219–229.

Yao, S., Fang, T., and Zhong, Y. (2011). Heat transfer of a generalized stretching/shrinking wall problem with convective boundary conditions. *Communications in Nonlinear Science and Numerical Simulation*, *16*: 752–760.

Yih, K.A. (1998). Heat Source/Sink effect on MHD mixed convection in stagnation flow on a vertical permeable plate in porous media. *International Communications in Heat and Mass Transfer*, *25*(3): 427-442.

Zhong, Y., and Fang, T. (2011). Unsteady stagnation-point flow over a plate moving along the direction of flow impingement. *International Journal of Heat and Mass Transfer*, *54*: 3103–3108.

Zhu, J. (2000). Numerical study of stagnation-point flows of incompressible fluid. *Japan Journal of Industrial and Applied Mathematics*, *17*: 209-228.

LIST OF PUBLICATIONS

Niranjan, H., Sivasankaran, S., Bhuvaneswari, M., and Siri, Z. (2015). Effects of chemical reaction on MHD mixed convection stagnation point flow toward a vertical plate in a porous medium with radiation and heat generation. *Journal of Physics: CS, 662, 012014*: 1-9.

Niranjan, H., Sivasankaran, S., and Bhuvaneswari, M. (2016). Analytical and numerical study on magneto-convection stagnation point flow in a porous medium with chemical reaction, radiation and slip effect. *Mathematical Problems in Engineering*, *4017076*: 1-12.

Niranjan, H., Sivasankaran, S., Siri, Z., and Bhuvaneswari, M. (2016). Chemical reaction, soret and dufour effects on MHD mixed convection stagnation point flow with radiation and slip condition. *Scientia Iranica*, *Transactions B: Mechanical Engineering, Accepted.*

Niranjan, H., Sivasankaran, S., Siri, Z., and Bhuvaneswari, M. (2016). Effects of slip and Newtonian heating on magneto-convection stagnation-point flow of chemically reacting fluid in a porous medium with radiation. *International Journal of Numerical Methods for Heat & Fluid Flow*, *Accepted*.

Niranjan, H., Sivasankaran, S., Siri, Z., and Bhuvaneswari, M. (2016). Effects of chemical reaction and radiation on MHD mixed convection stagnation point flow towards a vertical plate in a porous medium with convective boundary condition. *Journal of the Taiwan Institute of Chemical Engineers, Revision Submitted*.